

**Heavy hadron spectrum on lattice with NRQCD
bottom and HISQ lighter quarks**

By

Protick Mohanta

PHYS11201204013

National Institute of Science Education and Research

Jatni, Odisha - 752050, India

A thesis submitted to the

Board of Studies in Physical Sciences

In partial fulfillment of requirements

for the Degree of

DOCTOR OF PHILOSOPHY

of

HOMI BHABHA NATIONAL INSTITUTE

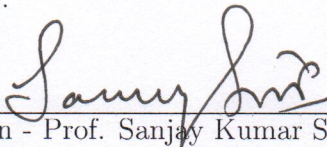
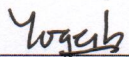


May, 2020

Homi Bhabha National Institute

Recommendations of the Viva Voce Committee

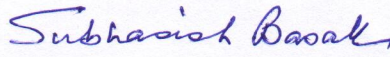
As members of the Viva Voce Committee, we certify that we have read the dissertation prepared by **Protick Mohanta** entitled “ **Heavy hadron spectrum on lattice with NRQCD bottom and HISQ lighter quarks**” and recommend that it may be accepted as fulfilling the thesis requirement for the award of Degree of Doctor of Philosophy.

 Chairman - Prof. Sanjay Kumar Swain	<u>30/12/20</u> Date
 Guide / Convener - Dr. Subhasish Basak	<u>30/12/2020</u> Date
 External Examiner - Prof. Dipankar Chakrabarti	<u>30/12/2020</u> Date
 Member 1 - Dr. Prolay Kumar Mal	<u>Dec 30, 2020</u> Date
 Member 2 - Dr. Yogesh Kumar Srivastava	<u>30/12/2020</u> Date
 External Member - Prof. Ajit Mohan Srivastava	<u>30-12-20</u> Date

Final approval and acceptance of this thesis is contingent upon the candidate's submission of the final copies of the thesis to HBNI.

I hereby certify that I have read this thesis prepared under my direction and recommend that it may be accepted as fulfilling the thesis requirement.

Date: 30/12/2020
Place: NISER Bhubaneswar


Dr. Subhasish Basak

STATEMENT BY AUTHOR

This dissertation has been submitted in partial fulfillment of requirements for an advanced degree at Homi Bhabha National Institute (HBNI) and is deposited in the Library to be made available to borrowers under rules of the HBNI.

Brief quotations from this dissertation are allowable without special permission, provided that accurate acknowledgement of source is made. Requests for permission for extended quotation from or reproduction of this manuscript in whole or in part may be granted by the Competent Authority of HBNI when in his or her judgment the proposed use of the material is in the interests of scholarship. In all other instances, however, permission must be obtained from the author.

Protick Mohanta

Protick Mohanta
30/12/2020

DECLARATION

I, Protick Mohanta, hereby declare that the investigation presented in the thesis has been carried out by me. The work is original and has not been submitted earlier as a whole or in part for a degree/diploma at this or any other Institution/University.

Protick Mohanta

Protick Mohanta
30/12/2020

List of publications arising from the thesis

Journal

Refereed journals

1. Protick Mohanta, Subhasish Basak, **Heavy baryon spectrum on the lattice with NRQCD bottom and HISQ lighter quarks.** Phys. Rev. D 101, 094503 (2020); arXiv:1911.03741 [hep-lat]
2. Protick Mohanta, Subhasish Basak, **Construction of $bb\bar{u}\bar{d}$ tetraquark states on lattice with NRQCD bottom and HISQ up/down quarks,** Phys. Rev. D 102, 094516 (2020), arXiv: 2008.11146 [hep-lat]

Conference proceedings

1. Protick Mohanta, Subhasish Basak, **Heavy hadrons spectra on lattice using NRQCD.** EPJ Web of Conferences 175, 05031 (2018).

Symposium and conference

1. **Heavy hadrons spectra on lattice using NRQCD.**
Lattice 2017: 35th International Symposium on Lattice Field Theory, 18th-24th June 2017, Granada, Spain.
2. **Charmed and strange B meson spectra on lattice using NRQCD.**
Helmholtz International Summer School: “Hadron Structure, Hadronic Matter, Lattice QCD” Bogoliubov Laboratory of Theoretical Physics, JINR, Dubna, Russia, August 20 - September 2, 2017.
3. **Heavy hadron spectrum on lattice using NRQCD.**

DAE-HEP Symposium: XXIII DAE-BRNS High Energy Physics Symposium,
10-14 Dec 2018, Indian Institute of Technology Madras, Chennai (India).

Protick Mohanta

Protick Mohanta
30/12/2020

Dedicated
to
All the people who inspired me to come this far.

Acknowledgements

I would like to begin by thanking my supervisor, Subhasish Basak for his invaluable guidance and decisive advice. I am grateful to him for giving me the opportunity to work in Lattice QCD. I am thankful to Stefan Meinel (University of Arizona, USA) and Rabeet Singh (Banaras Hindu University, India) for useful discussion. My heartfelt gratitude to Dipankar Chakrabarti (IIT-Kanpur) for his constant help. I shall thank my thesis monitoring committee members for their constructive suggestions. I would like to thank DAE (India) and HBNI (India) for providing me the financial support. I would like to express my gratitude to the NISER and SPS where I learned to develop a research career.

I owe a lot of thanks to all of my friends and my family, without their constant support I could hardly survive the last few struggling years.

Protick Mohanta

Protick Mohanta
30/12/2020

Contents

Summary	xii
List of Figures	xiv
List of Tables	xvii
1 Introduction	1
1.0.1 Heavy hadrons	3
1.0.2 Tetraquarks	5
1.0.3 QCD in continuum space-time	6
2 QCD on Lattice	13
2.1 Gauge action	17
2.2 Fermion action	18
2.2.1 Staggered fermions	21
2.2.2 HISQ action	25
2.3 NRQCD action	26
2.3.1 NRQCD on Lattice	33
2.3.2 $\mathcal{O}(a^4)$ Improvement	34
2.3.3 NRQCD Propagator	35

3	Heavy baryons on lattice	40
3.1	Two-point functions	41
3.1.1	Light-light meson two-point function	44
3.1.2	Bottom-bottom meson two-point function	45
3.1.3	Heavy-light meson two-point function	47
3.1.4	Bottom baryon two-point function	49
3.1.5	Triply bottom baryon	50
3.1.6	Bottom-light-light baryon	52
3.1.7	Bottom-bottom-light baryon	57
4	Quark mass tuning and Results	62
4.1	m_b tuning	63
4.2	m_c tuning	64
4.3	m_s tuning	66
4.4	$m_{u/d}$ tuning	67
4.5	Numerical results	70
5	Tetraquark	84
5.1	Doubly bottom tetraquark	85
5.1.1	Quark mass tuning	88
5.1.2	$bb\bar{u}\bar{d}$ spectrum	94
5.1.3	Variational analysis	98
5.2	Bottom-charm tetraquark	106
6	Summary and Outlook	111
A	Zeroth Order NRQCD	118

List of Figures

2.1	A graphic illustration of discrete space-time lattice with quark fields of flavor f on site n , $\psi^f(n)$ and the gluon fields $U_\mu(n)$ on the link between lattice sites n and $n + a\hat{\mu}$	15
2.2	Distribution of fermionic degrees of freedom in two dimensional lattice.	22
2.3	Clover operator in $\mu - \nu$ plane	34
4.1	Tuning of s and u/d quark masses in various lattices. The experimental values of B^0 and B_s^0 are shown by bands whose thickness are to enhance visibility and have nothing to do with experimental errors.	68
4.2	$\Sigma_b, \widetilde{\Omega}_b$ and $\widetilde{\Omega}_{ccb}$ correlators in $28^3 \times 96$ lattice.	72
4.3	Effective mass plots for the states in Figure 4.2. The bands are placed over what we consider plateau.	72
4.4	Variation of single b baryon masses in MeV against the same light quark masses as in Figure 4.1. $m_q = 0.085$ and 0.114 are the tuned $u/d, s$ quark masses respectively, indicated by dashed vertical lines. The bands correspond to the PDG values, except for Ξ_{cb} which is taken from [16].	73
4.5	Ratio of correlators for the calculation of the two splittings shown in Table 4.8. The bands overlaid on the data points represent single exponential fits.	77

4.6	Hyperfine splittings at various m_s and $m_{u/d}$ for a selected few bottom baryons on $28^3 \times 96$ lattice. Horizontal bands are the average values of the splittings.	77
4.7	Ω_{bbb}^* , $\widetilde{\Omega}_{cbb}^*$ and $\widetilde{\Omega}_{ccb}$ effective masses.	78
5.1	Molecular tetraquark state viewed as bound state of two B mesons, which is similar to two hydrogen atoms forming a hydrogen molecule.	89
5.2	Schematic diagram of helium-like Λ_b and $[bb][\bar{u}\bar{d}]$ tetraquark state used for Hartree-Fock treatment.	91
5.3	Variation of tetraquark mass in MeV versus am_q . The $am_q = 0.105$ and 0.155 are the Λ_b and B^0 tuned u/d quark masses.	94
5.4	Effective mass plot of the states of the operators \mathcal{O}_D and \mathcal{O}_{M_1} calculated on $16^3 \times 48$, $20^3 \times 64$ and $28^3 \times 96$ lattices. Dashed lines are $B - B^*$ thresholds for different lattices. For easy viewing, the effective masses and thresholds on $20^3 \times 64$ (purple colored) are multiplied by a common factor of 0.85, while that of $28^3 \times 96$ (green colored) by 0.70.	95
5.5	Variation of ground and excited state energies \mathcal{E}_m of the equation (5.24) with t_0 , obtained by solving 2×2 GEVP of the correlation matrices $\mathcal{O}_{M_1} \times \mathcal{O}_{M_2}$, $\mathcal{O}_D \times \mathcal{O}_{M_1}$ and $\mathcal{O}_D \times \mathcal{O}_{M_2}$. In this plot we used Λ_b -tuned $am_{u/d}$ for all the operators.	100
5.6	Histogram plots of normalized components $(v_0^{M_1}, v_0^{M_2})$ which define the energy eigenstate $ 0\rangle = v_0^{M_1} M_1\rangle + v_0^{M_2} M_2\rangle$	102
5.7	The histogram plot of $v_1^{M_1}$ and $v_1^{M_2}$ that define the energy eigenstate $ 1\rangle = v_1^{M_1} M_1\rangle + v_1^{M_2} M_2\rangle$	103
5.8	Histogram plots of normalized eigenvector components v_0^X, v_1^X and v_2^X of 3×3 correlation matrix, where $X = D, M_1, M_2$, on $28^3 \times 96$ lattice.	105

6.1	Comparison of our single bottom baryon spectra with Brown <i>et al.</i> [2], Burch [5], Mathur <i>et al.</i> [6] and PDG [4] where available.	113
6.2	Comparison of our triple and double bottom baryon spectra with Brown <i>et al.</i> [2] and Burch [5].	114
6.3	Comparison of our hyperfine splittings with Brown <i>et al.</i> [2], Burch [5], Mathur <i>et al.</i> [6] and PDG [4] where available.	115

List of Tables

3.1	Operators for single bottom baryons. Q is used for b field. Interchange in the position of two lighter quarks keeps the operator unchanged.	57
3.2	Operators for triple and double bottom baryons. Q is used for b field and l for any of the $c, s, u/d$ lighter quarks.	59
4.1	Tuned b, c and s quark bare masses for lattices used in this work. For s -quark mass, we mentioned the particle states to which it is tuned to. The values of ϵ -parameter used for c -quark are given in the last column.	65
4.2	Ω_c and Ω_{cc} baryon masses. Interpolating operator and two-point function used to calculate the masses of these triply light baryons are given in Appendix B.	66
4.3	D and B meson masses in MeV with the tuned am_b, am_c and am_s	67
4.4	Values of $am_{u/d}$ used in this work.	68
4.5	MILC configurations used in this work. The gauge coupling is β , lattice spacing a , u/d and s sea quark masses are m_l and m_s respectively and lattice size is $L^3 \times T$. The N_{cfg} is number of configurations used in this work.	70
4.6	Masses, in lattice unit, of baryons involving single b quark and no s quark. The bare u/d -quark masses are 0.165 for $16^3 \times 48$, 0.115 for $20^3 \times 64$ and 0.085 for $28^3 \times 96$	74

4.7	Masses, in lattice unit, of baryons containing single b -quark and s -quark(s).	75
4.8	Single bottom baryons mass splittings in MeV.	76
4.9	Triple and double bottom non-strange baryon masses.	79
4.10	Double bottom strange baryon spectra.	80
4.11	Double bottom baryon mass splittings in MeV. None of the splittings have PDG entries.	81
4.12	Ratio of hyperfine splittings of double bottom baryons to corresponding B -mesons in the heavy quark limit in $28^3 \times 96$ lattice.	81
5.1	Comparison of $m_{u/d}$ obtained from various lattices with quark mass parameters in the equations (5.10) and (5.17).	94
5.2	Masses of tetraquark states for different $am_{u/d}$ tuning in lattice unit aE_{latt} . We also include the B and B^* states that are used for threshold calculation.	96
5.3	Masses of tetraquark states for different $am_{u/d}$ tuning (M_{latt}) in MeV.	96
5.4	Mass differences of “bound” $ D\rangle$ and “molecular” $ M_1\rangle, M_2\rangle$ states from $B - B^*$ threshold. The X subscript denotes any of the D, M_1, M_2	97
5.5	Energy eigenvalues in lattice unit from GEVP analysis of the B -tuned $\mathcal{O}_{M_1} \times \mathcal{O}_{M_2}$ and Λ_b -tuned $\mathcal{O}_D \times \mathcal{O}_{M_1} \times \mathcal{O}_{M_2}$	101
5.6	Energy differences from the $B - B^*$ threshold of the GEVP values of Table 5.5 for the $\mathcal{O}_{M_1} \times \mathcal{O}_{M_2}$ and Λ_b -tuned $\mathcal{O}_D \times \mathcal{O}_{M_1} \times \mathcal{O}_{M_2}$ correlation matrices. Threshold values are taken from Table 5.2.	101
6.1	Bottom baryon mass differences in MeV. PDG values without error is simply the differences of the two states.	116

Chapter 1

Introduction

Standard Model of particle physics is a remarkably successful theory in explaining the fundamental interactions of the elementary particles at high energy. The theory provides a unified description of the electromagnetic, weak and strong interactions in the framework of the perturbation theory and local $SU(3)_c \times SU(2)_L \times U(1)_Y$ gauge group broken spontaneously to $SU(3)_c \times U(1)_{EM}$ [1]. The electromagnetic interaction between electrically charged particles is mediated by the photons γ . The weak interaction is responsible for the flavor changing processes like the radioactive β decay and its mediators are the Z, W^\pm bosons. The strong interaction is the forces between the color charged particles *i.e.* quarks and gluons and is carried by the colored gluons g . Besides these bosonic force carrying particles, the Standard Model contains fermionic matter particles that appear in three generations of *leptons* and *quarks*. The final ingredient of the Model is Higgs boson which provides a mechanism to give masses to the Z, W^\pm bosons as well as the leptons and quarks in a gauge invariant way. The Higgs boson is the last particle to be discovered in 2012 by ATLAS[2] and CMS[3] collaborations at CERN, almost two decades after the *top* quark was discovered and more than three decades from the discovery of Z and W^\pm

bosons.

Of the three interactions in the Standard Model, the strong interaction is rather different from the other two. QCD is the non-Abelian SU(3) gauge theory of strong interaction that exist among the quarks and gluons. The SU(3) gauge group leads to the self interaction of gluons and the nonpareil properties of QCD, namely asymptotic freedom and quark confinement are believed to be the consequence of gluon self interaction. Asymptotic freedom means that at short distances or high energies, *i.e.* high momentum transfer, the interaction between quarks and gluons is weak enough to be treated perturbatively. But at lower energy or at large distances, the quark-gluon coupling gets stronger which is believed to be the reason behind confinement of the quarks within the hadrons. Quarks and gluons can only exist inside a colorless bound state. Such colorless bound state of quarks and gluons are called “hadrons”. Based on the number of quarks contained, hadrons are further categorized into “mesons” and “baryons”. The bound states of antiquark and quark are called mesons whereas three quark bound states of are referred to as baryons. SU(3) flavor is approximately realized as global symmetry of the hadrons, which is manifested through octet and decuplet arrangements of the baryons and octet of the mesons.

Although the Standard Model is very successful in describing the dynamics and interactions of the elementary particles, both quarks and leptons, it does so at high energy when the gauge couplings are weak and perturbative expansion is valid. However, at lower energies the couplings become large, courtesy asymptotic freedom, and perturbative treatment becomes inappropriate. The characteristic energy scale above which the quarks and gluons become relevant degrees of freedom in Standard Model is known as $\Lambda_{QCD} \approx 200$ MeV. Below this scale the gluons and quarks are bound or confined within the hadrons. Masses of hadrons range from below Λ_{QCD} to orders of magnitude above. At energies below Λ_{QCD} , the strong coupling is too large and these

hadronic states are, therefore, not accessible to the perturbative calculations. In this region non-perturbative technique like lattice gauge theory can be used to calculate various important physical properties, simplest of which is hadron masses.

1.0.1 Heavy hadrons

The three generations of quark content of Standard Model *i.e.* six flavors of quarks are commonly grouped into three light flavors u, d, s and three heavy quarks c, b, t .

$$\begin{pmatrix} m_u \approx 0.003 \text{ GeV} \\ m_d \approx 0.005 \text{ GeV} \\ m_s \approx 0.095 \text{ GeV} \end{pmatrix} \ll 1 \text{ GeV} \leq \begin{pmatrix} m_c \approx 1.30 \text{ GeV} \\ m_b \approx 4.18 \text{ GeV} \\ m_t \approx 173.20 \text{ GeV} \end{pmatrix} \quad (1.1)$$

Because of the large mass, top quark decays typically in $\sim 10^{-25}$ sec and consequently cannot form hadrons. The rest five quarks form bound states – hadrons. The lightest hadrons containing s, d, u quark-antiquark pairs are mostly pseudoscalar mesons like η 's, K 's and π 's in the mass range 1.00 GeV – 0.14 GeV, while the lightest vector meson ρ 's are ~ 0.77 GeV. The light baryons are made of three light valence quarks, the lightest being the Nucleons (~ 1.0 GeV) the bound state of uud and heaviest is the Ω ($sss \sim 1.67$ GeV). From these numbers it is obvious that the masses of the light constituent quarks accounts for only fractional percentages of the hadron masses, the majority contribution is from the nonlinear strong color interaction between quarks and gluons.

However, this fact is not exactly true for heavy hadrons. In heavy mesons like $J/\psi, \eta_c, \Upsilon, \eta_b$ etc, a major contribution in the masses comes from the rest mass of the heavy quarks. We find the mass differences between the vector and pseudoscalar light quarkonia is one order larger than the corresponding heavy quarkonia states. For

instance $m_\rho - m_\pi \approx 635$ MeV whereas $m_\Upsilon - m_{\eta_b} \approx 70$ MeV. This perhaps shows that the dynamics of heavy quarks in heavy quarkonia and light quarks in light quarkonia are very different. The heavy quarks, being heavy, moves slowly compared to the light quarks to the extent that they can essentially be considered as nonrelativistic in nature. This prompts us to study heavy quarks using effective theories and potential model calculations [4]. In heavy-light mesons like B, B_s , the heavy quark is even slower than heavy-heavy mesons.

The light hadron spectra, both meson and baryon ground states and resonances, have been extensively studied using lattice QCD and the underlying nonperturbative phenomena are well understood. Lattice QCD results together with the chiral perturbation theory for light hadrons have made substantial impact not only on phenomenology of hadron physics (decay constants, CKM elements, structure constants, form factors etc.) but also deeply influenced the associated experiments. Numbers from lattice QCD calculations now regularly appear in Particle Data Group (PDG) compilation. The same is also true for heavy mesons, both B and D systems, and charmed baryons, which have been studied on lattice extensively over the last few decades, see for example [5, 6]).

However, lattice study of heavy baryons with bottom quark(s) is relatively a recent pursuit. Only a few lattice investigations of heavy baryons containing one or more bottom quarks have been carried out. On the experimental side, a slew of low lying $J^P = 1/2^+$ bottom baryons, such as $\Lambda_b, \Sigma_b, \Xi'_b, \Omega_b$ and $J^P = 3/2^+$ bottom baryons, such as $\Xi_b(5945), \Sigma_b^*$ have made entries in PDG. Possibilities of discoveries of other $J^P = 3/2^+$ bottom baryons are rather high. Along with well established light qqq baryons, such as $\Delta^{++} (uuu)$ and $\Omega^- (sss)$, QCD predicts the existence of both $\Omega^{++} (ccc)$ and $\Omega^- (bbb)$. Neither of these heavy qqq baryons have been observed in experiment, of course, as of now. The discoveries of doubly charmed baryons

Ξ^+ (ccd) and Ξ^{++} (ccu) [7], have led to strong expectation of the existence of the QCD predicted doubly bottom baryon states. But observation of such doubly and triply bottom states have very high energy threshold and is beyond the reaches of the present experiments. In this situation lattice QCD certainly can provide necessary insights into the masses, mass splittings and other physical properties of such bottom baryons states from the first principle.

1.0.2 Tetraquarks

The multiquark hadronic states other than the mesons and baryons are relatively new entrants particularly in the heavy quark sector, although QCD has long hold the possibility of four and five quark colorless states. The signature of some of such states containing four or more quarks and/or antiquarks have been found in experiments [8, 9, 10, 11, 12]. Such states are characterized by J^{PC} quantum numbers that cannot be arrived at from quark model. However, existence of four quark heavy hadronic states $QQ\bar{q}\bar{q}$ and their stability in the infinite quark mass limit have been studied in [13, 14] which raised the possibility of existence of heavy four quark bound states below the $Q\bar{q} - Q\bar{q}$ threshold. Of late, the observations of $Z^-(4430, 1^+)$ of minimal quark content being $c\bar{c}d\bar{u}$ [9] and subsequently the 1^+ states like $Z_b(10610)$ and $Z'_b(10650)$, having minimal quark content of four quarks (containing a $b\bar{b}$ pair), are found to be a few MeV above the thresholds of $B^*\bar{B}(10604.6)$ and $B^*\bar{B}^*(10650.2)$ [8, 15], have been reported. The proximity of Z_b, Z'_b to the $B^*\bar{B}^*$ threshold values perhaps suggest molecular, instead of bound nature of the states. Lattice QCD is the most appropriate tool to employ to investigate such bound and/or molecular nature of the heavy tetraquark states not only to understand the above observed states but also to identify possible other bound tetraquark states, both 0^+ and 1^+ .

If QCD is able to describe the strong interaction perfectly then it should reproduce

the hadron masses and their resonance spectra from the first principle, nonperturbative though they are. Therefore, the formidable machinery of perturbation theory cannot be employed to explore the low energy regime of QCD, it requires truly non-perturbative techniques. Lattice gauge theory grew out of the works of Wilson [16], Polyakov [17] and Wegner [18] was formulated precisely to investigate the territories of nonperturbative phenomena. After the numerical studies of lattice gauge theory using Monte Carlo simulation by Creutz *et. al.* [19], the lattice techniques became the strongest contender to investigate nonperturbative behavior of field theories by combined use of analytical and numerical methods.

1.0.3 QCD in continuum space-time

Quantum field theory has emerged as a framework to describe fundamental interactions at the sub-nuclear level among the elementary particles. The idea of gauge interactions and principle of local gauge invariance in field theory play a central role in our understanding of physics of elementary particles. Quantum field theory can be employed in perturbative setup, as is done in QED and weak interaction, as well as in nonperturbative regime, such as in QCD. The underlying gauge group of QCD is $SU(3)_c$, and the Lagrangian obtained from the gauge principle gives

$$\mathcal{L}_{\text{QCD}} = \sum_f \bar{\psi}_f(x) (i\not{D} - m_f) \psi_f(x) - \frac{1}{4} F_a^{\mu\nu} F_{\mu\nu}^a \quad (1.2)$$

where f stands for the quark flavors. The quark fields $\psi(x)$ transform as $\mathbf{3}_c$ which denotes the fundamental representation of the color $SU(3)_c$ and the covariant derivative is defined as,

$$D_\mu = \partial_\mu - ig \frac{\lambda_a}{2} A_\mu^a(x) \quad (1.3)$$

where $a = 1, \dots, 8$ and λ_a being eight Gell-Mann matrices. The strength tensor $F_{\mu\nu}^a$ is given by

$$F_{\mu\nu}^a = \partial_\mu A_\nu^a - \partial_\nu A_\mu^a + g f^{abc} A_\mu^b A_\nu^c. \quad (1.4)$$

Under $SU(3)_c$ gauge transformation, the fermionic quark fields $\psi(x)$ and the gauge fields $A_\mu^a(x)$ transform as

$$\psi(x) \rightarrow G(x) \psi(x) \quad \text{and} \quad A_\mu(x) \rightarrow G(x) A_\mu(x) G^{-1}(x) - \frac{i}{g} G(x) \partial_\mu G^{-1}(x) \quad (1.5)$$

where $G(x) = \exp(-ig\alpha^a(x)\lambda^a/2)$. As a consequence of $SU(3)_c$ gauge group, the self interaction of the gauge fields $gf^{abc}A_\mu^bA_\nu^c$ in Eq. (1.4) is believed to be the reason for the asymptotic freedom and quark confinement in the QCD. The quantum theory of strong interaction is achieved through Feynman's path integral. The partition function of the quantum theory can be written as

$$\mathcal{Z} = \int \mathcal{D}A \mathcal{D}\bar{\psi} \mathcal{D}\psi \exp\left(i \int d^4x \mathcal{L}_{\text{QCD}}\right). \quad (1.6)$$

The physical quantities or observables required to describe properties of strong interaction, such as the resonance spectra, are calculated from the vacuum expectation value of relevant field operator by varying the fields near their classical configurations,

$$\langle \mathcal{O}[A, \bar{\psi}, \psi] \rangle = \frac{1}{\mathcal{Z}} \int \mathcal{D}A \mathcal{D}\bar{\psi} \mathcal{D}\psi \mathcal{O}[A, \bar{\psi}, \psi] \exp\left(i \int d^4x \mathcal{L}_{\text{QCD}}\right). \quad (1.7)$$

In the high energy or short distance region, asymptotic freedom renders the strong coupling α_s weak and, consequently, the perturbative expansion in the strong coupling has successfully yielded essentially all the known perturbative QCD phenomena in colliders. But for calculating the Feynman processes when the energy is rather low or distance is large, the perturbative expansion cannot be carried out as α_s gets larger.

Lattice offers a nonperturbative way to calculate QCD processes in this low energy region, which is where hadronic physics lie.

An additional aspect of any quantum field theory are the infinities that arise in the action $\int d^4x \mathcal{L}$, in Eq. 1.6, in the loops of physical processes in higher order. To extract sensible results, the quantum theory must be regulated to prevent it from running to infinities. Keeping in close ties with perturbation theory, programs like Pauli-Villars (employing momentum cut-off) and dimensional regularization are typically employed to regularize the infinities and renormalize the theory. Lattice gauge theory is a nonperturbative regularization scheme, framed on discrete space-time grid. The lattice spacing a , *i.e.* the distance between two discrete space-time points, provides the required ultraviolet cut-off $\sim 1/a$ to the field theory, while restricting the 4-momenta to the first Brillouin zone.

We can carry out lattice QCD calculations numerically on discrete space-time lattices, provided the lattice spacing is small enough to accommodate all of the relevant physical distance scales. For spectrum calculation, one particularly needs $am_q \ll 1$, where a is the lattice spacing and m_q is the mass of the quark under consideration. This condition is satisfied for the light quarks u, d, s , to an extent for c quark ($am_c \gtrsim 0.7$) but for b quark $am_b > 2$ at a lattice spacing $a = 0.12$ fm. Comparison of the heavy quarkonium masses to the radial excitation energies showed that velocities of the heavy quarks inside a hadron are very non-relativistic, *i.e.* $v^2 \sim 0.1$ for $b\bar{b}$ systems [20]. For bottom hadrons containing lighter valence quarks, the velocity of the bottom quark is even smaller. This fact allows us to study the dynamics of bottom quark using Nonrelativistic QCD (NRQCD) [21, 22]. The NRQCD, therefore, will remain action of choice for b quark until finer lattices with $am_b < 1$ become widely available. Hence, in our present work, for the heavy-light baryon systems we treated the b quark nonrelativistically with NRQCD action and the lighter $u/d, s$

and c quarks relativistically. We have used the relativistic Highly Improved Staggered Quark (HISQ) action [23] for the u/d , s and c quarks.

The first step in the lattice calculation of bottom baryons containing light quarks is the construction of the creation (or annihilation) operators for the baryons of intended quantum numbers. Constructing baryonic operators using HISQ quark is challenging because the Heavy Quark Effective Theory (HQET) [24] motivated operators $(l_1^T C \gamma_k l_2) Q$, where l_1, l_2 are lighter relativistic quarks and Q is the heavy bottom quark, make the baryonic two-point correlation function to vanish. We get around this problem by swapping one of the l quarks with Q .

In the next step, the bottom baryon or tetraquark propagators or two-point correlation functions are constructed using the NRQCD b quark propagator(s) and HISQ u/d , s , c quark propagators on three different lattice spacings. An important part of this step is the quark mass tuning, particularly for b , c and s . The b quark mass is tuned with a spin average mass of Υ and η_b particles using the *kinetic mass* of both Υ and η_b and comparing them to the modified experimental spin average masses of Υ and η_b . The c quark mass is tuned using the spin average of η_c and J/ψ experimental masses. The s quark mass is tuned to two different values, hypothetical η_s meson (689 MeV) and B_s meson (5366 MeV). The extraction of the masses of the bottom baryons and tetraquarks are calculated from the exponential falloff of two-point functions, *i.e.* correlators of the states with quantum numbers of interest. The hyperfine and other mass splittings of the baryons, and tetraquark bound and molecular states are obtained from the exponential falloff of the ratio of the associated correlators.

In this dissertation, we present a detailed report of our work on heavy bottom baryon and tetraquark spectroscopy. The general organization is, in this Chapter 1 we provide an overview of particle phenomenology with emphasis on heavy

hadrons, baryons and tetraquarks, and their underlying theory QCD. In the Chapter 2 we briefly review the formulation of lattice gauge theory highlighting the staggered fermion proposal whose improved version is used in this work and some of the numerical techniques. In this chapter we also introduced NRQCD action used for bottom quarks. In the following two Chapters 3, 4 and 5, we discuss at length our main work of this thesis viz. heavy baryon operator construction and their spectra and heavy tetraquark spectroscopy. Finally, we summarize our results in the context of contemporary research in the concluding Chapter 6.

Bibliography

- [1] M. Tanabashi *et al.* (Particle Data Group), Phys. Rev. D 98, 030001 (2018).
- [2] ATLAS Collaboration, G. Aad *et al.*, Phys.Lett. B716, 1 (2012), 1207.7214.
- [3] CMS Collaboration, S. Chatrchyan *et al.* Phys.Lett. B716, 30 (2012), 1207.7235.
- [4] E. Klempt, and J. M. Richard, Rev. Mod. Phys. 82, 1095 (2010)
- [5] R. J. Dowdall *et al.* Phys. Rev. D 85, 054509 (2012).
- [6] Eric B. Gregory *et al.* Phys. Rev. D 83, 014506 (2011).
- [7] M. Mattson *et al.* (SELEX Collaboration) Phys. Rev. Lett. 89, 112001 (2002)
- [8] A. Bondar *et al.* (Belle Collaboration), Phys. Rev. Lett. **108**, 122001 (2012).
- [9] R. Aaij *et al.* (LHCb Collaboration), Phys. Rev. Lett **112**, 222002 (2014).
- [10] R.F. Lebed, R.E. Mitchell and E.S. Swanson, Prog. Part. Nucl. Phys. **93**, 143 (2017).
- [11] A. Esposito, A. Pilloni and A.D. Polosa, Phys. Rep. **668**, 1 (2017).
- [12] S.L. Olsen, T. Skwarnicki and D. Zieminska, Rev. Mod. Phys. **90**, 015003 (2018).
- [13] A.V. Manohar and M.B. Wise, Nucl. Phys. **B399**, 17 (1993).

- [14] E.J. Eichten and C. Quigg, Phys. Rev Lett. **119**, 202002 (2017).
- [15] A.E. Bondar, A. Garmash, A.I. Milstein, R. Mizuk and M.B. Voloshin, Phys. Rev. D **84**, 054010 (2011).
- [16] K.G. Wilson, Phys. Rev. D10 (1974) 2445.
- [17] A. Polyakov, Phys. Lett. B59 (1975) 79.
- [18] F. Wegner, J. Math. Phys. 12 (1971) 2259.
- [19] M. Creutz, L. Jacobs and C. Rebbi, Phys. Rev. Lett. 42 (1979) 1390.
- [20] C.T.H.Davies, K.Hornbostel, G.P.Lepage, A.J.Lidsey, J.Shigemitsu, J.Sloan, Phys.Lett. B382 (1996) 131-137
- [21] G.P. Lepage, L. Magnea, C. Nakhleh, U. Magnea, and K. Hornbostel, Phys. Rev. D46, 4052 (1992).
- [22] B.A. Thacker and G.P. Lepage, Phys. Rev. D43, 196 (1991).
- [23] E. Follana, Q. Mason, C. Davies, K. Hornbostel, G.P. Lepage, J. Shigemitsu, H. Trotter, and K. Wong, Phys. Rev. D75, 054502 (2007).
- [24] J.G. Korner, M. Kramer, and D. Pirjol, Prog. Part. Nucl. Phys. 33, 787 (1994), Howard Georgi, Phys. Lett. B. Volume 240, Issues 34, 26 April 1990, Pages 447-450

Chapter 2

QCD on Lattice

Lattice gauge theory is presently a powerful tool to investigate the nonperturbative properties of quantum field theories, QCD in particular. Lattice is a nonperturbative regulator formulated on discrete space-time grid. Specifically, lattice formulation of QCD makes calculations of physical quantities in the low energy region possible. To transcribe a Minkowski 3 + 1 dimensional continuum field theory action on lattice, we go over to the Euclidean space-time with

$$\vec{x}^M \rightarrow \vec{x}^E, \quad x_0^M \rightarrow -i x_4^E \quad \text{hence,} \quad \partial_0^M \rightarrow i\partial_4^E \quad (2.1)$$

then discretize both space and time by setting the space-time coordinate x_μ to a set of integers n_μ ($x_\mu \equiv an_\mu$), where a is the *lattice constant* or *lattice spacing*. Later, we will interchangeably use x and n (omitting a in an_μ) to denote the space-time coordinates on lattice. Lattice spacing is the distance between two nearest discrete space-time points and is assumed to be the same in all four directions. It is technically considered as *isotropic* lattice, which is used throughout this work. Often it is imperative to have two different lattice spacings, one for the time direction and the other for the 3-space

direction, which is called *anisotropic lattice*. Either way, the nearest neighbor to the site n in the μ -direction is denoted by $n + a\hat{\mu}$. This amounts to replacing the derivatives with discrete differences and the integrals by sum over sites as shown below (for free theory) in Eq. (2.2).

$$\begin{aligned} \partial_\mu \phi(x) &\rightarrow a \Delta_\mu^+ \phi_n = (\phi_{n+a\hat{\mu}} - \phi_n) \quad \text{and} \quad a \Delta_\mu^- = (\phi_n - \phi_{n-a\hat{\mu}}) \\ S^{\text{cont}} &= \int d^4x \mathcal{L}^{\text{cont}} \rightarrow S^{\text{latt}} = a^4 \sum_x \mathcal{L}^{\text{latt}}, \end{aligned} \quad (2.2)$$

The discrete space-time lattice provides an ultraviolet cut-off ($\sim 1/a$) to the theory. To define a quantum theory on lattice, Feynman path integral quantization is employed. The theory is then defined by the partition function

$$Z = \int \mathcal{D}\phi \exp\left(-\frac{S^{\text{latt}}}{\hbar}\right) \quad (2.3)$$

and the expectation value of some observable Θ is calculated as,

$$\langle \Theta \rangle = \frac{1}{Z} \int \mathcal{D}\phi \Theta(\phi) \exp\left(-\frac{S^{\text{latt}}}{\hbar}\right), \quad (2.4)$$

where ϕ is a collection of fields and the measure $\mathcal{D}\phi = \prod d\phi$. The finite dimensional functional integrals are defined precisely on lattice and no infinities are encountered. A very good guide to basic formulation of lattice gauge theory can be found in [1, 2].

The generic continuum action for QCD in Euclidean space-time is

$$S_{\text{QCD}}^E[A, \psi, \bar{\psi}] = S_{\text{F}}[A, \psi, \bar{\psi}] + S_{\text{G}}[A] \quad (2.5)$$

where the pure gauge (gluon) and fermion (quark) parts respectively are

$$S_G[A] = \frac{1}{4} \int d^4x F_{\mu\nu}^B F_{\mu\nu}^B \quad (2.6)$$

$$S_F[A, \psi, \bar{\psi}] = \int d^4x \bar{\psi}(x) (\not{\partial} + ig\gamma_\mu A_\mu + m) \psi(x) \quad (2.7)$$

The $\psi(x)$ are the quark fields of mass m and $A_\mu(x) = A_\mu^B(x)\lambda^B/2$ where A_μ^B are the colored gauge fields. The field strength tensor $F_{\mu\nu}^B$ is therefore,

$$F_{\mu\nu}^B = \partial_\mu A_\nu^B - \partial_\nu A_\mu^B - gf_{BCD}A_\mu^C A_\nu^D \quad (2.8)$$

While going over to the lattice, the quark fields $\psi(x)$ are placed at each site *i.e.* space-time point of lattice, denoted as $\psi(n)$ and the gluon fields $U_\mu(n)$ are defined on the links between lattice sites,

$$U(n, n + a\hat{\mu}) \equiv U_\mu(n) = e^{igaA_\mu(n)} \quad (2.9)$$

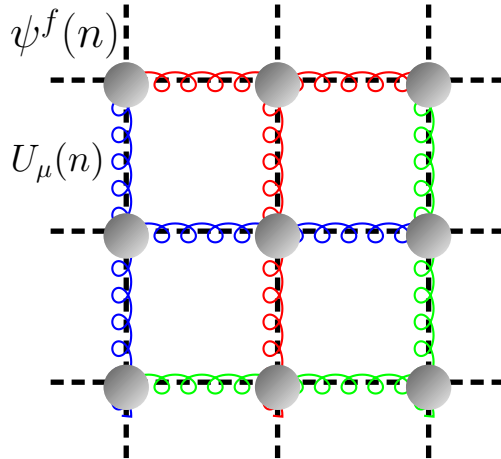


Figure 2.1: A graphic illustration of discrete space-time lattice with quark fields of flavor f on site n , $\psi^f(n)$ and the gluon fields $U_\mu(n)$ on the link between lattice sites n and $n + a\hat{\mu}$

Under the local $SU(3)_c$ gauge transformation, the gluon and quark fields, $U_\mu(n)$ and $\psi(n)$ respectively, transform as

$$\begin{aligned} U_\mu(n) &\rightarrow G(n) U_\mu(n) G^{-1}(n + \mu) \\ \psi(n) &\rightarrow G(n) \psi(n) \quad \text{and} \quad \bar{\psi}(n) \rightarrow \bar{\psi}(n) G^{-1}(n). \end{aligned} \quad (2.10)$$

which in the naive continuum limit boils down to the familiar form,

$$A_\mu(x) \rightarrow G(x) A_\mu(x) G^{-1}(x) - \frac{i}{g} G(x) \partial_\mu G^{-1}(x) \quad (2.11)$$

Once the lattice version of QCD action is obtained, expectation value of the operator Θ is given as,

$$\langle \Theta \rangle = \frac{1}{Z} \int \mathcal{D}U \mathcal{D}\psi \mathcal{D}\bar{\psi} \Theta(U, \psi, \bar{\psi}) \exp(-S_{\text{QCD}}^{\text{latt}}) \quad (2.12)$$

where $\mathcal{D}U = \prod_n dU(n)$ is the Harr measure. After the fermionic variables $\bar{\psi}$ and ψ are integrated out, the above equation becomes

$$\langle \Theta \rangle = \frac{1}{Z} \int \mathcal{D}U \Theta(U) \det[M(U)] \exp(-S_G^{\text{latt}}) \quad (2.13)$$

Here $M(U)$ is the quark propagator which is just the inverse of Dirac operator and S_G^{latt} is the lattice version of the gluon (gauge) action. Even for the small lattices, the number of variables to be integrated over to carry out the above integration becomes very large. In such a situation, the Monte Carlo simulation becomes the tool of choice. Monte Carlo steps approximate the above integral by the average of the observable calculated on N gauge configurations $\{U(n)\}$ generated with the

probability $P[U(n)] \propto \det[M(U)] \exp\{-S_G^{\text{latt}}(U(n))\}$

$$\langle \Theta \rangle \approx \frac{1}{N} \sum_n \Theta(U(n)). \quad (2.14)$$

2.1 Gauge action

The gauge fields defined as link variables $U_\mu(n)$ and the gauge transformation given by Eq. (2.10) imply that the trace of product of path ordered link variables around any closed loop is a gauge invariant object. The simplest of such a loop is the 1×1 elementary *plaquette*

$$U_{\mu\nu}(n) = U_\mu(n) U_\nu(n + \mu) U_\mu^\dagger(n + \nu) U_\nu^\dagger(n). \quad (2.15)$$

Building on this plaquette, Wilson proposed plaquette action for the pure $SU(3)_c$ gauge field action,

$$S_G = \frac{6}{g^2} \sum_n \sum_{\mu < \nu} \left[1 - \frac{1}{6} \text{Tr}(U_{\mu\nu}(n) + U_{\mu\nu}^\dagger(n)) \right] \quad (2.16)$$

The plaquette variable $U_{\mu\nu}$ and the Euclidean field strength tensor $F_{\mu\nu}$, up to $\mathcal{O}(a^2)$ are related as $U_{\mu\nu} = \exp(iga^2 F_{\mu\nu})$. In the continuum limit $a \rightarrow 0$, the gauge action S_G of Eq.(2.16) boils down to the familiar form

$$S_G = \frac{1}{4} \int d^4x \text{Tr} [F_{\mu\nu}(x) F_{\mu\nu}(x)] \quad (2.17)$$

Gauge action defined above in Eq. (2.16) has discretization error of $\mathcal{O}(a^2)$ which can be improved by adding more gauge invariant terms (such as *clover-leaf*) to the action. This improvement scheme will be discussed in the NRQCD action section.

2.2 Fermion action

The free fermion action for single flavor of mass m_f in Euclidean space-time is given by

$$S_F = \int d^4x \bar{\psi}(x) (\gamma_\mu \partial_\mu + m_f) \psi(x) \quad (2.18)$$

which is then transcribed on discrete space-time lattice. The lattice fermion action, in terms of dimensionless fermion fields $\hat{\psi}$, has the form

$$S_F = \sum_{n,m,\alpha,\beta} \bar{\hat{\psi}}_\alpha(n) K_{\alpha\beta}(n,m) \hat{\psi}_\beta(m) \quad (2.19)$$

where the matrix $K_{\alpha\beta}(n,m)$ is given by

$$K_{\alpha\beta}(n,m) = \sum_{\mu} \frac{1}{2} (\gamma_\mu)_{\alpha\beta} [\delta_{m,n+\hat{\mu}} - \delta_{m,n-\hat{\mu}}] + \hat{m}_f \delta_{\alpha\beta} \delta_{m,n} \quad (2.20)$$

The fermion propagator is obtained from the inverse of the matrix $K(n,m)$. The Fourier transformation of the fermion matrix to momentum space reveals a crucial property of the discretized fermion action.

$$K_{\alpha\beta}(n,m) = \int_{-\pi}^{\pi} \frac{d^4\hat{p}}{(2\pi)^4} \left[\sum_{\mu} i\gamma_\mu \sin(\hat{p}_\mu) + \hat{m}_f \right]_{\alpha\beta} e^{i\hat{p}\cdot(n-m)} \quad (2.21)$$

To arrive at the expression in Eq. (2.21), we made use of the property of Kronecker- δ ,

$$\delta_{mn} = \int_{-\pi}^{\pi} \frac{d\hat{p}}{2\pi} e^{i\hat{p}(n-m)}. \quad (2.22)$$

The Fourier transforms of the fermion matrix on lattice develops a periodic part in momentum space with periodicity 2π . Therefore, all the components of four momenta get restricted to the first Brillouin zone, $-\pi < \hat{p}_\mu \leq \pi$. From Eq. (2.21) it is evident

that not only the free fermion propagator has a pole at $\hat{p}_\mu = 0$ for $\hat{m}_f = 0$ but also at $\hat{p}_\mu = \pm\pi$, i.e. at the corners of Brillouin zone. So naive discretization of fermionic action leads to sixteen fermion states, fifteen of which have no continuum analog. This is the famous *fermion doubling* problem and the extra species of fermions are called doublers. Doubling turns out to be a general feature of the lattice fermions [3] and it underwent thorough investigations. Numerous solutions have been proposed by many authors including Wilson himself. His proposal was to add a term to the action such that it goes to zero in the continuum limit

$$S_F^W = S_F - \frac{r}{2} \sum_n \bar{\psi}(n) \hat{\square} \psi(n) \quad (2.23)$$

where r is the Wilson parameter, which for all practical purpose is taken as $r = 1$. The dimensionless lattice Laplacian $\hat{\square}$ is defined as

$$\hat{\square} \hat{\psi}_\alpha(n) = \sum_\mu [\hat{\psi}_\alpha(n + \hat{\mu}a) + \hat{\psi}_\alpha(n - \hat{\mu}a) - 2\hat{\psi}_\alpha(n)] \quad (2.24)$$

The kernel of the fermionic action becomes

$$K_{\alpha\beta}^W(n, m) = \int_{-\pi}^{\pi} \frac{d^4 \hat{p}}{(2\pi)^4} \left[\sum_\mu i\gamma_\mu \sin(\hat{p}_\mu) + \hat{m}_f + 2r \sum_\mu \sin^2\left(\frac{\hat{p}_\mu}{2}\right) \right]_{\alpha\beta} e^{i\hat{p} \cdot (n-m)} \quad (2.25)$$

The addition of this Wilson term amounts to change of the mass term as

$$m_f(p) = m_f + \frac{2r}{a} \sum_\mu \sin^2(p_\mu a/2) \quad (2.26)$$

which diverges as $a \rightarrow 0$. In the above equation, we used dimensioned parameters and the reason why we did this will be clear later. Setting $r = 1$, $p_1 = p_2 = p_3 = 0$ and $p_4 = iE$ (and dropping the indices and the label W) we find the pole of the Wilson

propagator to be

$$\begin{aligned}
& K(p)K(p)^\dagger = 0 \\
\Rightarrow & \sinh(Ea) = 1 + m_F a - \cosh(Ea) \\
\Rightarrow & E = \frac{1}{a} \ln(1 + m_f a) \\
\Rightarrow & \frac{m_f^{phys}}{m_f^{lat}} = 1 - \frac{m_f^{lat} a}{2} + \frac{m_f^{lat^2} a^2}{3} + \dots
\end{aligned} \tag{2.27}$$

As we set three momentum $\vec{p} = 0$ we substitute E by m_f^{phys} . From the above Eq. (2.27) we can see that in order to obtain m_f^{phys} we need $m_f^{lat} a \ll 1$. Though the Wilson term solves the doubling problem, it does so by breaking the chiral symmetry of the theory maximally even with $m_f = 0$. However, breaking of chiral symmetry and removal of doublers have a deeper connection which is summarized in terms of the well-known Nielsen-Ninomiya theorem. This theorem essentially implies that the doublers cannot be removed without sacrificing any of the desired properties of translational invariance, locality, hermiticity and chiral symmetry of the lattice action [3]. Among the other proposals, perhaps numerically the least demanding formalism is Kogut-Susskind or Staggered fermion [4]. In the staggered fermion formalism, the fermion fields (Dirac spinors) are spin diagonalized [5] and consequently numerically one order faster than the Wilson fermion. In the next section we discuss the Staggered fermion proposal in details because an improved form of this fermion, known as Highly Improved Staggered Fermion (HISQ), is employed in the present work for the light quarks.

2.2.1 Staggered fermions

The basic idea of the Staggered fermion method is to reduce the Brillouin zone by half through doubling the effective lattice spacing, thus eliminating some of the spurious fermionic degrees of freedom *i.e.* the doublers. This is achieved by distributing the doublers over the alternating lattice sites so that the lattice spacing effectively becomes $2a$. In Figure 2.2 we depicted the case of a 2-dimensional lattice. In an even d -dimensional space-time lattice, the gamma matrices have $2^{d/2}$ eigen vectors so only $2^{d/2}$ different species of fermions fields are needed to reduce the Brillouin zone by a factor of two. This is accomplished by the so-called *spin diagonalization* *i.e.* yielding one component staggered fermion fields $\chi(n), \bar{\chi}(n)$ rather than four component Dirac spinors $\hat{\psi}(n), \bar{\hat{\psi}}(n)$. These $2^{d/2}$ numbered fields are used as physical degrees of freedom. These remaining fermion degrees of freedom are called *tastes*, having poles only at $\hat{p}_\nu = 0$. The staggered fermions χ are defined through the Kawamoto-Smit transformation [5],

$$\hat{\psi}(n) = \Omega(n) \chi(n), \quad \bar{\hat{\psi}}(n) = \bar{\chi}(n) \Omega(n)^\dagger \quad (2.28)$$

$$\Omega(n) = \gamma_1^{n_1} \gamma_2^{n_2} \gamma_3^{n_3} \gamma_4^{n_4} \quad (2.29)$$

where $\Omega(n)$ are unitary 4×4 matrices which diagonalize the γ -matrices,

$$\Omega(n)^\dagger \gamma_\nu \Omega_{n+\nu} = \eta_\nu(n) \mathbf{1} \quad \text{where, } \eta_\nu(n) = (-1)^{n_1 + \dots + n_{\nu-1}} \quad \text{with } \eta_1(n) = 1. \quad (2.30)$$

Thus the space-time discretized free fermion action

$$S_F = \frac{1}{2} \sum_{n,\nu} \left[\bar{\hat{\psi}}(n) \gamma_\nu \hat{\psi}(n + \hat{\nu}) - \bar{\hat{\psi}}(n) \gamma_\nu \hat{\psi}(n - \hat{\nu}) \right] + \hat{m}_f \sum_n \bar{\hat{\psi}}(n) \hat{\psi}(n) \quad (2.31)$$

transforms to the Staggered fermion action of 1-component fermion fields, $\chi, \bar{\chi}$,

$$S_F^{\text{stag}} = \frac{1}{2} \sum_{n,\nu} \eta_\nu(n) [\bar{\chi}(n) \chi(n + \hat{\nu}) - \bar{\chi}(n) \chi(n - \hat{\nu})] + \hat{m}_f \sum_n \bar{\chi}(n) \chi(n). \quad (2.32)$$

The fermion action above in Eq. (2.32) no longer contains the gamma matrices, they are spin diagonalized.

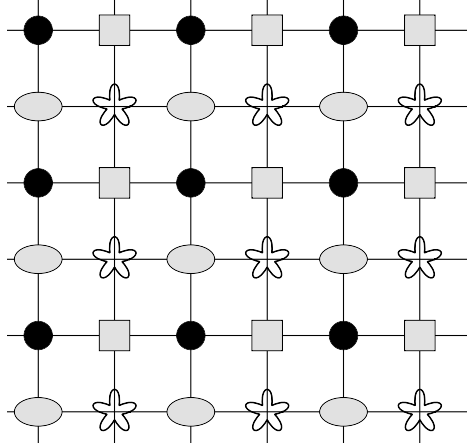


Figure 2.2: Distribution of fermionic degrees of freedom in two dimensional lattice.

Let us consider a hypercube with origin at $2N_\nu$, where N_ν are integers, then the coordinates of the sixteen ($2^d, d = 4$) corners are given by

$$n_\nu = 2N_\nu + s_\nu \quad (2.33)$$

where the components of s can take values either zero or one $s_\nu = 0, 1$. Now the sixteen sites of the hypercube are grouped together and the degrees of freedom sitting at those sixteen sites are interpreted as four species of fermions (say quarks), each of them having 4-component spinor. The relabeling of sites given in Eq.(2.33) suggests the following renaming of fermion fields

$$\chi(2N + s) \equiv \chi_s(N) \quad (2.34)$$

With this labeling of sites $\eta_\nu(n)$ becomes independent of N

$$\eta_\nu(n) = \eta_\nu(2N + s) = \eta_\nu(s) \quad (2.35)$$

Therefore the action becomes

$$S = \frac{1}{2} \sum_{N,s,\nu} \eta_\nu(s) \bar{\chi}(2N+s) [\chi(2N+s+\hat{\nu}) - \chi(2N+s-\hat{\nu})] + \hat{m}_f \sum_{N,s} \bar{\chi}(2N+s) \chi(2N+s) \quad (2.36)$$

First consider the term $\chi(2N + s + \hat{\nu})$, If $s + \hat{\nu}$ is a s type vector i.e. if it has components either zero or one, then $2N + s + \hat{\nu}$ labels sites within a hypercube with origin at $2N$. Hence $\chi(2N + s + \hat{\nu})$ can be relabeled as $\chi_{s+\hat{\nu}}(N)$. Similarly if $s + \hat{\nu}$ is not a s type vector then $s - \hat{\nu}$ is a vector of such type and we can rename $\chi(2N + s + \hat{\nu}) = \chi_{s-\hat{\nu}}(N + \hat{\nu})$. So we can write

$$\chi(2N + s + \hat{\nu}) = \sum_{s'} [\delta_{s+\hat{\nu},s'} \chi_{s'}(N) + \delta_{s-\hat{\nu},s'} \chi_{s'}(N + \hat{\nu})] \quad (2.37)$$

Here s' is a vector having components either zero or one. Similarly $\chi(2N + s - \hat{\nu})$ can be written as

$$\chi(2N + s - \hat{\nu}) = \sum_{s'} [\delta_{s-\hat{\nu},s'} \chi_{s'}(N) + \delta_{s+\hat{\nu},s'} \chi_{s'}(N - \hat{\nu})] \quad (2.38)$$

So the action becomes

$$\begin{aligned} S &= \frac{1}{2} \sum_{N,s,s',\nu} \eta_\nu(s) \bar{\chi}_s(N) [\delta_{s+\hat{\nu},s'} \{\chi_{s'}(N) - \chi_{s'}(N - \hat{\nu})\} \\ &\quad + \delta_{s-\hat{\nu},s'} \{\chi_{s'}(N + \hat{\nu}) - \chi_{s'}(N)\}] + \hat{m}_f \sum_{N,s} \bar{\chi}_s(N) \chi_s(N) \end{aligned} \quad (2.39)$$

Terms in the curly brackets are analogous to left and right block derivatives. Defining

the Fourier transformation of the fields as

$$\begin{aligned}\chi_s(N) &= \int_{-\pi}^{\pi} \frac{d^4 \hat{p}}{(2\pi)^4} \tilde{\chi}_s(\hat{p}) e^{i\hat{p}\cdot N} \\ \bar{\chi}_s(N) &= \int_{-\pi}^{\pi} \frac{d^4 \hat{p}}{(2\pi)^4} \tilde{\bar{\chi}}_s(\hat{p}) e^{-i\hat{p}\cdot N}\end{aligned}\quad (2.40)$$

we get

$$S = \sum_{s,s'} \int_{-\pi}^{\pi} \frac{d^4 \hat{p}}{(2\pi)^4} \tilde{\bar{\chi}}_s(\hat{p}) K_{ss'}(\hat{p}) \tilde{\chi}_{s'}(\hat{p}) \quad (2.41)$$

where

$$K_{ss'}(\hat{p}) = \sum_{\nu} i\Gamma_{ss'}^{\nu}(\hat{p}) \sin(\hat{p}_{\nu}/2) + \hat{m}_f \delta_{ss'} \quad (2.42)$$

$$\Gamma_{ss'}^{\nu}(\hat{p}) = \eta_{\nu}(s) e^{i\hat{p}\cdot(s-s')/2} [\delta_{s+\hat{\nu},s'} + \delta_{s-\hat{\nu},s'}] \quad (2.43)$$

The inverse of the fermionic matrix Eq.(2.42) in momentum space becomes

$$K^{-1}(p) = \frac{-i \sum_{\nu} \Gamma^{\nu}(\hat{p}) \sin(\hat{p}_{\nu}/2) + \hat{m}_f}{\sum_{\nu} \sin^2(\hat{p}_{\nu}/2) + \hat{m}_f^2}, \quad (2.44)$$

Due to the presence of the factor 1/2 the staggered propagator does not have doubling problem. Coupling to the gauge fields $U_{\nu}(n)$ in a gauge invariant way is straight forward,

$$S_F^{\text{stag}} = \frac{1}{2} \sum_{n,\nu} \eta_{\nu}(n) [\bar{\chi}(n) U_{\nu}(n) \chi(n + \hat{\nu}) - \bar{\chi}(n) U_{\nu}^{\dagger}(n - \hat{\nu}) \chi(n - \hat{\nu})] + \hat{m} \sum_n \bar{\chi}(n) \chi(n) \quad (2.45)$$

The staggered action above in Eq. (2.45) suffers from several discretization errors, for example it has $O(a^2)$ error as well as errors coming from taste-changing effects. These errors are removed in the Highly Improved Staggered Quark (HISQ) formulation.

2.2.2 HISQ action

The HISQ action is defined through [6]

$$S^{\text{HISQ}} = \sum_n \bar{\psi}(n) (\gamma^\mu D_\mu^{\text{HISQ}} + m_f) \psi(n) \quad (2.46)$$

where ψ 's are 4-component Dirac spinors and

$$D_\mu^{\text{HISQ}} = \Delta_\mu(W) - \frac{a^2}{6} (1 + \epsilon) \Delta_\mu^3(X). \quad (2.47)$$

Here $W_\mu(n) = F_\mu^{\text{HISQ}} U_\mu(n)$ and $X_\mu(n) = \mathcal{U} F_\mu U_\mu(n)$. The F_μ^{HISQ} has the form

$$F_\mu^{\text{HISQ}} = \left(F_\mu - \sum_{\rho \neq \mu} \frac{a^2 (\delta_\rho)^2}{2} \right) \mathcal{U} F_\mu \quad (2.48)$$

The \mathcal{U} is the unitarizing operator, it unitarizes whatever it acts on, and F_μ is the smearing operator given by

$$F_\mu = \prod_{\rho \neq \mu} \left(1 + \frac{a^2 \delta_\rho^{(2)}}{4} \right). \quad (2.49)$$

The δ_ρ and $\delta_\rho^{(2)}$ in the Eqs. (2.48) and (2.49) are covariant first and second order derivatives. The second term of Eq. (2.47) removes $\mathcal{O}(a^2)$ discretization error. The doubly smeared operator F_μ^{HISQ} removes the taste-changing errors. Because HISQ action reduces $\mathcal{O}(\alpha_s a^2)$ discretization errors, it is well suited for c , s and u/d quarks. The parameter ϵ in the coefficient of Naik term can be tuned appropriately to use the action for c quark. For s and u/d quarks, the $\epsilon = 0$. The 1-component staggered action can be obtained in the usual way using the spin diagonalization of Eq. (2.29).

Propagators obtained from HISQ action have only one spin component. The full

4×4 spin structure can be regained by multiplying the propagators by Kawamoto-Smit multiplicative phase factor given in Eq. (2.29). Although the ϵ -parameter of the Naik term can be tuned appropriately to use HISQ action for c quarks, it can not be used for heavier b quarks. It is well known that in order to simulate b quark one needs $a \ll 1/m_b$, at the same time the length of the lattice should be larger than the de Broglie wavelength of the b quark. To achieve this one needs to work with lattice grids of size $\sim 80^4$. This requires enormous computing power untenable on today's computing facilities. This inability to describe b quarks using relativistic lattice actions calls for an alternative.

2.3 NRQCD action

It follows from the potential models [7] that the dynamics of b quarks in bottomonium states is rather nonrelativistic $v^2 \sim 0.1$, where v being the velocity of the b quarks in hadrons. This is also supported by the fact that the mass of Υ , $M_\Upsilon = 9460$ MeV whereas $2 \times m_b = 8360$ MeV in \overline{MS} scheme. These potential models have two disadvantages – firstly, they are nonlocal and secondly, in order to have sufficient accuracy one needs to increase the number of parameters which makes the models complex. On the other hand, on lattice one can use effective theories like Heavy Quark Effective Theory. HQET explores the infinite mass limit of Dirac theory *i.e.* the static limit. The expansion parameter for HQET is $1/M$, where M is the mass of heavy quark. Therefore, HQET is suitable for singly heavy hadrons *i.e.* hadrons having only one bottom quark / anti-quark. This leaves NRQCD the most suitable candidate to study bottom hadrons, mesons and baryons both. NRQCD explores the nonrelativistic limit of the Dirac action. The nonrelativistic expansion contains three energy scales - the mass of the b quark m_b , momentum of the b quark $m_b v$ and the

kinetic energy $m_b v^2$. In NRQCD, the rest mass term is excluded making $m_b v$ *i.e.* b quark momentum the highest energy scale of the theory. This allows one to simulate b quark with lattices having much larger lattice spacings compared to $1/m_b$. One of the major advantages of using NRQCD is that one can expand the Dirac Lagrangian up to any desired order in quark velocity v . Hence by adding more terms to the Hamiltonian, one can include relativistic corrections to any desired order. NRQCD has other advantages too, for example the quark field decouples from the anti-quark field and it uses a simple evolution equation and is free from the doubling problem.

The NRQCD Lagrangian can be found in analogy with the Lagrangian of non-relativistic QED *i.e.* NRQED. In what follows, we outline how one can construct NRQED Lagrangian and then upgrade it to NRQCD.

Non-relativistic limit of Dirac equation is reached using Foldy-Wouthuysen transformation [8]. Consider the Dirac equation of an electron in EM field (ϕ, \vec{A}) ,

$$H\psi = i \frac{\partial \psi}{\partial t} \quad \text{where, } H = \vec{\alpha} \cdot (\vec{p} - e\vec{A}) + e\phi + m\beta \quad (2.50)$$

where $\vec{\alpha}$ and β are the Dirac matrices that have their usual definitions in terms of γ matrices. The transformation

$$\psi' = e^{iS} \psi \quad \text{where, } S = -\frac{i}{2m} \beta \vec{\alpha} \cdot (\vec{p} - e\vec{A}) \quad (2.51)$$

changes the Dirac equation to $H'\psi' = i\partial\psi'/\partial t$, where

$$\begin{aligned} H' &= e^{iS} H e^{-iS} - i e^{iS} \frac{\partial e^{-iS}}{\partial t} \\ &= H + [S, H]i - [S, [S, H]]\frac{1}{2} - [S, [S, [S, H]]]\frac{i}{6} + \dots \\ &\quad - \dot{S} - \frac{i}{2}[S, \dot{S}] + \frac{1}{6}[S, [S, \dot{S}]] + \dots \end{aligned} \quad (2.52)$$

Defining $\theta = \vec{\alpha} \cdot (\vec{p} - e\vec{A})$, we have

$$S = -\frac{i}{2m}\beta\theta \quad \text{and} \quad \dot{S} = -\frac{i}{2m}\beta\dot{\theta} \quad (2.53)$$

The first term in H' then is,

$$\begin{aligned} i[S, H] &= \frac{1}{2m}[\beta\theta, H] = \frac{1}{2m}[\beta\theta, \theta + e\phi + m\beta] \\ &= \frac{\beta\theta^2}{m} + \frac{e\beta}{2m}[\theta, \phi] - \theta \end{aligned} \quad (2.54)$$

In the last line, we have used the fact that the θ anticommutes with β . The next few terms in H' , similarly, are

$$-\frac{1}{2}[S, [S, H]] = -\frac{\theta^3}{2m^2} - \frac{\beta\theta^2}{2m} - \frac{e}{8m^2}[\theta, [\theta, \phi]] \quad (2.55)$$

$$-\frac{i}{6}[S, [S, [S, H]]] = \frac{\theta^3}{6m^2} - \frac{\beta\theta^4}{6m^3} \quad (2.56)$$

$$\frac{i}{24}[S, [S, [S, [S, H]]]] = \frac{\beta\theta^4}{24m^3} + \frac{\theta^5}{24m^4} \quad (2.57)$$

and so on. Similarly, the terms with \dot{S} can be derived. Hence, under the Foldy-Wouthusyen transformation, the Hamiltonian H' corrected up to $\mathcal{O}(v^4/c^4)$ can be written as,

$$\begin{aligned} H' &= \beta \left(m + \frac{\theta^2}{2m} - \frac{\theta^4}{8m^3} \right) + e\phi - \frac{e}{8m^2}[\theta, [\theta, \phi]] \\ &\quad - \frac{i}{8m^2}[\theta, \dot{\theta}] + \frac{e\beta}{2m}[\theta, \phi] + i\beta \frac{\dot{\theta}}{2m} - \frac{\theta^3}{3m^2} \end{aligned} \quad (2.58)$$

The third, fourth and fifth term of the above Hamiltonian in Eq. (2.58) is off-diagonal and can be removed using suitable transformation. Remaining terms can be further

simplified by observing that

$$\begin{aligned}\theta^2 &= [\vec{\alpha} \cdot (\vec{p} - e\vec{A})][\vec{\alpha} \cdot (\vec{p} - e\vec{A})] \\ &= \begin{pmatrix} [\vec{\sigma} \cdot (\vec{p} - e\vec{A})]^2 & 0 \\ 0 & [\vec{\sigma} \cdot (\vec{p} - e\vec{A})]^2 \end{pmatrix}\end{aligned}\quad (2.59)$$

If we replace \vec{p} by its operator representation $-i\vec{\nabla}$, then the diagonal blocks of Eq. (2.59) becomes

$$[\vec{\sigma} \cdot (\vec{p} - e\vec{A})]^2 = \left[-\sum_j D_j^2 - e\vec{\sigma} \cdot \vec{B} \right]. \quad (2.60)$$

The D_j above is the covariant derivative given by $D_j = \partial_j - ieA_j$ and $\vec{B} = \vec{\nabla} \times \vec{A}$. In terms of (ϕ, \vec{A}) ,

$$e[\theta, \phi] = e\vec{\alpha} \cdot \vec{p}\phi \quad (2.61)$$

$$i\dot{\theta} = -ie\vec{\alpha} \cdot \dot{\vec{A}} \quad (2.62)$$

In Eq. (2.62) we have used $\dot{\vec{p}} = 0$. The above two expressions, when added, yield

$$e[\theta, \phi] + i\dot{\theta} = ie\vec{\alpha} \cdot \vec{E} \quad (2.63)$$

The Dirac matrices $\vec{\alpha}$ satisfy $\alpha_i\alpha_j = \delta_{ij} + i\epsilon_{ijk}\sigma_k$ and the i -th component of the curl

of \vec{E} is $(\vec{\nabla} \times \vec{E})_i = \epsilon_{ijk} \partial_j E_k$. The third and fourth term of Eq. (2.58) thus become

$$\begin{aligned}
-\frac{1}{8m^2}[\theta, ie \vec{\alpha} \cdot \vec{E}] &= -\frac{ie}{8m^2}[\vec{\alpha} \cdot (\vec{p} - e\vec{A}), \vec{\alpha} \cdot \vec{E}] \\
&= -\frac{ie}{8m^2} \left\{ \alpha_i (\vec{p} - e\vec{A})_i \alpha_j E_j - \alpha_j E_j \alpha_i (\vec{p} - e\vec{A})_i \right\} \\
&= -\frac{ie}{8m^2} \left\{ (\delta_{ij} + i \epsilon_{ijk} \sigma_k) (\vec{p} - e\vec{A})_i E_j - (\delta_{ji} + i \epsilon_{jik} \sigma_k) E_j (\vec{p} - e\vec{A})_i \right\} \\
&= -\frac{ie}{8m^2} \left\{ \delta_{ij} p_i E_j + i \vec{\sigma} \cdot [(\vec{p} - e\vec{A}) \times \vec{E}] - i \vec{\sigma} \cdot [\vec{E} \times (\vec{p} - e\vec{A})] \right\} \\
&= -\frac{e}{8m^2} \left\{ i \vec{\sigma} \cdot (\vec{D} \times \vec{E}) + \vec{\nabla} \cdot \vec{E} - i \vec{\sigma} \cdot (\vec{E} \times \vec{D}) \right\} \quad (2.64)
\end{aligned}$$

If we think of ψ' as a two two-component spinor

$$\psi' = \begin{pmatrix} u \\ v \end{pmatrix} \quad (2.65)$$

then we arrive at the NRQED Lagrangian

$$\begin{aligned}
i \frac{\partial u}{\partial t} &= \left[m - \frac{1}{2m} \sum_j D_j^2 - \frac{e}{2m} \vec{\sigma} \cdot \vec{B} - \frac{1}{8m^3} \left(\sum_j D_j^2 \right)^2 \right. \\
&\quad \left. + e\phi - \frac{e}{8m^2} \vec{\nabla} \cdot \vec{E} - \frac{ie}{8m^2} \vec{\sigma} \cdot (\vec{\nabla} \times \vec{E} - \vec{E} \times \vec{\nabla}) \right] u \quad (2.66)
\end{aligned}$$

The $i\partial/\partial t$ together with the D^2 (Laplacian) and $(m + e\phi)$ (potential) is just the Schrödinger equation. The remaining terms are the relativistic corrections of which $\vec{\nabla} \cdot \vec{E}$ is the well-known Darwin term.

For the NRQCD, let us write the Lagrangian to $\mathcal{O}(v^6/c^6)$ as

$$\mathcal{L}_{\text{NRQCD}} = \mathcal{L}_0 + \delta\mathcal{L}_{v^4} + \delta\mathcal{L}_{v^6} \quad (2.67)$$

Following the NRQED Lagrangian above in Eq. (2.66), we equate the \mathcal{L}_0 to the

Schrödinger lagrangian without the rest mass term.

$$\mathcal{L}_0 = \psi^\dagger \left(iD_0 + \frac{\vec{D}^2}{2m} \right) \psi \quad (2.68)$$

The implication of the absence of the rest mass in the Lagrangian is that the pole mass of the hadrons containing nonrelativistic quark(s) will not render their physical mass. The details of extracting heavy hadron mass from the pole mass will be discussed later in Chapter 4.

The extension to NRQCD to $\mathcal{O}(v^4/c^4)$ order almost mimic the NRQED terms of the same order with $\vec{\nabla} \rightarrow \vec{D}$,

$$\begin{aligned} \delta\mathcal{L}_{v^4} = & c_1 \frac{1}{8m^3} \psi^\dagger D^4 \psi + c_3 \frac{ie}{8m^2} \psi^\dagger \vec{\sigma} \cdot \left(\vec{D} \times \vec{E} - \vec{E} \times \vec{D} \right) \psi \\ & + c_2 \frac{g}{8m^2} \psi^\dagger \left(\vec{D} \cdot \vec{E} - \vec{E} \cdot \vec{D} \right) \psi + c_4 \frac{g}{2m} \psi^\dagger \vec{\sigma} \cdot \vec{B} \psi \end{aligned} \quad (2.69)$$

The coefficients c_1 through c_4 are equal to 1 at the tree level (as in NRQED Lagrangian). It is to note that the leading term in this order is the c_4 term which is $\propto 1/m$ and contribute significantly to hyperfine splitting among the hadrons. Tuning the c_4 is an important step in this work as this leads to correct hyperfine splittings among heavy baryons.

The $\mathcal{O}(v^6/c^6)$ terms in $\delta\mathcal{L}_{v^6}$ are obtained by using the power counting method keeping in mind the symmetries of the action, for details see [9].

$$\begin{aligned} \delta\mathcal{L}_{v^6} = & c_5 \frac{g}{m^3} \psi^\dagger \left\{ \vec{D}^2, \vec{\sigma} \cdot \vec{B} \right\} \psi + c_6 \frac{ig^2}{m^3} \psi^\dagger \left(\vec{\sigma} \cdot \vec{E} \times \vec{E} \right) \psi \\ & + c_7 \frac{ig}{m^4} \psi^\dagger \left\{ \vec{D}^2, \vec{\sigma} \cdot \left(\vec{D} \times \vec{E} - \vec{E} \times \vec{D} \right) \right\} \psi \end{aligned} \quad (2.70)$$

The coefficients c_5 through c_7 in the $\delta\mathcal{L}_{v^6}$ are obtained by considering suitable interactions of the original action in the non-relativistic limit. For example, c_7 can be

calculated from the interaction $T_E = \bar{\psi}(q)\gamma^0 g\phi(q-p)\psi(p)$. If we substitute $\psi(p)$ by the positive energy spinor

$$\psi(p) = \left(\frac{E_p + m}{2E_p}\right)^{\frac{1}{2}} \begin{bmatrix} u \\ \frac{\vec{\sigma}\cdot\vec{p}}{E_p+m}u \end{bmatrix}$$

in the expression of T_E , we get

$$\begin{aligned} T_E &= \sqrt{\frac{(E_p + m)(E_q + m)}{4E_p E_q}} \\ &\quad \times u^\dagger \left[1 + \frac{\vec{p}\cdot\vec{q} + i\vec{\sigma}\cdot(\vec{q}\times\vec{p})}{(E_q + m)(E_p + m)} \right] g\phi(q-p)u \\ &= V_E(p, q) + S_E(p, q) \end{aligned} \quad (2.71)$$

where $V_E(p, q)$ contains the σ dependent part of the above expression and $S_E(p, q)$ contains the rest. Written explicitly,

$$\begin{aligned} V_E(p, q) &= \frac{i u^\dagger \vec{\sigma}\cdot(\vec{q}\times\vec{p})g\phi(q-p)u}{\sqrt{(E_q + m)(E_p + m)4E_q E_p}} \\ &= \frac{i u^\dagger \vec{\sigma}\cdot(\vec{q}\times\vec{p})g\phi(q-p)u}{4m^2} \left(1 + \frac{p^2}{4m^2}\right)^{-\frac{1}{2}} \left(1 + \frac{q^2}{4m^2}\right)^{-\frac{1}{2}} \left(1 + \frac{p^2}{2m^2}\right)^{-\frac{1}{2}} \left(1 + \frac{q^2}{2m^2}\right)^{-\frac{1}{2}} \\ &= \frac{i u^\dagger \vec{\sigma}\cdot(\vec{q}\times\vec{p})g\phi(q-p)u}{4m^2} \left(1 - \frac{p^2}{8m^2} - \frac{q^2}{8m^2} - \frac{p^2}{4m^2} - \frac{q^2}{4m^2}\right) \\ &= \frac{i u^\dagger \vec{\sigma}\cdot(\vec{q}\times\vec{p})g\phi(q-p)u}{4m^2} \left(1 - \frac{3p^2}{8m^2} - \frac{3q^2}{8m^2}\right) \\ &= u^\dagger \vec{\sigma}\cdot(\vec{q}\times\vec{p})g\phi(q-p)u \left[\frac{i}{4m^2} - \frac{3i}{32m^4}(p^2 + q^2) \right] \end{aligned} \quad (2.72)$$

$$S_E(p, q) = \left[1 - \frac{(p-q)^2}{8m^3} \right] u^\dagger g\phi(q-p)u \quad (2.73)$$

Comparing the c_7 term in Eq. (2.70) with the $(p^2 + q^2)$ term in Eq. (2.72), we find $c_7 = \frac{3}{64}$. Additionally we can compare the first term in Eq. (2.72) with the c_3 in Eq. (2.69) and we find $c_3 = 1$. Similarly from Eq. (2.73) we get $c_2 = 1$. In the same way,

c_5 can be calculated from an interaction $T_B(p, q) = -g \bar{\psi}(q) \vec{\gamma} \cdot \vec{A}(q - p) \psi(p)$ which gives us $c_5 = \frac{1}{8}$. From the double scattering of quark off an external static electric field one can $c_6 = -\frac{1}{8}$ [9].

2.3.1 NRQCD on Lattice

NRQCD action on lattice is realized by replacing the Euclidean covariant derivatives in \mathcal{L}_0 , $\delta\mathcal{L}_{v^4}$ and $\delta\mathcal{L}_{v^6}$ in Eqs. (2.68), (2.69) and (2.70) with the lattice covariant derivatives. The discrete derivatives acting on the quark fields are,

$$\begin{aligned} a\Delta_\nu^+ \psi(x) &= U_\nu(x) \psi(x + a\hat{\nu}) - \psi(x) \\ a\Delta_\nu^- \psi(x) &= \psi(x) - U_\nu^\dagger(x - a\hat{\nu}) \psi(x - a\hat{\nu}) \end{aligned} \quad (2.74)$$

and that on the gauge fields are,

$$\begin{aligned} a\Delta_\rho^+ F_{\mu\nu}(x) &= U_\rho(x) F_{\mu\nu}(x + a\hat{\rho}) U_\rho^\dagger(x) - F_{\mu\nu}(x) \\ a\Delta_\rho^- F_{\mu\nu}(x) &= F_{\mu\nu}(x) - U_\rho^\dagger(x - a\hat{\rho}) F_{\mu\nu}(x) U_\rho(x - a\hat{\rho}) \end{aligned} \quad (2.75)$$

The Δ^+ and Δ^- above are the forward and backward derivatives respectively. We can define symmetric derivative Δ^\pm and the lattice Laplacian Δ^2 in terms of forward and backward derivatives as

$$\Delta^\pm \equiv \frac{1}{2} (\Delta^- + \Delta^+) \quad (2.76)$$

$$\Delta^2 \equiv \sum_k \Delta_k^- \Delta_k^+ = \sum_k \Delta_k^+ \Delta_k^- \quad (2.77)$$

2.3.2 $\mathcal{O}(a^4)$ Improvement

By Taylor expanding the Laplacian operator and the symmetric derivative, we can find their $\mathcal{O}(a^4)$ improved forms. This improved version of the lattice symmetric derivative and the Laplacian operator are respectively given by,

$$\begin{aligned}\tilde{\Delta}_k^\pm &= \Delta_k^\pm - \frac{a^2}{6} \Delta_k^+ \Delta_k^\pm \Delta_k^- \\ \tilde{\Delta}^2 &= \Delta^2 - \frac{a^2}{12} \sum_k [\Delta_k^+ \Delta_k^-]^2\end{aligned}\tag{2.78}$$

The next step is to improve the gauge fields to the same order. It is generally done by substituting the 1×1 Wilson plaquette action of Eq. (2.15) with the clover-leaf plaquette action. The clover-leaf plaquette is illustrated in the Fig. 2.3.

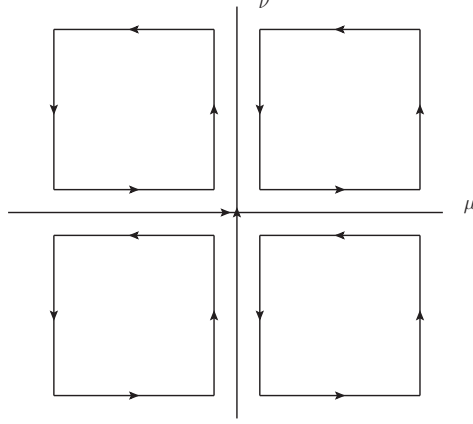


Figure 2.3: Clover operator in $\mu - \nu$ plane

In the Abelian gauge theory the clover-leaf plaquette amounts to

$$\begin{aligned}a^2 g F_{\mu\nu}^c(x) &= -\text{Im} \left(1 - \frac{ig}{4} \oint_{(2 \times 2)} A \cdot dy + \dots \right) \\ &= \frac{g}{4} \oint_{(2 \times 2)} (\partial_\mu A_\nu - \partial_\nu A_\mu) dy^\mu dy^\nu + \mathcal{O}(a^6) \\ &= a^2 g F_{\mu\nu}(x) + \frac{a^4}{6} (\partial_\mu^2 + \partial_\nu^2) g F_{\mu\nu}(x) + \mathcal{O}(a^6),\end{aligned}\tag{2.79}$$

where the surface integral is over the clover-leaf 2×2 plaquette in the (μ, ν) plane centered at x . The a^3 and a^5 terms in the Taylor expansion vanish because of the limits of the integrations. The non-Abelian generalization of the above leads to the gauge fields that are improved to $\mathcal{O}(a^4)$,

$$g\tilde{F}_{\mu\nu}(x) = gF_{\mu\nu}(x) - \frac{a^2}{6} [\Delta_\mu^+ \Delta_\mu^- + \Delta_\nu^+ \Delta_\nu^-] gF_{\mu\nu}(x). \quad (2.80)$$

2.3.3 NRQCD Propagator

The heavy quark propagators, which go in the two-point function for the calculation of heavy hadron propagators, are generated by the time evolution of the NRQCD Hamiltonian. The Lagrangian in Eq. (2.67) can be written as,

$$\mathcal{L} = \psi^\dagger(x, t) \Delta_4 \psi(x, t) + \psi^\dagger(x, t) H \psi(x, t) \quad (2.81)$$

In the above Eq. (2.81), the $H = H_0 + \delta H$ is the NRQCD Hamiltonian where,

$$H_0 = -\frac{\Delta^2}{2m_b} \quad \text{and} \quad \delta H = \sum_i \delta H^{(i)} \quad (2.82)$$

The H_0 is the leading $\mathcal{O}(v^2)$ term whereas the $\mathcal{O}(v^4)$ and $\mathcal{O}(v^6)$ terms with the coefficients c_1 through c_7 of Eqs. (2.69) and (2.70) are collected in δH . The Hamiltonian H contains only the spatial derivatives. The equation of motion corresponding to the ψ^\dagger is

$$U_t(\vec{x}, t)\psi(\vec{x}, t+a) - \psi(\vec{x}, t) + aH\psi(\vec{x}, t) = 0 \quad (2.83)$$

and the corresponding Green's function equation is

$$\begin{aligned}
& U_t(\vec{x}, t)G(\vec{x}, t + a; \vec{0}, 0) - (1 - aH)G(\vec{x}, t; \vec{0}, 0) = \delta_{\vec{x}, \vec{0}}\delta_{t, 0} \\
\Rightarrow & G(\vec{x}, t + a; \vec{0}, 0) = U_t^\dagger(\vec{x}, t)(1 - aH)G(\vec{x}, t; \vec{0}, 0)
\end{aligned} \tag{2.84}$$

In momentum space, the Green function in the Eq. (2.84) with H replaced by the leading order Hamiltonian H_0 takes the following form

$$G(\vec{p}, t + a; 0) = \left(1 - \sum_i \frac{4 \sin^2(\frac{p_i a}{2})}{2m_b a}\right) G(\vec{p}, t; 0) \tag{2.85}$$

At higher momenta $p_i \approx \pi/a$, the above equation reduces to the following form,

$$G(\vec{p}|_{p_i \approx \pi/a}, t + a; 0) = \left(1 - \frac{12}{2m_b a}\right) G(\vec{p}, t; 0). \tag{2.86}$$

which is unstable for $am_b < 3$. To avoid this numerical instability, a factor n is introduced to ensure numerical stability at small am_b which is achieved by replacing $(1 - aH_0)$ by $(1 - aH_0/n)^n$

$$G(\vec{x}, t + a; \vec{0}, 0) = U_t^\dagger(\vec{x}, t)(1 - aH_0/n)^n G(\vec{x}, t; \vec{0}, 0). \tag{2.87}$$

The requirement for numerical stability is now $am_b > 3/n$. This form of evolution equation was first used in [10]. However, instead of Eq. (2.87), if one uses the time reversal symmetric evolution equation

$$G(\vec{x}, t + a; \vec{0}, 0) = \left(1 - \frac{aH_0}{2n}\right)^n U_t^\dagger(\vec{x}, t) \left(1 - \frac{aH_0}{2n}\right)^n G(\vec{x}, t; \vec{0}, 0) \tag{2.88}$$

then it leads to smaller wave function renormalization [9]. Using (forward) lattice derivative in the evolution introduces $\mathcal{O}(a)$ error in the theory. To account for this error, an effective Hamiltonian is defined which, ignoring the gauge fields, is

$$G(\vec{x}, t + a; \vec{0}, 0) = \left(1 - \frac{aH_0}{2n}\right)^{2n} G(\vec{x}, t; \vec{0}, 0) = e^{-aH_{\text{eff}}} G(\vec{x}, t; \vec{0}, 0) \quad (2.89)$$

where we have defined

$$H_{\text{eff}} = -\frac{2n}{a} \ln \left(1 - \frac{aH_0}{2n}\right) = H_0 + \frac{a}{4n} H_0^2 + \dots \quad (2.90)$$

we can remove the $\mathcal{O}(a)$ error if H_0 is replaced by $H_0 - \frac{a}{4n} H_0^2$. Taking this into consideration, the final form of the evolution equation becomes

$$\begin{aligned} G(\vec{x}, t + 1; 0, 0) = & \\ & \left(1 - \frac{aH_0}{2n}\right)^n \left(1 - \frac{a\delta H}{2}\right) U_4(\vec{x}, t)^\dagger \times \\ & \left(1 - \frac{a\delta H}{2}\right) \left(1 - \frac{aH_0}{2n}\right)^n G(\vec{x}, t; 0, 0) \end{aligned} \quad (2.91)$$

where

$$G(\vec{x}, t; 0, 0) = \begin{cases} \delta_{\vec{x}, 0} & \text{for } t = 0 \\ 0 & \text{for } t < 0 \end{cases}$$

The modified NRQCD Hamiltonian which we used in this work is given by

$$H_0 = -\frac{\tilde{\Delta}^2}{2m_b} - \frac{a}{4n} \frac{(\Delta^2)^2}{4m_b^2} \quad \text{and} \quad \delta H = \sum_i \delta H^{(i)}. \quad (2.92)$$

Here, H_0 is the leading $\mathcal{O}(v^2)$ term while the $\mathcal{O}(v^4)$ and $\mathcal{O}(v^6)$ terms are assembled in δH with the coefficients c_1 through c_7 ,

$$\begin{aligned}
\delta H^{(1)} &= -c_1 \frac{(\Delta^2)^2}{8m_b^3} \\
\delta H^{(2)} &= c_2 \frac{ig}{8m_b^2} \left(\vec{\Delta}^\pm \cdot \vec{E} - \vec{E} \cdot \vec{\Delta}^\pm \right) \\
\delta H^{(3)} &= -c_3 \frac{g}{8m_b^2} \vec{\sigma} \cdot \left(\vec{\Delta}^\pm \times \vec{E} - \vec{E} \times \vec{\Delta}^\pm \right) \\
\delta H^{(4)} &= -c_4 \frac{g}{2m_b} \vec{\sigma} \cdot \vec{B} \\
\delta H^{(5)} &= -c_5 \frac{g}{8m_b^3} \left\{ \Delta^2, \vec{\sigma} \cdot \vec{B} \right\} \\
\delta H^{(6)} &= -c_6 \frac{3g}{64m_b^4} \left\{ \Delta^2, \vec{\sigma} \cdot \left(\vec{\Delta}^\pm \times \vec{E} - \vec{E} \times \vec{\Delta}^\pm \right) \right\} \\
\delta H^{(7)} &= -c_7 \frac{ig^2}{8m_b^3} \vec{\sigma} \cdot \vec{E} \times \vec{E}
\end{aligned} \tag{2.93}$$

$n > 3/2m_b$ is the requirement for the numerical stability of the equation of motion with the above modified NRQCD Hamiltonian.

Bibliography

- [1] H.J. Rothe, World Scientific Publishing Co. Pte. Ltd. Third edition, 2005.
- [2] Glattringer C., Lang C.B., Lect. Notes Phys. 788 (Springer, Berlin Heidelberg 2010),
- [3] H. B. Nielsen and M. Ninomiya, Nucl. Phys. B185 (1981) 20.
- [4] L. Susskind, Phys. Rev. D16, 3031 (1977).
- [5] N. Kawamoto and J. Smit, Nucl. Phys. B192, 100 (1981).
- [6] E. Follana, Q. Mason, C. Davies, K. Hornbostel, G. P. Lepage, J. Shigemitsu, H. Trotter, and K. Wong, Phys. Rev. D75, 054502 (2007).
- [7] G. S. Bali, K. Schilling, and A. Wachter, Phys. Rev. D56, 2566 (1997).
- [8] L.L. Foldy and S.A. Wouthusyen, Phys. Rev. 78, 29 (1950)
- [9] G.P. Lepage, L. Magnea, C. Nakhleh, U. Magnea, and K. Hornbostel, Phys. Rev. D46, 4052 (1992).
- [10] B.A. Thacker and G.P. Lepage, Phys. Rev. D43, 196 (1991).

Chapter 3

Heavy baryons on lattice

In QCD, the baryons are color contracted bound states of three quarks. Lattice QCD has been extensively employed to investigate the spectroscopy of baryons, both light and heavy, from the first principle. The lattice QCD results of light baryons and their resonance spectra over the last few decades have led to significant improvement in our understanding of quark dynamics inside the baryons and other hadronic physical properties not accessible to the models and perturbation theory [1]. The remarkable progress is largely due to improved actions, large volume simulations with physical quark masses, high statistics and control of systematic uncertainties.

The charm baryon spectroscopy became accessible to lattice QCD with availability of lattices with smaller spacings and theoretical developments in actions like Fermilab action [2] and HISQ [3], which allowed for using relativistic actions for the charm quark. The lattice results for charm baryons are found to be in very good agreement with the experimental results, particularly those coming from the LHCb. The impressive agreement between lattice estimates for $\Xi_{cc}(1/2^+)$ and that measured by LHCb is a case in point. This is a good indication that lattice QCD techniques can make reliable predictions in the heavy baryon sector. This encourages the lattice

community for serious exploration of the bottom quark sector.

For baryons containing bottom quark(s), many of the ground states are yet to be observed or discovered in experiments. In this context the lattice QCD calculation for such states becomes important in the sense that it can guide their future discoveries in experiments, the way it happened in the charm sector. The lattice simulations of bottom baryons have been on the forefront of research over the last several years. Rather recently there has been a spurt in discovery of low lying $J^P = 1/2^+$ as well as $3/2^+$ bottom baryons, such as Λ_b , Σ_b , Ξ'_b , Ω_b and $\Xi_b(5945)$, Σ_b^* having made entries in the PDG [4]. Possibilities of discoveries of other $J^P = 3/2^+$ bottom baryons are getting increasingly high. In this scenario, it is widely believed that lattice QCD can provide important insight into the masses, mass splittings and other properties of such bottom baryons. In this thesis, our primary goal is to determine the mass spectra of such heavy baryons containing one or more bottom quarks using NRQCD action for the bottom and relativistic HISQ action for the light charm, strange and up/down quarks.

Before we can compute bottom baryon spectra and their mass splittings we need operators to create and annihilate them. This is usually done taking clue from the quantum numbers of their continuum states. In this chapter, we discuss in details the construction of the baryonic operators using nonrelativistic heavy and relativistic light quarks and describe necessary strategy for numerical simulation.

3.1 Two-point functions

Baryons come in many combinations of quantum numbers such as flavor content, spin-parity etc. Therefore, the first step towards computing baryon masses is the construction of the creation / annihilation operators with the correct baryonic quan-

tum numbers followed by their correlation *i.e.* two-point functions or, in other word, baryon propagators. This two-point functions contains the information of the mass of the baryon and hence necessary for computing the spectra. For this purpose, we need to compute the quark propagators for both the heavy and light quarks on the gauge configurations. We combine these propagators suitably to obtain the baryon propagators. After performing averages over all gauge configurations, the masses of the heavy baryons are then calculated from the exponential fall-off of the two-point functions. Consider the following two-point function

$$C(t) = \sum_{\vec{z}} \langle \mathcal{O}_H(\vec{z}, t) \mathcal{O}_H(\vec{0}, 0)^\dagger \rangle \quad (3.1)$$

where \mathcal{O}_H is any generic lattice hadron operator. The Eq. (2.13) helps us to calculate the expectation value *i.e.* gauge averaged value of the two-point correlation function $C(t)$. For large t , below baryon decay threshold, we can write [5]

$$C(t) \underset{t \rightarrow \infty}{=} A e^{-Et} [1 + O(e^{-t\Delta E})] \quad (3.2)$$

Here E is the zero momentum energy of the lowest contributing state and ΔE is the energy difference to the first excited state. As the spatial coordinates are summed over, the above expression projects out the states with zero momentum. Thus E gives the mass of the hadron considered. Therefore, in the large t limit, the mass of the hadrons can be obtained as

$$M_{\text{eff}} = \ln \left[\frac{\text{Re}[C(t)]}{\text{Re}[C(t+1)]} \right] \quad (3.3)$$

often called *effective mass*. Apart from the zero momentum states, often one needs to simulate the energy of particles at different lattice momenta, particularly while

calculating the kinetic mass of Υ or η_b . In order to do that first consider Fourier transformation of a continuous function $f(x)$. The Fourier transformation to momentum space is given by

$$F(k) = \frac{1}{\sqrt{2\pi}} \int_{-\infty}^{\infty} f(x) e^{ikx} dx \quad (3.4)$$

However, when x takes discrete values $0, \pm a, \pm 2a, \dots$, the discrete version of the above transformation becomes

$$F(k) = \frac{a}{\sqrt{2\pi}} \sum_{n=-\infty}^{\infty} f(na) e^{ikna} \quad (3.5)$$

In practice, instead of taking infinitely long 1-D lattices, we take lattice of finite length Na and impose periodic (or anti-periodic) boundary condition. This leads to momentum taking discrete values $k_q = \frac{2\pi}{Na}q$ with $q = 0, 1, 2, \dots$ etc., which amounts to

$$F(k_q) = \frac{a}{\sqrt{2\pi}} \sum_{n=0}^N f(na) e^{i\frac{2\pi q}{N}n} \quad (3.6)$$

Therefore if we have a correlator $C(\vec{z}, t)$, then its value for a given momentum allowed in lattice can be obtained from

$$C(\vec{p}, t) = \mathcal{N} \sum_{\vec{z}} e^{i\vec{p}\cdot\vec{z}} C(\vec{z}, t) \quad (3.7)$$

where \mathcal{N} is normalization constant.

Heavy baryon spectroscopy requires a couple of additional steps before the mass can be calculated. They are the tuning of the bottom quark mass and the parameter c_4 of the NRQCD Hamiltonian 2.93 with the help of Υ and η_b bottomonium states and the corresponding hyperfine splitting respectively. Besides, we need appropriately tuned charm and strange quark masses to reproduce correctly the B_c and B_s states. Therefore, we start our discussion of operator construction with the light-light,

bottom-bottom and bottom-light meson states.

3.1.1 Light-light meson two-point function

For mesons having light quark and light antiquark, the corresponding interpolating operator is given as $\mathcal{O}_{l_1 l_2}(z) = \bar{l}^{f_1}(z)\Gamma l^{f_2}(z)$ with $\Gamma = \gamma_5, \gamma_4\gamma_5, \gamma_k, \gamma_4\gamma_k, \gamma_k\gamma_5$ and so on. Here $l^f(z)$ stands for the light quark field of flavor f , which can be any of up/down, strange and charm, and $\bar{l}(z) = l(z)^\dagger\gamma_4$.

This construction of mesonic operator is innately relativistic – $l^f(z)$ are the Dirac spinors and are solution of Dirac equation. In principle, bottom quark can also be included in $l^f(z)$, but the usefulness of the corresponding operator construction depends on lattice spacings of the gauge ensembles used. For currently available gauge configurations, am_b is greater than 1 and therefore needs to be treated differently. The nonrelativistic treatment for b quark has been discussed at length in the previous chapter and operators for bottom hadrons will be discussed in the later sections in this chapter. But for c quark, $am_c < 1$ for most of the available gauge configurations, particularly the publicly available MILC configurations. The charm quark is usually implemented using the Fermilab formulation [2]. Details regarding the use of relativistic action for charm will be discussed in the section of charm mass tuning in the next chapter.

Getting back to the meson operator $\mathcal{O}_{l_1 l_2}$, in order to evaluate the Euclidean correlator we need to find the corresponding $\mathcal{O}_{l_1 l_2}^\dagger(z)$ which creates the $\bar{l}^{f_1} l^{f_2}$ meson from the vacuum.

$$(\bar{l}^{f_1}\Gamma l^{f_2})^\dagger = -l^{f_2\dagger}\Gamma^\dagger\bar{l}^{f_1\dagger} = -\bar{l}^{f_2}\gamma_4\Gamma^\dagger\gamma_4 l^{f_1} = \pm\bar{l}^{f_2}\Gamma l^{f_1} \quad (3.8)$$

For any choice of Γ listed above, it satisfies $\gamma_4\Gamma^\dagger\gamma_4 = \pm\Gamma$. Different choices of Γ leads

to mesonic states having different spin-parity (J^P). For instance, $\Gamma = \gamma_5$ corresponds to $J^P = 0^-$ pseudoscalar mesons, $\Gamma = \gamma_k$ corresponds to $J^P = 1^-$ vector mesons and so on. Under parity transformation $l^f(z) \rightarrow \gamma_4 l^f(z)$, the pseudoscalar operator $\bar{l}^{f_1} \gamma_5 l^{f_2}$ changes as

$$\bar{l}^{f_1} \gamma_5 l^{f_2} \rightarrow \bar{l}^{f_1} \gamma_4 \gamma_5 \gamma_4 l^{f_2} = -\bar{l}^{f_1} \gamma_5 l^{f_2} \quad (3.9)$$

It follows from the Eq. (3.7) the two-point correlation function for light-light meson is

$$\begin{aligned} C_{l_1 l_2}(\vec{p}, t) &= \sum_{\vec{z}} \langle 0 | e^{i\vec{p}\cdot\vec{z}} \mathcal{O}_{l_1 l_2}(\vec{z}, t) \mathcal{O}_{l_1 l_2}^\dagger(\vec{0}, 0) | 0 \rangle \\ &= \sum_{\vec{z}} e^{i\vec{p}\cdot\vec{z}} \langle 0 | \bar{l}^{f_1}(\vec{z}, t) \Gamma l^{f_2}(\vec{z}, t) \bar{l}^{f_1}(\vec{0}, 0) \Gamma l^{f_1}(\vec{0}, 0) | 0 \rangle \\ &= \sum_{\vec{z}} e^{i\vec{p}\cdot\vec{z}} \langle 0 | \bar{l}_{c_1; s_1}^{f_1}(\vec{z}, t) \Gamma_{s_1, s_2} l_{c_1; s_2}^{f_2}(\vec{z}, t) \bar{l}_{c_2; s_3}^{f_1}(\vec{0}, 0) \Gamma_{s_3, s_4} l_{c_2; s_4}^{f_1}(\vec{0}, 0) | 0 \rangle \\ &= - \sum_{\vec{z}} e^{i\vec{p}\cdot\vec{z}} \left[M_{c_2, c_1; s_4, s_1}^{f_1}(0, z) \Gamma_{s_1, s_2} M_{c_1, c_2; s_2, s_3}^{f_2}(z, 0) \Gamma_{s_3, s_4} \right] \\ &= - \sum_{\vec{z}} e^{i\vec{p}\cdot\vec{z}} \text{Tr} \left[M^{f_1}(0, z) \Gamma M^{f_2}(z, 0) \Gamma \right] \\ &= - \sum_{\vec{z}} e^{i\vec{p}\cdot\vec{z}} \text{Tr} \left[\gamma_5 M^{f_1 \dagger}(z, 0) \gamma_5 \Gamma M^{f_2}(z, 0) \Gamma \right] \end{aligned} \quad (3.10)$$

Here c_1, c_2 are the color indices and s_1, s_2, s_3, s_4 are the spin indices. The light quark propagators are denoted by M and we have used $\gamma_5 M(z, 0) \gamma_5 = M^\dagger(0, z)$ [6], where z stands for $z = (\vec{z}, t)$. In the Eq. (3.10) and later in Eqs. (3.12), (3.13) and (3.16), the traces are taken over both the spin and color indices.

3.1.2 Bottom-bottom meson two-point function

The b quark, as discussed in the previous chapter, requires nonrelativistic treatment and this is done in the framework of NRQCD. In NRQCD, the upper and lower component of the Dirac field decouple and the b quark field becomes a two component

spinor. The heavy-heavy meson (often referred to as quarkonium) creation operator is then obtained by combining the two component quark and anti-quark creation operators ψ_h^\dagger and χ_h^\dagger [7, 8]. Since the antiquarks transform as $\bar{3}$ under color rotation, we rename the antiquark spinor as $\chi_h \equiv \chi_h^*$ [9]. The heavy quarkonium creation operator thus becomes,

$$\mathcal{O}_{hh}(z) = \psi_h^\dagger(z) \Gamma \chi_h(z). \quad (3.11)$$

where $\Gamma = I$ for the pseudoscalar and σ_i for vector mesons. Heavy-heavy, which in our case is bottom-bottom, meson two-point function is then given by [9, 11],

$$\begin{aligned} C_{hh}(\vec{p}, t) &= \sum_{\vec{z}} \langle 0 | e^{i\vec{p}\cdot\vec{z}} \mathcal{O}_{hh}^\dagger(z) \mathcal{O}_{hh}(0) | 0 \rangle \\ &= \sum_{\vec{z}} e^{i\vec{p}\cdot\vec{z}} \langle 0 | \chi^\dagger(z) \Gamma^\dagger \psi(z) \psi^\dagger(0) \Gamma \chi(0) | 0 \rangle \\ &= \sum_{\vec{z}} e^{i\vec{p}\cdot\vec{z}} \langle 0 | \chi_{c1;s1}^\dagger(z) \Gamma_{s1,s2}^\dagger \psi_{c1;s2}(z) \psi_{c2;s3}^\dagger(0) \Gamma_{s3,s4} \chi_{c2;s4}(0) | 0 \rangle \\ &= - \sum_{\vec{z}} e^{i\vec{p}\cdot\vec{z}} \langle 0 | \chi_{c2;s4}(0) \chi_{c1;s1}^\dagger(z) \Gamma_{s1,s2}^\dagger \psi_{c1;s2}(z) \psi_{c2;s3}^\dagger(0) \Gamma_{s3,s4} | 0 \rangle \\ &= - \sum_{\vec{z}} e^{i\vec{p}\cdot\vec{z}} \text{Tr} [G_\chi(0, z) \Gamma^\dagger G(z, 0) \Gamma] \\ &= \sum_{\vec{z}} e^{i\vec{p}\cdot\vec{z}} \text{Tr} [G^\dagger(z, 0) \Gamma^\dagger G(z, 0) \Gamma] \end{aligned} \quad (3.12)$$

Heavy quark propagator $G(z, 0)$ is 2×2 matrix in spin space and G_χ is heavy antiquark propagator which is the equal to the hermitian conjugate of quark propagator G , *i.e* $G_\chi(0, z) = -G^\dagger(z, 0)$ [9]. If we think $G(z, 0)$ as a 4×4 matrix with vanishing lower components then we can rewrite the above Eq. (3.12) as [10]

$$C_{hh}(\vec{p}, t) = \sum_{\vec{z}} e^{i\vec{p}\cdot\vec{z}} \text{Tr} [\gamma_5 G^\dagger(z, 0) \gamma_5 \Gamma^\dagger G(z, 0) \Gamma] \quad (3.13)$$

where the Γ matrix now replaces I and σ_i with γ_5 and γ_i for pseudoscalar and vector mesons respectively.

3.1.3 Heavy-light meson two-point function

The bottom quark field ψ_h has only two spin components, as discussed before. However, to combine it with a 4-component spinor field *i.e.* with the relativistic lighter quarks, the ψ_h is converted to a 4-component spinor Q having vanishing lower components,

$$Q = \begin{pmatrix} \psi_h \\ 0 \end{pmatrix} \quad (3.14)$$

With this definition of heavy *i.e.* bottom quark field Q we can combine the b and light quark fields in the usual way,

$$\mathcal{O}_{hl}(x) = \bar{Q}(x) \Gamma l(x) \quad (3.15)$$

where $\bar{Q} = Q^\dagger \gamma_4$ and depending on pseudoscalar and vector mesons $\Gamma = \gamma_5$ and γ_k respectively. In passing we note that in the Dirac representation of gamma matrices $\gamma_4 Q = Q$. Following the steps used to arrive at Eq. (3.8), we obtain the hermitian conjugate of the $\mathcal{O}_{hl}(x)$, which is $\mathcal{O}_{hl}^\dagger(x) = \bar{l}(x) \Gamma Q(x)$. The bottom-light two-point

function is therefore [12, 13],

$$\begin{aligned}
C_{hl}(t) &= \sum_{\vec{x}} \langle 0 | e^{i\vec{p}\cdot\vec{x}} \mathcal{O}_{hl}^\dagger(x) \mathcal{O}_{hl}(0) | 0 \rangle \\
&= \sum_{\vec{x}} e^{i\vec{p}\cdot\vec{x}} \langle 0 | \bar{l}_{c1;s1}(x) \Gamma_{s1;s2} Q_{c1;s2}(x) \bar{Q}_{c2;s3}(0) \Gamma_{s3;s4} l_{c2;s4}(0) | 0 \rangle \\
&= - \sum_{\vec{x}} e^{i\vec{p}\cdot\vec{x}} \langle 0 | l_{c2;s4}(0) \bar{l}_{c1;s1}(x) \Gamma_{s1;s2} Q_{c1;s2}(x) \bar{Q}_{c2;s3}(0) \Gamma_{s3;s4} | 0 \rangle \\
&= - \sum_{\vec{x}} e^{i\vec{p}\cdot\vec{x}} [M_{s4,s1}^{c2,c1}(0,x) \Gamma_{s1;s2} G_{s2,s3}^{c1,c2}(x,0) \Gamma_{s3,s4}] \\
&= - \sum_{\vec{x}} e^{i\vec{p}\cdot\vec{x}} \text{Tr} [M(0,x) \Gamma G(x,0) \Gamma] \\
&= - \sum_{\vec{x}} e^{i\vec{p}\cdot\vec{x}} \text{Tr} [\gamma_5 M^\dagger(x,0) \gamma_5 \Gamma G(x,0) \Gamma] \tag{3.16}
\end{aligned}$$

In the above expression, $M(x,0)$ is the usual light quark propagator having full 4×4 spin structure. As before, $G(x,0)$ is the b quark propagator having vanishing lower components. To avoid repetition of steps, here we omitted the explicit spin and color indices while deriving the Eq. (3.16).

For the numerical implementation of the operators with heavy quarks, we have to keep in mind that NRQCD uses Dirac representation of gamma matrices but the MILC library suit, that we use for the implementation of the HISQ light quarks, uses a MILC-Weyl representation of gamma matrices. These two representations of gamma matrices are related by the unitary transformation of the form

$$S \gamma_\mu^{\text{MILC}} S^\dagger = \gamma_\mu^{\text{NR}} \quad \text{where,} \quad S = \frac{1}{\sqrt{2}} \begin{pmatrix} \sigma_y & \sigma_y \\ -\sigma_y & \sigma_y \end{pmatrix} \tag{3.17}$$

Therefore, it is imperative to rotate $G(x,0)$ to the MILC basis before implementing the Eq. (3.16).

3.1.4 Bottom baryon two-point function

Before addressing the problem of heavy baryon operators, we discuss briefly the construction of local baryon operators for light quarks for use in lattice QCD. The discussion has been given in details in Appendix B. Baryons are half-integer spin particles, therefore they are fermions and have spinor index. Based on the spin-parity of the baryon that we are after, in the first step we combine the two light quarks into a Lorentz scalar, pseudoscalar, vector or pseudovector

$$l^{f_1 T}(x) \Gamma l^{f_2}(x) \quad \text{for } \Gamma = C, C\gamma_5, C\gamma_\mu, C\gamma_\mu\gamma_5 \quad (3.18)$$

respectively and $C = \gamma_4\gamma_2$. This 2-quark part of the baryon operator is customarily called *diquark*. Next add the third light quark and the operator becomes, showing explicitly the color and spinor indices,

$$\mathcal{B}(x) = \epsilon_{abc} \left(l_{a\alpha}^{f_1}(x) \Gamma_{\alpha\beta} l_{b\beta}^{f_2}(x) \right) l_{c\gamma}^{f_3}(x) \quad (3.19)$$

For instance, the well-known Nucleon ($I = 1/2$) spin-1/2 operator is

$$\mathcal{N}(x) = \epsilon_{abc} \left(u_{a\alpha}(x) (C\gamma_5)_{\alpha\beta} d_{b\beta}(x) \right) u_{c\gamma}(x) \quad (3.20)$$

Here α, β, γ are the spinor indices and a, b, c are the color indices. A typical Δ ($I = 3/2$) operator, according to the above prescription is

$$\Delta(x) = \epsilon_{abc} \left(u_{a\alpha}(x) (C\gamma_i)_{\alpha\beta} u_{b\beta}(x) \right) u_{c\gamma}(x). \quad (3.21)$$

But, the above Δ operator corresponds to a mixed spin-1/2 as well as spin-3/2 state and the individual spin states are required to be projected out. More on this spin

projection will be discussed later in the context of heavy baryon. In our present discussion, we are interested only in the spin-1/2 and 3/2 heavy baryons containing one or more b quark(s). Defining the b field in Eq. (3.14), we now proceed to construct the operators for the bottom baryons.

First we highlight a couple of complication involved in the construction of the two-point functions for bottom baryons.

1. Since the heavy quark field Q has vanishing lower components it can be projected to positive parity states only.
2. Beacuse of Pauli exclusion principle, we cannot insert $C\gamma_5$ in a diquark made from same flavor *i.e.* $l^T C\gamma_5 l$. This is because the diquark operator thus defined creates a combination which is antisymmetric in spin indices, while the presence of ϵ_{abc} also makes the combination antisymmetric in color indices. This amounts to an operator becoming overall symmetric under the interchange of the same flavored quark fields.

With these points in mind, we construct bottom baryon operators as described in the following subsections.

3.1.5 Triply bottom baryon

The baryonic states of three identically flavored quarks Ω_{qqq} have been well studied on lattice for both $q = s$ and c , although Ω_{ccc} is yet to be discovered. For the Ω_{bbb} state we are no where near any experimental signature, but is studied on lattice because of its potential importance in phenomenology. The operator for the baryon with 3 bottom quarks is defined as

$$(\mathcal{O}_k^{hhh})_\alpha = \epsilon_{abc} (Q^{aT} C\gamma_k Q^b) Q_\alpha^c \quad (3.22)$$

Here k is the Lorentz index which runs from 1 to 3. The hermitian conjugate of \mathcal{O}_k^{hhh} is given by

$$(\mathcal{O}_k^{hhh})^\dagger_\delta = \epsilon_{fgh} \bar{Q}_\delta^h \bar{Q}_\rho^g (\gamma_k \gamma_2)_{\rho\sigma} \bar{Q}_\sigma^f \quad (3.23)$$

Here we have used $\bar{Q} = Q^\dagger \gamma_4 = Q^\dagger$ and have ignored the overall negative sign because we will eventually consider the absolute value of the correlation functions in our simulation. The zero momentum two-point function becomes,

$$\begin{aligned} C_{jk;\alpha\delta}^{hhh}(t) &= \sum_{\vec{z}} \langle 0 | [\mathcal{O}_j^{hhh}(z)]_\alpha [\mathcal{O}_k^{hhh}(0)]^\dagger_\delta | 0 \rangle \\ &= \sum_{\vec{z}} \epsilon_{abc} \epsilon_{fgh} \langle 0 | Q_\mu^a(z) (C\gamma_j)_{\mu\nu} Q_\nu^b(z) Q_\alpha^c(z) \bar{Q}_\delta^h(0) \bar{Q}_\rho^g(0) (\gamma_k \gamma_2)_{\rho\sigma} \bar{Q}_\sigma^f(0) | 0 \rangle \\ &= \sum_{\vec{z}} \epsilon_{abc} \epsilon_{fgh} G_{\alpha\delta}^{ch}(z, 0) (C\gamma_j)_{\mu\nu} G_{\nu\rho}^{bg}(z, 0) (\gamma_k \gamma_2)_{\rho\sigma} G_{\mu\sigma}^{af}(z, 0) \\ &= \sum_{\vec{z}} \epsilon_{abc} \epsilon_{fgh} G_{\alpha\delta}^{ch}(z, 0) \times \text{Tr} \left[C\gamma_j G^{bg}(z, 0) \gamma_k \gamma_2 G^{afT}(z, 0) \right] \end{aligned} \quad (3.24)$$

In the above Eq. (3.24) and the subsequent ones, the transpose and traces are taken over the spin indices. Baryon operators having $C\gamma_k$ in the diquark part have overlap with both spin-3/2 and 1/2 states. For example, correlator given in Eq. (3.24) can be written explicitly as an overlap of both spin-1/2 and 3/2 states [14],

$$C_{ij}^{hhh}(t) = Z_{3/2}^2 e^{-E_{3/2}t} \Pi P_{ij}^{3/2} + Z_{1/2}^2 e^{-E_{1/2}t} \Pi P_{ij}^{1/2} \quad (3.25)$$

with $\Pi = (1 + \gamma_4)/2$ and $P_{ij}^{1/2} = \gamma_i \gamma_j / 3$ and $P_{ij}^{3/2} = \delta_{ij} - \gamma_i \gamma_j / 3$ are the spin projection operator for spin-1/2 and 3/2 respectively. The individual contribution to the respective spin states can be obtained by taking appropriate projections,

$$\begin{aligned} P_{ij}^{1/2} C_{jk}^{hhh} &= Z_{1/2}^2 \Pi e^{-E_{1/2}t} P_{ik}^{1/2} \\ P_{ij}^{3/2} C_{jk}^{hhh} &= Z_{3/2}^2 \Pi e^{-E_{3/2}t} P_{ik}^{3/2} \end{aligned} \quad (3.26)$$

These projection operators are used to separate the different spin states. The spin-1/2 state of triply bottom baryon, however, is not a physical state as it violates Pauli exclusion principle even though, in practice, we can take the projection anyway and get non-zero correlation function.

3.1.6 Bottom-light-light baryon

The bottom-light-light baryons (hll) have the most promising experimental signatures and some like Λ_b (5620, $1/2^+$), Σ_b (5810, $1/2^+$), Ω_b (6046, $1/2^+$) and a couple more have entered PDG database. It is, therefore, absolutely imperative for the heavy baryon lattice calculations to capture these states with enough precision for confident exploration and extension into the multi-bottom sector. Because of presence of multiple light quarks, different relativistic actions like clover, overlap, twisted mass, staggered etc. are needed to be explored to gain understanding and control of the systematics. In this thesis, we chose to use HISQ (highly improved staggered quark) action for the light quarks u/d and s including c .

Using staggered quark for constructing baryons brings its own problem, which we see below. The natural choice for (hll) baryon interpolating operator is motivated by the Heavy Quark Effective Theory (HQET) [15]. The Lagrangian of HQET is obtained by going to the infinite mass limit of the Dirac Lagrangian by replacing Q with $\frac{1 + \gamma_0}{2} Q$

$$\mathcal{L}_{\text{QCD}} = \bar{Q} (i\gamma^\mu D_\mu - m_Q) Q \Rightarrow \mathcal{L} = \bar{Q} (iD_0 - m_Q) Q \quad (3.27)$$

The Eq.(3.27) represents the Lagrangian of a static heavy quark. Generalization of

the above formula is obtained by making the following transformation

$$Q = \frac{1 + \not{v}}{2} e^{-imv_\mu x^\mu} h_v + O(1/m_Q) \quad (3.28)$$

where h_v is the heavy quark field which satisfies $\not{v}.h_v = h_v$ and v being velocity of the bound state containing the heavy quark. The basic assumption here is that a heavy quark bound inside a hadron moves more or less with the hadron's velocity v . The momentum of the heavy quark is defined as

$$p_Q^\mu = m_Q v^\mu + k^\mu \quad (3.29)$$

where k is called the residual momentum and its components are much smaller than m_Q . Upon substitution of Eq.(3.28) we get the zeroth $O(1/M)$ order HQET Lagrangian

$$\mathcal{L}_{\text{HQET}} = i\bar{h}_v v^\mu D_\mu h_v \quad (3.30)$$

The above HQET Lagrangian $\mathcal{L}_{\text{HQET}}$ is invariant under the transformation

$$h_v \rightarrow \exp\left(\frac{i}{2}\vec{\Sigma} \cdot \vec{n}\theta\right) h_v \quad (3.31)$$

where $\vec{\Sigma}$ is the spin operator defined as

$$\vec{\Sigma} = \begin{pmatrix} \vec{\sigma} & 0 \\ 0 & \vec{\sigma} \end{pmatrix}$$

and \vec{n}, θ are the rotation axis and the rotation angle respectively. The above symmetry Eq.(3.31) implies that in the infinite mass limit the heavy quark becomes insensitive to the spin orientation of the light quark(s). So the natural choice of

interpolating operator for hll -baryon kind is

$$(\mathcal{O}_k^{l_1 l_2 h})_\alpha = \epsilon_{abc} (l_1^{aT} C \gamma_k l_2^b) Q_\alpha^c \quad (3.32)$$

The hermitian conjugate of $\mathcal{O}_k^{l_1 l_2 h}$ is given by

$$\begin{aligned} (\mathcal{O}_k^{l_1 l_2 h})_\delta^\dagger &= \epsilon_{fgh} \bar{Q}_\delta^h \left[l_2^{g\dagger} (C \gamma_k)^\dagger (l_1^{f\dagger})^T \right] \\ &= \epsilon_{fgh} \bar{Q}_\delta^h \left[l_2^{g\dagger} \gamma_k \gamma_2 \gamma_4 (l_1^{f\dagger})^T \right] \\ &= \epsilon_{fgh} \bar{Q}_\delta^h \left[\bar{l}_2^g \gamma_4 \gamma_k \gamma_2 (l_1^f)^\dagger \gamma_4 \right]^T \\ &= \epsilon_{fgh} \bar{Q}_\delta^h \left[\bar{l}_2^g \gamma_k \gamma_2 \gamma_4 (\bar{l}_1^f)^T \right] \end{aligned} \quad (3.33)$$

Here we have used the fact that in both MILC and Dirac representation of γ matrices $\gamma_4^T = \gamma_4$. The bottom-light-light baryon two-point correlation function is

$$\begin{aligned} C_{jk;\alpha\delta}^{l_1 l_2 h}(t) &= \sum_{\vec{z}} \langle 0 | [\mathcal{O}_j^{l_1 l_2 h}(z)]_\alpha [\mathcal{O}_k^{l_1 l_2 h}(0)]_\delta^\dagger | 0 \rangle \\ &= \sum_{\vec{z}} \epsilon_{abc} \epsilon_{fgh} \langle 0 | l_{1\mu}^a(z) (\gamma_4 \gamma_2 \gamma_j)_{\mu\nu} l_{2\nu}^b(z) Q_\alpha^c(z) \bar{Q}_\delta^h(0) \bar{l}_{2\rho}^g(0) (\gamma_k \gamma_2 \gamma_4)_{\rho\sigma} \bar{l}_{1\sigma}^f(0) | 0 \rangle \\ &= \sum_{\vec{z}} \epsilon_{abc} \epsilon_{fgh} G_{\alpha\delta}^{ch}(z, 0) (\gamma_4 \gamma_2 \gamma_j)_{\mu\nu} M_{2\nu\rho}^{bg}(z, 0) (\gamma_k \gamma_2 \gamma_4)_{\rho\sigma} M_{1\mu\sigma}^{af}(z, 0) \\ &= \sum_{\vec{z}} \epsilon_{abc} \epsilon_{fgh} G_{\alpha\delta}^{ch}(z, 0) \times \text{Tr} \left[\gamma_4 \gamma_2 \gamma_j M_2^{bg}(z, 0) \gamma_k \gamma_2 \gamma_4 M_1^{afT}(z, 0) \right] \end{aligned} \quad (3.34)$$

In HISQ formalism, which we use for the lighter quarks, the corresponding propagators $M_1(z, 0)$ and $M_2(z, 0)$ have the same Kawamoto-Smit multiplicative factor $\Omega(z)$ as given in Eq. (2.29). This means they have the same spin structure irrespective of color indices. As a result, the trace over spin indices in Eqn. (3.34) vanishes if $\gamma_j \neq \gamma_k$. Therefore, we can not separate the two spin-3/2 and 1/2 states. Here we want mention that though the operator given in Eq.(3.32) couples to both spin-1/2

as well as spin-3/2 states, it is suitable for spin-3/2 states. Operator for spin-1/2 baryons having different light quark flavors l_1, l_2 , is given by

$$(\mathcal{O}_5^{l_1 l_2 h})_\alpha = \epsilon_{abc} (l_1^{aT} C \gamma_5 l_2^b) Q_\alpha^c \quad (3.35)$$

and the corresponding two-point function is

$$\begin{aligned} C_{55;\alpha\delta}^{l_1 l_2 h}(t) &= \sum_{\vec{z}} \langle 0 | [\mathcal{O}_5^{l_1 l_2 h}(z)]_\alpha [\mathcal{O}_5^{l_1 l_2 h}(0)]_\delta^\dagger | 0 \rangle \\ &= \sum_{\vec{z}} \epsilon_{abc} \epsilon_{fgh} G_{\alpha\delta}^{ch}(z, 0) \times \text{Tr} \left[\gamma_4 \gamma_2 \gamma_5 M_2^{bg}(z, 0) \gamma_5 \gamma_2 \gamma_4 M_1^{afT}(z, 0) \right] \end{aligned} \quad (3.36)$$

To get around the problem arising from the operator form in Eq. (3.32), we define our $hl_2 l_1$ -operator as

$$(\mathcal{O}_k^{hl_2 l_1})_\alpha = \epsilon_{abc} (Q^{aT} C \gamma_k l_2^b) l_{1\alpha}^c \quad (3.37)$$

This construction of operator of $(hl_2 l_1)$ baryon is possible because, unlike HQET, the NRQCD Lagrangian is not invariant under arbitrary rotations. The hermitian conjugate of $\mathcal{O}_k^{hl_2 l_1}$ is given by

$$(\mathcal{O}_k^{hl_2 l_1})_\delta^\dagger = \epsilon_{fgh} (\bar{l}_1 \gamma_4)_\delta^h [\bar{l}_2^g \gamma_k \gamma_2 (\bar{Q}^f)^T] \quad (3.38)$$

The corresponding two-point function is then given by

$$\begin{aligned}
C_{jk,\alpha\delta}^{hl_2l_1}(t) &= \sum_{\vec{z}} \langle 0 | [\mathcal{O}_j^{hl_2l_2}(z)]_\alpha [\mathcal{O}_k^{hl_2l_1}(0)]_\delta^\dagger | 0 \rangle \\
&= \sum_{\vec{z}} \epsilon_{abc} \epsilon_{fgh} \langle 0 | Q_\mu^a(z) (C\gamma_j)_{\mu\nu} l_{2\nu}^b(z) l_{1\alpha}^c(z) \bar{l}_{1\beta}^h(0) \gamma_{4\beta\delta} \bar{l}_{2\rho}^g(0) (\gamma_k \gamma_2)_{\rho\sigma} \bar{Q}_\sigma^f(0) | 0 \rangle \\
&= \sum_{\vec{z}} \epsilon_{abc} \epsilon_{fgh} M_{1\alpha\beta}^{ch}(z, 0) \gamma_{4\beta\delta} (\gamma_4 \gamma_2 \gamma_j)_{\mu\nu} M_{2\nu\rho}^{bg}(z, 0) (\gamma_k \gamma_2)_{\rho\sigma} G_{\mu\sigma}^{af}(z, 0) \\
&= \sum_{\vec{z}} \epsilon_{abc} \epsilon_{fgh} [M_1^{ch}(z, 0) \gamma_4]_{\alpha\delta} \times \text{Tr} \left[\gamma_4 \gamma_2 \gamma_j M_2^{bg}(z, 0) \gamma_k \gamma_2 G^{afT}(z, 0) \right] \quad (3.39)
\end{aligned}$$

Because the light quark propagators $M_1(z, 0)$ and $M_2(z, 0)$ are proportional to each other, the relative positions of the quark fields l_1 and l_2 in Eq. (3.39) are irrelevant. This definition of hll -operator has overlap with both the spin-3/2 and 1/2 states and can be projected out by appropriate projection operators $P_{ij}^{1/2, 3/2}$. The heavy propagator $G(z, 0)$ is required to be rotated to MILC basis using the unitary matrix S defined in the Eq. (3.17).

We can also define an additional spin-1/2 operator,

$$(\mathcal{O}_5^{hl_2l_1})_\alpha = \epsilon_{abc} (Q^{aT} C \gamma_5 l_2^b) l_{1\alpha}^c \quad (3.40)$$

The two-point function for this operator has the same form as in Eq. (3.39) with γ_j and γ_k replaced by γ_5 . With this set up, we identify various singly bottom baryon with the corresponding interpolating operators given in the table below.

In Table 3.1, we tabulate our full list of single bottom baryon operators that are made use of in this work. We have mostly followed the nomenclature used in [16] but with certain modifications as needed for this work. The baryons having the same quark content and J^P are obtained in two different ways, as mentioned above. The operators with “tilde”, for instance $\tilde{\Omega}_{ccb}(1/2^+)$, are obtained by projecting the relevant

Baryon	Quark content	J^P	Operator
$\tilde{\Omega}_{ccb}^*, \tilde{\Omega}_{ccb}$	ccb	$\frac{3}{2}^+, \frac{1}{2}^+$	$\epsilon_{abc}(Q^{aT} C \gamma_k c^b) c^c$
Ω'_{ccb}	ccb	$\frac{1}{2}^+$	$\epsilon_{abc}(Q^{aT} C \gamma_5 c^b) c^c$
Ω_{cb}	scb	$\frac{1}{2}^+$	$\epsilon_{abc}(s^{aT} C \gamma_5 c^b) Q^c$
$\tilde{\Omega}_{cb}^*, \tilde{\Omega}_{cb}$	scb	$\frac{3}{2}^+, \frac{1}{2}^+$	$\epsilon_{abc}(Q^{aT} C \gamma_k c^b) s^c$
Ω'_{cb}	scb	$\frac{1}{2}^+$	$\epsilon_{abc}(Q^{aT} C \gamma_5 c^b) s^c$
Ξ_{cb}	ucb	$\frac{1}{2}^+$	$\epsilon_{abc}(u^{aT} C \gamma_5 c^b) Q^c$
$\tilde{\Xi}_{cb}^*, \tilde{\Xi}_{cb}$	ucb	$\frac{3}{2}^+, \frac{1}{2}^+$	$\epsilon_{abc}(Q^{aT} C \gamma_k c^b) u^c$
Ξ'_{cb}	ucb	$\frac{1}{2}^+$	$\epsilon_{abc}(Q^{aT} C \gamma_5 c^b) u^c$
$\tilde{\Omega}_b^*, \tilde{\Omega}_b$	ssb	$\frac{3}{2}^+, \frac{1}{2}^+$	$\epsilon_{abc}(Q^{aT} C \gamma_k s^b) s^c$
Ω'_b	ssb	$\frac{1}{2}^+$	$\epsilon_{abc}(Q^{aT} C \gamma_5 s^b) s^c$
Ξ_b	usb	$\frac{1}{2}^+$	$\epsilon_{abc}(u^{aT} C \gamma_5 s^b) Q^c$
$\tilde{\Xi}_b^*, \tilde{\Xi}_b$	usb	$\frac{3}{2}^+, \frac{1}{2}^+$	$\epsilon_{abc}(Q^{aT} C \gamma_k s^b) u^c$
Ξ'_b	usb	$\frac{1}{2}^+$	$\epsilon_{abc}(Q^{aT} C \gamma_5 s^b) u^c$
$\tilde{\Sigma}_b^*, \tilde{\Sigma}_b$	uub	$\frac{3}{2}^+, \frac{1}{2}^+$	$\epsilon_{abc}(Q^{aT} C \gamma_k u^b) u^c$
Σ'_b	uub	$\frac{1}{2}^+$	$\epsilon_{abc}(Q^{aT} C \gamma_5 u^b) u^c$
Λ_b	udb	$\frac{1}{2}^+$	$\epsilon_{abc}(u^{aT} C \gamma_5 d^b) Q^c$

Table 3.1: Operators for single bottom baryons. Q is used for b field. Interchange in the position of two lighter quarks keeps the operator unchanged.

$(Q C \gamma_k c) c$ operator with $P_{ij}^{1/2}$. The operators with “prime”, such as Ω'_{ccb} ($1/2^+$), are obtained from $(Q C \gamma_5 c) c$ diquark construction. The “prime” states so constructed on lattice correspond to the “prime” continuum states, such as Ξ'_b or till unobserved Ω'_{cb} for instance. It is obvious that baryon states calculated by projecting out definite spin states from a two-point function share the same interpolating operator. The star-ed baryons are for $J^P = 3/2^+$ states.

3.1.7 Bottom-bottom-light baryon

The staggered operators for bottom-bottom-light (hhl) are relatively straight forward as they do not involve any complications coming from Pauli exclusion law. The

interpolating operator for doubly bottom baryons can be constructed in two ways – firstly, the conventional way as motivated by HQET and secondly, through heavy-light diquark construction the way we did above for the singly bottom baryons. The operators for (hhl) baryons, having two b quarks and a light quark, can be constructed based on how the diquark component is formed [17].

$$(\mathcal{O}_k^{hhl})_\alpha = \epsilon_{abc} (Q^{aT} C \gamma_k Q^b) l_\alpha^c \quad (3.41)$$

$$(\mathcal{O}_k^{hlh})_\alpha = \epsilon_{abc} (Q^{aT} C \gamma_k l^b) Q_\alpha^c \quad (3.42)$$

The corresponding baryon correlators can be obtained in a similar way as is done for single bottom baryons,

$$\begin{aligned} C_{jk;\alpha\delta}^{hhl}(t) &= \sum_{\vec{z}} \langle 0 | [\mathcal{O}_j^{hhl}(z)]_\alpha [\mathcal{O}_k^{hhl}(0)]_\delta^\dagger | 0 \rangle \\ &= \sum_{\vec{z}} \epsilon_{abc} \epsilon_{fgh} [M^{ch}(z, 0) \gamma_4]_{\alpha\delta} \times \text{Tr} \left[\gamma_4 \gamma_2 \gamma_j G^{bg}(z, 0) \gamma_k \gamma_2 G^{afT}(z, 0) \right] \end{aligned} \quad (3.43)$$

$$\begin{aligned} C_{jk;\alpha\delta}^{hlh}(t) &= \sum_{\vec{z}} \langle 0 | [\mathcal{O}_j^{hlh}(z)]_\alpha [\mathcal{O}_k^{hlh}(0)]_\delta^\dagger | 0 \rangle \\ &= \sum_{\vec{z}} \epsilon_{abc} \epsilon_{fgh} G_{\alpha\delta}^{ch}(z, 0) \times \text{Tr} \left[\gamma_4 \gamma_2 \gamma_j M^{bg}(z, 0) \gamma_k \gamma_2 G^{afT}(z, 0) \right] \end{aligned} \quad (3.44)$$

Very much like hll -baryon, here too we can define an additional spin-1/2 operator for doubly bottom baryon

$$(\mathcal{O}_5^{hlh})_\alpha = \epsilon_{abc} (Q^{aT} C \gamma_5 l^b) Q_\alpha^c \quad (3.45)$$

The two-point function for this operator is obtained by replacing γ_j and γ_k by γ_5 in Eq. (3.44). However, we cannot have a $C \gamma_5$ between two Q in diquark and hence, unlike \mathcal{O}_5^{hhl} there is no \mathcal{O}_5^{hhl} operator.

In the following Table 3.2 we have listed the full set of triple and double bottom baryon operators that are used in this work. However these operators are not the only local operators which can be used in the simulation of baryon spectrum. The lattice symmetry group – octahedral and double-covered octahedral group allows for many different local and non-local baryon operators. For a detailed discussion of such baryonic operators see [18, 19].

Baryon	Quark content	J^P	Operator
Ω_{bbb}	bbb	$\frac{3}{2}^+, \frac{1}{2}^+$	$\epsilon_{abc}(Q^{aT} C \gamma_k Q^b) Q^c$
$\Omega_{cbb}^*, \Omega_{cbb}$	cbb	$\frac{3}{2}^+, \frac{1}{2}^+$	$\epsilon_{abc}(Q^{aT} C \gamma_k Q^b) l^c$
$\tilde{\Omega}_{cbb}^*, \tilde{\Omega}_{cbb}$	cbb	$\frac{3}{2}^+, \frac{1}{2}^+$	$\epsilon_{abc}(Q^{aT} C \gamma_k l^b) Q^c$
Ω'_{cbb}	cbb	$\frac{1}{2}^+$	$\epsilon_{abc}(Q^{aT} C \gamma_5 l^b) Q^c$
$\Omega_{bb}^*, \Omega_{bb}$	sbb	$\frac{3}{2}^+, \frac{1}{2}^+$	$\epsilon_{abc}(Q^{aT} C \gamma_k Q^b) l^c$
$\tilde{\Omega}_{bb}^*, \tilde{\Omega}_{bb}$	sbb	$\frac{3}{2}^+, \frac{1}{2}^+$	$\epsilon_{abc}(Q^{aT} C \gamma_k l^b) Q^c$
Ω'_{bb}	sbb	$\frac{1}{2}^+$	$\epsilon_{abc}(Q^{aT} C \gamma_5 l^b) Q^c$
Ξ_{bb}^*, Ξ_{bb}	ubb	$\frac{3}{2}^+, \frac{1}{2}^+$	$\epsilon_{abc}(Q^{aT} C \gamma_k Q^b) l^c$
$\tilde{\Xi}_{bb}^*, \tilde{\Xi}_{bb}$	ubb	$\frac{3}{2}^+, \frac{1}{2}^+$	$\epsilon_{abc}(Q^{aT} C \gamma_k l^b) Q^c$
Ξ'_{bb}	ubb	$\frac{1}{2}^+$	$\epsilon_{abc}(Q^{aT} C \gamma_5 l^b) Q^c$

Table 3.2: Operators for triple and double bottom baryons. Q is used for b field and l for any of the $c, s, u/d$ lighter quarks.

Having defined the single and double bottom baryon two-point functions, we can now simulate their masses. The details of our simulation has been discussed in the next chapter.

Bibliography

- [1] Huey-Wen Lin arXiv: 1106.1608 [hep-lat], CJP 49 (2011) 827
- [2] Aida X. El-Khadra, Andreas S. Kronfeld, and Paul B. Mackenzie, Phys. Rev. D55, 3933 (1997).
- [3] E. Follana, Q. Mason, C. Davies, K. Hornbostel, G. P. Lepage, J. Shigemitsu, H. Trotter, and K. Wong, Phys. Rev. D75, 054502 (2007).
- [4] M. Tanabashi *et al.* (Particle Data Group), Phys. Rev. D98, 030001 (2018) and 2019 update.
- [5] Istvan Montvay, Gernot Munster. *Quantum Fields on a Lattice*, Cambridge University Press, First edition 1994.
- [6] Glattinger C., Lang C.B., Lect. Notes Phys. 788 (Springer, Berlin Heidelberg 2010).
- [7] C.T.H. Davies, K. Hornbostel, A. Langnau, G.P. Lepage, A. Lidsey, J. Shigemitsu, and J. Sloan, Phys. Rev. D50, 6963 (1994).
- [8] C.T.H. Davies, K. Hornbostel, G.P. Lepage, A.J. Lidsey, J. Shigemitsu, and J. Sloan, Phys. Rev. D52, 6519 (1995).
- [9] B.A. Thacker and G.P. Lepage, Phys. Rev. D43, 196 (1991).

- [10] Stefan Meinel, Phys. Rev. D82, 114514 (2010).
- [11] Howard D. Trottier, Phys. Rev. D55, 6844 (1997).
- [12] Tommy Burch, arxiv:1502.00675
- [13] M. Wingate, J. Shigemitsu, C.T.H. Davies, G.P. Lepage, and H.D. Trottier, Phys. Rev. D67, 054505 (2003).
- [14] K. C. Bowler, R. D. Kenway, O. Oliveira, D. G. Richards, P. Ueberholz, L. Lellouch, J. Nieves, C. T. Sachrajda, N. Stella, and H. Wittig (UKQCD Collaboration) , Phys. Rev. D54, 3619 (1996).
- [15] J.G. Korner, M. Kramer, and D. Pirjol, Prog. Part. Nucl. Phys. 33, 787 (1994).
- [16] Zachary S. Brown, William Detmold, Stefan Meinel, and Kostas Orginos, Phys. Rev. D90, 094507 (2014).
- [17] J.M. Flynn, F. Mescia, and A.S.B. Tariq, JHEP 0307, 066 (2003).
- [18] S. Basak, R. G. Edwards, G. T. Fleming, U. M. Heller, C. Morningstar, D. Richards, I. Sato, and S. Wallace, Phys. Rev. D72, 094506
- [19] Subhasish Basak, Robert Edwards, George T. Fleming, Urs M. Heller, Colin Morningstar, David Richards, Ikuro Sato, and Stephen J. Wallace Phys. Rev. D72, 074501

Chapter 4

Quark mass tuning and Results

The bottom baryon correlators constructed in the last Chapter are evaluated by computing quark propagators, both light and heavy, against the background $SU(3)_c$ gauge configurations. At this step of fermion matrix inversion for calculating the propagators, we need to fix the bare quark masses that appear as parameters in the actions given in the Eqs. (2.46), (2.92) and (2.93). This quark mass fixing has to be done for all the quarks, namely bottom, charm, strange and up/down. The fixing of u/d -quark mass is where it gets different from light baryon calculations. For light baryons, the general practice is to vary the bare u/d quark masses necessary to approach the chiral limit $am_{u/d} \rightarrow 0$ *i.e.* $(am_\pi)^2 \rightarrow 0$, but usually restricted by the requirement $m_\pi L \approx 4$. Therefore, $m_{u/d}$ needed to be tuned and fixed instead of a naive $m_{u/d} \rightarrow 0$ limit. The tuning of s also departs from the way it is done in light hadron spectroscopy, where a fictitious pseudoscalar state η_s is used. In our work we find that using B_s state, instead of η_s , for fixing s gives a more accurate $S = -1$, $B = -1, -2$ baryon spectrum. The tuning of c and b conventionally involves calculation of kinetic masses of the pseudoscalar $(\bar{\psi}\gamma_5\psi)$ and vector $(\bar{\psi}\gamma_i\psi)$ mesons, $\eta_c - J/\psi$ for c and $\eta_b - \Upsilon$ for b and followed by equating them with the physical *i.e.*

experimental spin average masses. In this work, we do not need kinetic mass to fix c -quark for reason discussed later but need it for b tuning. In what follows, we discuss in detail our tuning strategy for various quarks starting with b .

4.1 m_b tuning

The tuning of b -quark mass involves computation of kinetic masses of η_b and Υ . Since the rest mass term is not included in the NRQCD formulation given in the Eqs. (2.68), (2.69) and (2.70), we can not determine the hadron masses directly from the leading exponential decay of the two-point functions of the bottomonium states. Hence the need for calculating the kinetic mass M_k instead [1]. Consider the energy-momentum relation, up to $\mathcal{O}(p^2)$

$$\begin{aligned} E(\vec{p}) - E(0) &= \sqrt{\vec{p}^2 + M_k^2} - M_k \\ \Rightarrow E(\vec{p})^2 &= E(0)^2 + \frac{E(0)}{M_k} \vec{p}^2 + \dots \end{aligned} \quad (4.1)$$

The above expression requires calculation of the $E(\vec{p})$ at different values of lattice momenta $\vec{p} = 2\vec{n}\pi/L$ where, $\vec{n} = (0,0,0), (1,0,0), (1,1,0), (1,1,1), (2,0,0), (2,1,0)$ and $(2,1,1)$. From the slope of the $E(\vec{p})^2$ vs \vec{p}^2 plot we extract the M_k . The mass of b quark is tuned from the spin average masses of η_b and Υ

$$M_{b\bar{b}} = \frac{3M_k^\Upsilon + M_k^{\eta_b}}{4} \quad (4.2)$$

using the kinetic mass for both η_b and Υ . The experimental spin average mass of Υ (9460) and η_b (9391) is 9443 but lattice spin average mass is tuned to 9450 MeV, denoted as $M_{\text{phys}}^{\text{mod}}$ later in the Eq. (4.3). The reasons being – (a) we are not considering the electromagnetic interactions among the quarks, (b) we do not have sea c quarks in

our simulation and (c) we have not considered disconnected diagrams while computing the bottomonium two-point functions thus not allowing b, \bar{b} quarks to annihilate to gluons [2].

The coefficient c_4 of Eq. (2.69) and b quark mass m_b are then tuned to obtain modified spin average mass and the hyperfine splitting of Υ and η_b . The c_4 term is the only term at order $\mathcal{O}(1/m_b)$ that contains Pauli spin matrices. It contributes maximally in the hyperfine splitting compared to other terms. Hence we tuned c_4 only to achieve the hyperfine splitting of Υ and η_b , which is $\sim 60 - 65$ MeV [3]. The one-loop radiative correction to c_4 [4] has been used to tune the hyperfine splitting in [5] where it was found to change, but only mildly, over lattice spacings $\sim 0.15 - 0.09$ fm for $N_f = 2 + 1 + 1$ HISQ gauge configurations. In our present mixed action study, the changes in the tuned c_4 on various lattice ensembles are small enough. Taking an average of those values we choose $c_4 = 1.9$ for which the hyperfine splittings obtained on three different lattices 0.15, 0.12 and 0.09 fm are 60.6 MeV, 61.1 MeV and 61.8 MeV respectively.

All the remaining coefficients c_i in Eq. (2.93) are set to 1. The stability factor n in Eq. (2.91) is set to $n = 4$ throughout our simulation. We list various tuned values of m_b for different lattice ensembles used in this work in the Table 4.1. Here we want to mention that HPQCD [6] also used the same lattices as we have used in our study but as we haven't used tadpole improved gauge links in our formulation we got different bare b -quark mass.

4.2 m_c tuning

Being heavy, the dynamics of the c quark is essentially governed by the nonrelativistic Hamiltonian. The typical velocity of c quark in mesons is quite nonrelativistic, $v^2 \sim$

a (fm)	am_b	am_c	am_s (η_s)	am_s (B_s)	ϵ [2]
0.15	2.76	0.850	0.065	0.215	-0.34
0.12	2.08	0.632	0.049	0.155	-0.21
0.09	1.20	0.452	0.0385	0.114	-0.115

Table 4.1: Tuned b , c and s quark bare masses for lattices used in this work. For s -quark mass, we mentioned the particle states to which it is tuned to. The values of ϵ -parameter used for c -quark are given in the last column.

0.35 in B_c meson and $v^2 \sim 0.3$ in charmonium states [2]. In D and D_s mesons, the c quark is even slower. The rest mass decouples from the interesting dynamics and the kinetic mass becomes very significant in such systems. For example, the radial and orbital excitations of charmonium states are governed by kinetic mass [1]. Therefore while simulating the c quark using Clover-Wilson type actions one must match the kinetic mass instead of the pole mass to the physical value.

HISQ action overcomes the above problem of tuning the kinetic mass. The Naik term of HISQ action can be appropriately tuned to eliminate the $\mathcal{O}(pa)^2$ errors which in turn allows one to match the pole mass to the physical values. As we are using HISQ action for c quark we use the pole mass instead of kinetic mass for the charmoniums. The mass of c quark is tuned to the spin average of η_c and J/ψ experimental masses. The modification to spin average value due to the absence of c -quarks in sea, electromagnetic interaction, and disconnected diagrams are very small and hence neglected. The bare c -quark masses used in this work are also given in the Table 4.1.

In order to check the correctness of the c quark tuning, we calculated the mass of Ω_c and Ω_{cc} states. These states contain s quark(s) which is tuned to η_s . Details of the s quark tuning is given in the next section. Here, in the Table 4.2 we compare our numbers with the recent available lattice results in the reference [7]. The doubly charmed strange baryon Ω_{cc} does not have any PDG entry, however the PDG value

Baryon	J^P	Quark content	This work (MeV)	Flynn <i>et al.</i> (MeV)
Ω_c	$\frac{1}{2}^+$	css	2630(3)	2627(16)
Ω_{cc}	$\frac{1}{2}^+$	ccs	3745(2)	3663(11)

Table 4.2: Ω_c and Ω_{cc} baryon masses. Interpolating operator and two-point function used to calculate the masses of these triply light baryons are given in Appendix B.

of Ω_c is 2698 MeV, which is significantly away from the lattice results.

4.3 m_s tuning

The s quark mass is tuned to two different values. First by using η_s meson, a hypothetical pseudoscalar meson which can not mix with physical η or η' meson via $s\bar{s}$ annihilation. So we do not need to consider disconnected diagrams while calculating the two point function. Using leading order chiral perturbation theory one can estimate its mass to be $m_{\eta_s} = \sqrt{2m_K^2 - m_\pi^2} = 689$ MeV [8, 9]. The s -quark mass thus tuned is checked against D_s meson ($c\bar{s}$), making use of the c -quark mass obtained above and found to agree with the experimental D_s (1968 MeV). The s quark tuned this way, however, fails to capture the strange bottom meson ($b\bar{s}$) or strange-baryon ($S = -1, B = -1, -2$) spectra *i.e.* when s -quark is in a bound state with a heavy b quark. We anticipate the s quark getting significant correction in its mass in the presence of b quark(s). For this reason we have to resort to B_s tuning.

The s quark mass, thus tuned using the B_s , reproduces the strange bottom baryon spectra satisfactorily. While calculating the mass of other baryons we assume that the potential experienced by the s quark in the field of b quark in B_s meson does not change in other strange bottom baryons and there is no spin-spin interaction between the s quark and the other quarks in the baryon. This assumption may be true for bbs

and bcs systems, but it might not be true for bss or bsu/bsd systems. Nevertheless, we still try and obtain the masses of such systems close to their physical masses without resorting to any extrapolation with this tuning strategy.

We will present our results obtained at these two different values of m_s . In Table 4.1, we listed these values of m_s for different lattices. In the Table 4.3 we calculate B_c and D_s mesons using tuned b , c and s masses. As is seen, when m_s is tuned with η_s , the D_s mass obtained is fairly close to PDG value whereas when tuned to B_s we see an upward shift by an average 200 MeV. We have observed similar differences when s quark appears together with c in (scb) -baryon masses.

$L^3 \times T$	B_c	D_s	
		η_s	B_s
$16^3 \times 48$	6260(8)	1994(3)	2197(2)
$20^3 \times 64$	6263(12)	1977(4)	2172(2)
$28^3 \times 96$	6255(10)	1971(3)	2167(2)
PDG [15]	6275	1968	

Table 4.3: D and B meson masses in MeV with the tuned am_b , am_c and am_s .

4.4 $m_{u/d}$ tuning

For the valence u/d quark mass, we varied the bare quark mass from the lightest sea quark masses all the way to a little above where s mass is tuned to B_s . We have worked in the isospin limit *i.e.* $m_u = m_d$. We tried to compute the bottom baryon spectra with u/d quark mass tuned to B mass, so whenever the mass of a bottom baryon containing u/d quark(s) is quoted, it corresponds to u/d quark mass tuned at B mass. This strategy differs from what is done for light baryons. The light baryon masses, obtained over a range of $am_{u/d}$ *i.e.* $(am_\pi)^2$, are extrapolated to $(am_\pi)^2 \rightarrow 0$. But in the present case of bottom baryons, we have fixed even the $(am_\pi)^2$ well away from the

chiral limit. This tuning of u/d mass to B works particularly well in reproducing the bottom baryon containing a single u/d quarks, such as (bsu) or (bcu) . Therefore, in short, all the quark mass parameters for bottom baryon simulation are fixed through pseudoscalar and vector D and B mesons. In Table 4.4, we listed u/d quark masses (am_q) against the lattice spacing.

$L^3 \times T$	$am_{u/d}$
$16^3 \times 48$ (0.15 fm)	0.065, 0.10, 0.13, 0.14, 0.155 0.165, 0.185, 0.215, 0.225
$20^3 \times 64$ (0.12 fm)	0.05, 0.075, 0.090, 0.10, 0.115, 0.13, 0.155, 0.165
$28^3 \times 96$ (0.09 fm)	0.04, 0.07, 0.085, 0.09, 0.10, 0.114, 0.12, 0.13

Table 4.4: Values of $am_{u/d}$ used in this work.

We show in the Figure 4.1 our strategy used to tune m_s and $m_{u/d}$ for all the three lattice ensembles used in this work.

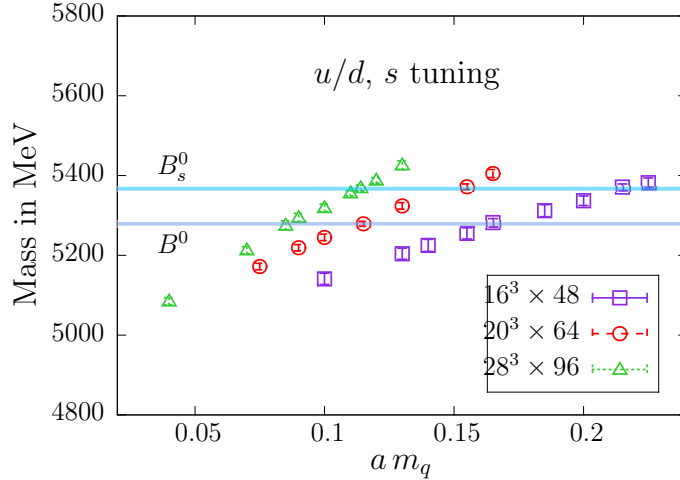


Figure 4.1: Tuning of s and u/d quark masses in various lattices. The experimental values of B^0 and B_s^0 are shown by bands whose thickness are to enhance visibility and have nothing to do with experimental errors.

We compute the B meson masses over the range of light quark masses given in

the Table 4.4 for the three different lattice ensembles we used. We fixed the $m_{u/d}$ and m_s whenever the corresponding B meson mass coincides with the physical B^0 and B_s^0 masses respectively. From the above figure, we extract the tuned $am_{u/d}$ at B^0 for different lattices to use with b quarks,

$$16^3 \times 48 : 0.165 \quad 20^3 \times 64 : 0.115 \quad 28^3 \times 96 : 0.085$$

The s and u/d masses so tuned, the ratio $m_s/m_{u/d}$ turns out to be ~ 1.3 compared to ~ 6 that we get when m_s is obtained from η_s and $m_{u/d}$ is the bare sea quark mass. The physical relevance of unusually high light and strange quark masses is not well understood from the context of this work. Here our main focus is to construct HISQ-NRQCD operators for various bottom baryons and tetraquarks for spectroscopic studies and, therefore, the issue has not been explored sufficiently.

For states containing two u/d quarks, such as Σ_b (uub) and Λ_b (udb), we have mixed success with the above tuning approach. When b and u form diquarks ($QC\gamma_{\{k,5\}}u$) for Σ_b state, the masses obtained are consistent with other lattice studies. However, this tuning scheme involving B fails for Λ_b where the diquark part is ($uC\gamma_5 d$) (see the Table 3.1). Hence for Λ_b , containing both u and d quarks, we have to resort to different tuning to account for the 190 MeV of mass difference with Σ_b . For details discussion see section 5.1.1. The mass of Λ_b is obtained from this specially tuned $m'_{u/d}$ (to be used only for Λ_b). Thus tuned differently, the mass differences $\Xi_b - \Lambda_b$ and $\Sigma_b^* - \Lambda_b$ are well within 2σ of PDG values while $\Lambda_b - B$ is about 60 MeV higher, see the Table 4.8.

4.5 Numerical results

The tuning of all the quark masses involved (b , c , s and u/d) and the subsequent calculation of bottom baryon spectra are carried out over three different gauge ensembles of dimensions $16^3 \times 48$, $20^3 \times 64$ and $28^3 \times 96$ all corresponding to the same physical spatial volume $(2.5 \text{ fm})^3$. In our simulation, We made use of the publicly available $N_f = 2+1$ Asqtad gauge ensembles generated by MILC Collaboration. Details about these lattices are given in [10]. It uses Asqtad action [11, 12] for the sea s and u/d quarks and Symanzik-improved Lüscher-Weisz action for the gluons. The lattices we choose have a fixed ratio of $am_l/am_s = 1/5$ and lattice spacings ranging from 0.15 fm to 0.09 fm corresponding to the same physical volume. We have not determined the lattice spacings ourselves but have taken the values of a from the [10]. In Table 4.5 we listed the various parameters of the ensembles used in this work.

$\beta = 10/g^2$	$a(\text{fm})$	am_l	am_s	$L^3 \times T$	N_{cfg}
6.572	0.15	0.0097	0.0484	$16^3 \times 48$	400
6.76	0.12	0.01	0.05	$20^3 \times 64$	400
7.09	0.09	0.0062	0.031	$28^3 \times 96$	300

Table 4.5: MILC configurations used in this work. The gauge coupling is β , lattice spacing a , u/d and s sea quark masses are m_l and m_s respectively and lattice size is $L^3 \times T$. The N_{cfg} is number of configurations used in this work.

For the present simulation, we are using different actions for valence and sea quarks, the so-called mixed action approach. As different lattice actions respect different symmetries of continuum QCD, mixed action inevitably violates unitarity, however, near the continuum limit one can construct an effective theory. One can tune the valence quark masses to have the desired meson masses in the mixed action to agree with unitarity. Since the valence and sea quarks have different discretization effects, it is not, however, possible to tune the mesons made up of purely sea and

valence quarks. One such quantity which is sensitive to unitarity violation is the scalar correlator. It becomes negative for sea quark mass larger than valence quark mass ($m_{val} < m_{sea}$) [13]. In mixed action simulation, therefore, it is imperative to keep $m_{val} > m_{sea}$. In our calculation it is not an issue since our tuned values of valence light quark masses stand far away from the sea quark masses.

To extract masses we perform two-exponential uncorrelated fit to the baryonic two-point functions. Fit range is suitably chosen by looking at the extent of the plateau of the effective mass plots from the correlators. But this zero momentum energy (or the pole mass) does not directly give us the mass of the bottom baryon. The reason being, as discussed before, the unphysical shift in zero of energy. Taking this into account, we arrive at the bottom baryon mass by using,

$$M_{\text{latt}} = E_{\text{latt}} + \frac{n_b}{2} (M_{\text{phys}}^{\text{mod}} - E_{\text{latt}}^{\eta_b}) \quad (4.3)$$

where E_{latt} is the lattice zero momentum energy in MeV, n_b is the number of b -quarks in the bottom baryon. $M_{\text{phys}}^{\text{mod}}$ is the modified spin averaged mass of η_b and Υ as discussed before. While calculating the above splittings in parenthesis, this shift in energies is canceled by subtraction among energies of hadrons having equal number of b quarks (n_b) in them. For this calculation of mass splittings, we use jack-knifed ratio of the correlation functions for fitting [14],

$$C^{Y-X}(t) = \frac{C^Y(t)}{C^X(t)} \sim e^{-(M_Y - M_X)t} \quad (4.4)$$

In the Figure 4.2 we show a few correlators for single b baryons containing exclusively either two c or s or u/d for the $28^3 \times 96$ lattices. The data from other lattices are similar. The “goodness” of the operators that we have constructed is reflected in the quality of the data. To illustrate how the fitting ranges are chosen, we plot in

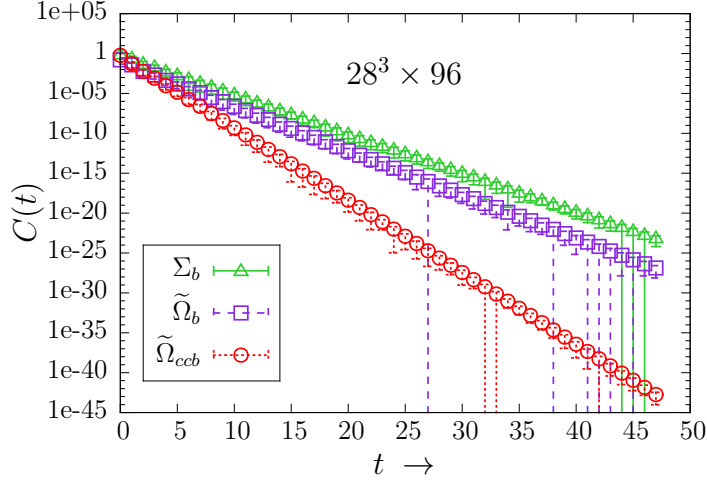


Figure 4.2: Σ_b , $\tilde{\Omega}_b$ and $\tilde{\Omega}_{ccb}$ correlators in $28^3 \times 96$ lattice.

tandem the corresponding effective mass plots in Figure 4.3. The fitting range is the

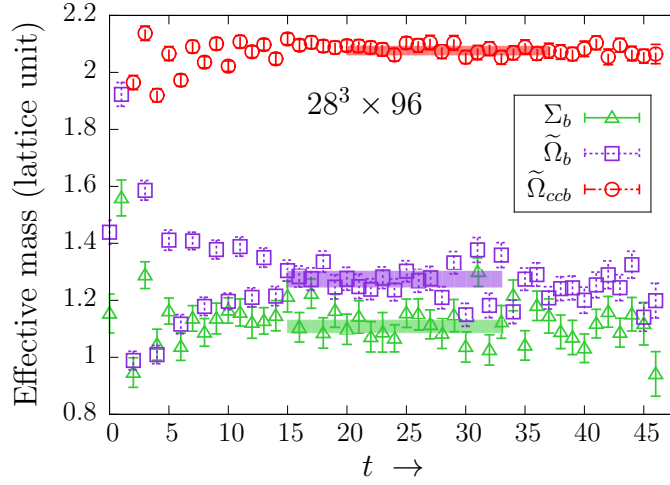


Figure 4.3: Effective mass plots for the states in Figure 4.2. The bands are placed over what we consider plateau.

extent of the plateau in the effective mass plots and the exponential fits of the correlators. Both fittings return same masses over suitably chosen range. In the effective mass plot Figure 4.3, the zero momentum energies and the errors of the same three states, as shown in the Figure 4.2, are represented by bands. The thickness of the

bands is proportional to statistical uncertainties of the fit values. The plots are similar, in trend and quality, for other two set of lattices, namely $16^3 \times 48$ and $20^3 \times 64$, but have shorter fitting range because of shorter time extent. The fitting range for a class of bottom baryons, say single bottom baryon, are kept the same (for a given lattice ensemble) unless convergence issue is encountered. This sometime necessitates small variation in the fitting range.

Single bottom baryons: A couple of single bottom baryon have been listed in the PDG [15], such as Λ_b (udb), Ω_b (ssb), Ξ'_b (usb) etc. and they provide a good matching opportunity for our lattice data. In the Figure 4.4, we show the agreement of some of these baryon masses with PDG at the tuned $m_{u/d}$ and m_s .

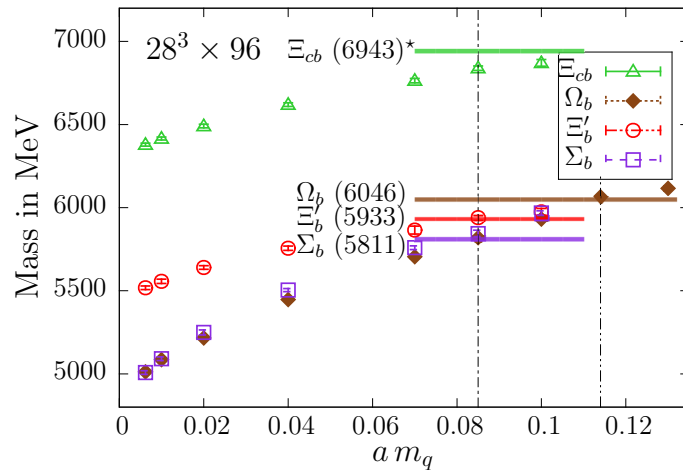


Figure 4.4: Variation of single b baryon masses in MeV against the same light quark masses as in Figure 4.1. $m_q = 0.085$ and 0.114 are the tuned u/d , s quark masses respectively, indicated by dashed vertical lines. The bands correspond to the PDG values, except for Ξ_{cb} which is taken from [16].

Ξ_{cb} has no entry in PDG and so compared with previous lattice result [16]. The disagreement in Ξ_{cb} values is possibly because of different action used for c and u/d .

In the following pages, we present our results of the single and multi b baryon

states corresponding to the operators listed in the Tables 3.1 and 3.2. In first, we collect our results for single bottom baryon, not containing s quark(s), in the Table 4.6 and those with s quark in Table 4.7.

Baryons	$16^3 \times 48$ (0.15 fm)	$20^3 \times 64$ (0.12 fm)	$28^3 \times 96$ (0.09 fm)	Average (MeV)
$\tilde{\Omega}_{ccb}^*$	2.954(5)	2.497(4)	2.088(3)	7807(11)
$\tilde{\Omega}_{ccb}$	2.933(5)	2.482(3)	2.078(3)	7780(9)
Ω'_{ccb}	2.952(4)	2.497(3)	2.078(3)	7797(11)
$\tilde{\Xi}_{cb}^*$	2.222(6)	1.899(4)	1.648(6)	6835(20)
Ξ_{cb}	2.177(11)	1.881(4)	1.623(5)	6787(12)
$\tilde{\Xi}_{cb}$	2.199(8)	1.886(4)	1.631(4)	6805(16)
Ξ'_{cb}	2.227(6)	1.904(4)	1.653(6)	6843(19)
$\tilde{\Sigma}_b^*$	1.468(8)	1.292(5)	1.189(5)	5836(22)
$\tilde{\Sigma}_b$	1.460(7)	1.290(3)	1.174(6)	5820(21)
Σ'_b	1.470(7)	1.305(3)	1.194(9)	5848(18)
Λ_b	1.322(7)	1.208(6)	1.109(9)	5667(14)

Table 4.6: Masses, in lattice unit, of baryons involving single b quark and no s quark. The bare u/d -quark masses are 0.165 for $16^3 \times 48$, 0.115 for $20^3 \times 64$ and 0.085 for $28^3 \times 96$.

In the columns corresponding to various lattice ensembles, we show the masses in lattice unit, aE_{latt} of the Eq. (4.3). In the last column of each table, we provide the average M_{latt} in MeV and the statistical errors, calculated assuming the lattice configurations of different lattice spacings are statistically independent. First we determined the individual aE_{latt} and their error from two-exponential fitting and used Eq. (4.3) to obtain M_{latt} for each lattice spacings. The average $\overline{M}_{\text{latt}}$ and the

error (square root of the variance) provided in the last column is arrived at by,

$$\overline{M}_{\text{latt}} = \frac{M_{\text{latt}}^{(0.15)} + M_{\text{latt}}^{(0.12)} + M_{\text{latt}}^{(0.09)}}{3} \quad (4.5)$$

$$\text{Var}(M_{\text{latt}}) = \frac{\text{Var}(M_{\text{latt}}^{(0.15)}) + \text{Var}(M_{\text{latt}}^{(0.12)}) + \text{Var}(M_{\text{latt}}^{(0.09)})}{3} + \frac{(M_{\text{latt}}^{(0.15)} - \overline{M}_{\text{latt}})^2 + (M_{\text{latt}}^{(0.12)} - \overline{M}_{\text{latt}})^2 + (M_{\text{latt}}^{(0.09)} - \overline{M}_{\text{latt}})^2}{3} \quad (4.6)$$

Since s quark has been tuned in two different ways, we quote both the b baryon masses at η_s and B_s points. As is evident from our results, the numbers coming from

Baryons	Tuning	$16^3 \times 48$ (0.15 fm)	$20^3 \times 64$ (0.12 fm)	$28^3 \times 96$ (0.09 fm)	Average (MeV)
$\tilde{\Omega}_{cb}^*$	η_s	2.035(5)	1.782(5)	1.542(3)	6611(9)
	B_s	2.292(7)	1.957(6)	1.693(4)	6930(19)
Ω_{cb}	η_s	2.010(8)	1.754(5)	1.532(3)	6578(9)
	B_s	2.248(11)	1.937(7)	1.684(2)	6893(16)
$\tilde{\Omega}_{cb}$	η_s	2.012(7)	1.765(5)	1.536(3)	6587(10)
	B_s	2.267(8)	1.943(7)	1.686(2)	6906(17)
Ω'_{cb}	η_s	2.052(5)	1.785(5)	1.548(3)	6625(8)
	B_s	2.297(6)	1.966(6)	1.705(2)	6946(17)
$\tilde{\Xi}_b^*$	η_s	0.987(4)	0.945(2)	0.918(3)	5237(8)
	B_s	1.541(8)	1.352(6)	1.235(6)	5935(22)
Ξ_b	η_s	0.986(5)	0.947(2)	0.909(4)	5231(11)
	B_s	1.520(9)	1.345(3)	1.207(6)	5901(20)
$\tilde{\Xi}_b$	η_s	0.978(5)	0.944(2)	0.904(5)	5222(13)
	B_s	1.532(11)	1.350(4)	1.224(4)	5921(19)
Ξ'_b	η_s	0.987(4)	0.948(3)	0.913(5)	5235(11)
	B_s	1.544(10)	1.366(4)	1.238(6)	5946(16)
$\tilde{\Omega}_b^*$	η_s	1.129(5)	1.058(3)	1.012(4)	5430(11)
	B_s	1.611(8)	1.412(6)	1.264(3)	6019(20)
$\tilde{\Omega}_b$	η_s	1.118(7)	1.050(3)	0.997(4)	5410(10)
	B_s	1.600(11)	1.411(7)	1.264(3)	6014(17)
Ω'_b	η_s	1.131(9)	1.057(3)	1.007(2)	5427(9)
	B_s	1.615(8)	1.425(7)	1.295(2)	6051(15)

Table 4.7: Masses, in lattice unit, of baryons containing single b -quark and s -quark(s).

s -quark tuned to η_s are about 300 MeV smaller from those tuned to B_s (600 MeV in baryons with two s). If we take $\Omega_b(bss)$ and compare with the PDG value of 6046 MeV, it becomes obvious.

One of the important phenomenological observables is the mass splittings of the baryons. Particularly important is the splitting between the spin-3/2 and 1/2 states, known as hyperfine splittings, which reveals the physics of spin-spin interactions among the quarks inside a baryon. We determine and assemble the results of the mass splittings in single bottom sector in the Table 4.8 below.

Baryon splittings	$16^3 \times 48$ (MeV)	$20^3 \times 64$ (MeV)	$28^3 \times 96$ (MeV)	Average (MeV)
$\tilde{\Omega}_{ccb}^* - \tilde{\Omega}_{ccb}$	28(3)	23(2)	–	26(3)
$\tilde{\Omega}_{cb}^* - \tilde{\Omega}_{cb}$	59(8)	62(13)	61(22)	61(15)
$\tilde{\Xi}_{cb}^* - \tilde{\Xi}_{cb}$	37(6)	44(5)	44(9)	42(7)
$\tilde{\Omega}_b^* - \tilde{\Omega}_b$	29(5)	28(11)	29(4)	29(7)
$\Omega'_b - \Lambda_b$	396(4)	391(9)	406(10)	398(9)
$\tilde{\Xi}_b^* - \tilde{\Xi}_b$	138(20)	122(38)	138(46)	133(36)
$\tilde{\Xi}_b - \Lambda_b$	170(9)	166(11)	163(6)	166(9)
$\Lambda_b - B$	391(20)	431(20)	397(22)	406(21)
$\tilde{\Sigma}_b^* - \tilde{\Sigma}_b$	30(9)	30(8)	29(8)	30(8)
$\tilde{\Sigma}_b^* - \Lambda_b$	224(13)	203(12)	175(13)	201(13)

Table 4.8: Single bottom baryons mass splittings in MeV.

A graphic illustration of the difference is made evident in the plots for ratio of correlators in Figure 4.5. Here, we have chosen the correlator plots for $\Omega'_b - \Lambda_b$ and $\Xi_b - \Lambda_b$, for all three lattice ensembles, for comfortable viewing because of their relatively large mass differences *i.e.* slopes are prominent and well separated. The fit ranges are chosen as before by comparing with the corresponding effective mass plateau. For smaller differences, for instance $\tilde{\Omega}_b^* - \tilde{\Omega}_b$ or $\tilde{\Xi}_{cb}^* - \tilde{\Xi}_{cb}$, the slopes of the ratio of correlators are rather small and not quite visible.

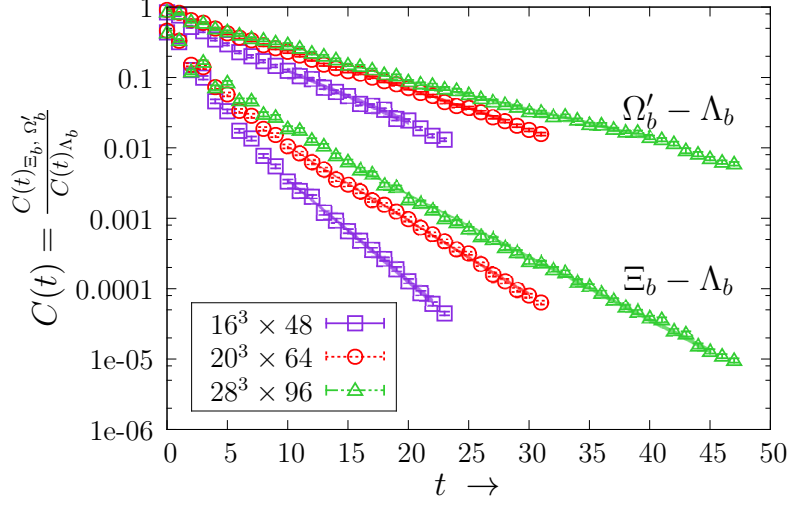


Figure 4.5: Ratio of correlators for the calculation of the two splittings shown in Table 4.8. The bands overlaid on the data points represent single exponential fits.

A heavy quark basically acts as a static color source, and therefore, we expect that the hyperfine splittings between states containing single or multiple s and u/d quark(s) to depend only weakly on the tuning of m_s and $m_{u/d}$. For $m_{u/d} \leq 0.085$ and two values of m_s we show this pattern for a few hyperfine splittings in Figure 4.6.

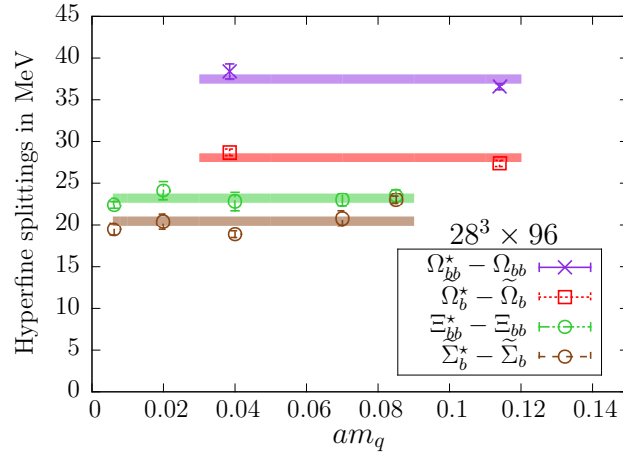


Figure 4.6: Hyperfine splittings at various m_s and $m_{u/d}$ for a selected few bottom baryons on $28^3 \times 96$ lattice. Horizontal bands are the average values of the splittings.

Double bottom baryons: For double bottom baryons, the data are relatively less noisy than the single bottom baryons. The effective mass plots in Figure 4.7, shown for only $16^3 \times 48$ lattices but similar for two other lattices, are an evidence for this. The fitting ranges are chosen the same way as is done for Figure 4.3. The plot for

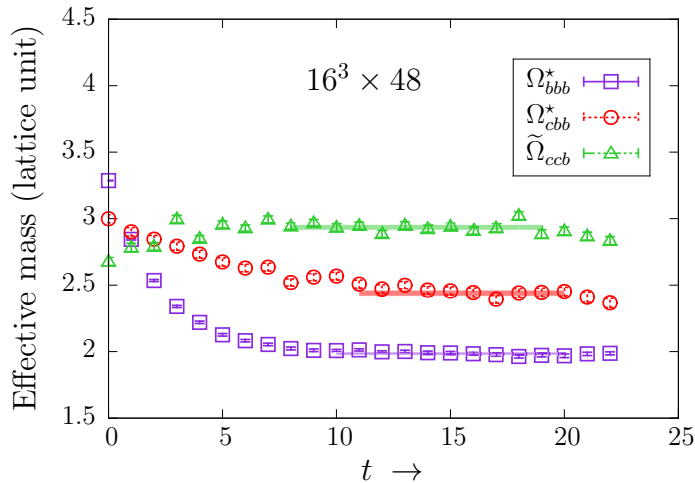


Figure 4.7: Ω_{bbb}^* , $\tilde{\Omega}_{cbb}^*$ and $\tilde{\Omega}_{ccb}^*$ effective masses.

Ω_{bbb}^* appears to be counter intuitive, since being the heaviest, it is showing lower mass compared to the other two. However, it gets large correction because of shift in rest mass of three b -quarks.

We tabulate our results for double bottom non-strange baryons in the Table 4.9 while those containing s quark in Table 4.10. It is to be noted that Ω_{bbb} is a spin-3/2 state having no spin-1/2 counterpart. But in practice we can take a spin-1/2 projection to get such a fictitious state. Therefore, we label the physical (bbb) spin-3/2 state with Ω_{bbb}^* to keep consistency with our remaining notation. In this case none of the states have PDG entries. Later in the summary chapter, we will compare our multi-bottom baryon results with previous lattice results wherever available.

Baryon	$16^3 \times 48$ (0.15 fm)	$20^3 \times 64$ (0.12 fm)	$28^3 \times 96$ (0.09 fm)	Average (MeV)
Ω_{bbb}^*	1.983(4)	2.031(3)	2.154(4)	14403(7)
Ω_{bbb}	1.974(4)	2.023(5)	2.148(4)	14390(8)
Ω_{cbb}^*	2.429(16)	2.259(4)	2.117(3)	11081(21)
Ω_{cbb}	2.409(16)	2.246(5)	2.110(3)	11060(23)
$\tilde{\Omega}_{cbb}^*$	2.431(8)	2.255(4)	2.113(3)	11077(14)
$\tilde{\Omega}_{cbb}$	2.432(10)	2.251(4)	2.113(3)	11075(13)
Ω'_{cbb}	2.434(8)	2.250(4)	2.114(4)	11076(12)
Ξ_{bb}^*	1.721(12)	1.643(10)	1.666(5)	10103(24)
Ξ_{bb}	1.700(12)	1.640(7)	1.664(5)	10091(17)
$\tilde{\Xi}_{bb}^*$	1.720(12)	1.635(8)	1.668(3)	10100(27)
$\tilde{\Xi}_{bb}$	1.703(16)	1.634(8)	1.661(4)	10087(22)
Ξ'_{bb}	1.704(16)	1.635(10)	1.672(3)	10096(24)

Table 4.9: Triple and double bottom non-strange baryon masses.

Baryon	Tuning	$16^3 \times 48$ (0.15 fm)	$20^3 \times 64$ (0.12 fm)	$28^3 \times 96$ (0.09 fm)	Average (MeV)
Ω_{bb}^*	η_s	1.545(11)	1.536(6)	1.576(4)	9902(12)
	B_s	1.791(12)	1.703(11)	1.716(3)	10203(22)
Ω_{bb}	η_s	1.553(9)	1.527(7)	1.570(4)	9896(13)
	B_s	1.768(12)	1.699(8)	1.715(3)	10190(17)
$\tilde{\Omega}_{bb}^*$	η_s	1.542(9)	1.529(7)	1.575(4)	9896(12)
	B_s	1.791(12)	1.693(10)	1.717(3)	10199(28)
$\tilde{\Omega}_{bb}$	η_s	1.541(12)	1.527(7)	1.571(4)	9891(13)
	B_s	1.789(9)	1.695(7)	1.714(3)	10197(24)
Ω'_{bb}	η_s	1.552(9)	1.539(7)	1.578(3)	9908(11)
	B_s	1.782(9)	1.699(7)	1.720(3)	10200(20)

Table 4.10: Double bottom strange baryon spectra.

We would like to point out that the variation of the Ξ_{bb} (ubb) masses with $m_{u/d}$ is almost absent as the major contribution to these baryons are coming from two b quarks. Similarly, in Table 4.10 we see different tuning of s quark has significantly less influence on double bottom baryon masses.

We listed the mass splittings in double bottom baryon sector in the Table 4.11. Two of the entries in the Table below are too noisy to be quoted.

The splittings between the spin-3/2 and 1/2 states in double bottom baryons are particularly interesting because HQET relates this mass differences with hyperfine splittings of heavy-light mesons, which in the heavy-quark limit [17]

$$\frac{\Delta M_{bb}^{\text{baryon}}}{\Delta m_b^{\text{meson}}} \rightarrow \frac{3}{4} \quad (4.7)$$

Baryon splittings	$16^3 \times 48$ (MeV)	$20^3 \times 64$ (MeV)	$28^3 \times 96$ (MeV)	Average (MeV)
$\tilde{\Omega}_{cbb}^* - \tilde{\Omega}_{cbb}$	–	25(5)	35(2)	30(5)
$\Omega_{bb}^* - \Omega_{bb}$	34(5)	25(8)	37(9)	32(7)
$\Xi_{bb}^* - \Xi_{bb}$	–	25(4)	39(7)	32(5)

Table 4.11: Double bottom baryon mass splittings in MeV. None of the splittings have PDG entries.

This behavior is consistent with our results within errors as given in Table 4.12.

Baryon splittings	Our results (MeV)	Meson splittings	Our results (MeV)	Ratio
$\tilde{\Omega}_{bbc}^* - \tilde{\Omega}_{bbc}$	35(2)	$B_c^* - B_c$	46(4)	0.76(4)
$\Omega_{bb}^* - \Omega_{bb}$	37(9)	$B_s^* - B_s$	45(9)	0.82(9)
$\Xi_{bb}^* - \Xi_{bb}$	39(7)	$B^* - B$	47(7)	0.83(8)

Table 4.12: Ratio of hyperfine splittings of double bottom baryons to corresponding B -mesons in the heavy quark limit in $28^3 \times 96$ lattice.

We also computed a few GMO mass relations involving b -quark [18] in this work,

$$M_{\Omega_{ccb}^*} - M_{\Omega_{ccb}} \approx M_{\Omega_{cbb}^*} - M_{\Omega_{cbb}} \quad (4.8)$$

$$M_{\Sigma_b^*} - M_{\Sigma_b} \approx M_{\Xi_{bb}^*} - M_{\Xi_{bb}} \quad (4.9)$$

For the GMO relation (4.8), the both sides are expected to be approximately 31 MeV but in our case for $20^3 \times 64$ lattice, for which we have data for both the sides, they are approximately equal but is around 24 MeV as against 31 MeV given in [18]. Our lattice data is also consistent with the approximate GMO relation (4.9), where each side is about 30 MeV against 20 MeV calculated in the reference [18].

Bibliography

- [1] Aida X. El-Khadra, Andreas S. Kronfeld, and Paul B. Mackenzie, *Phys. Rev. D* 55, 3933 (1997).
- [2] Eric B. Gregory, Christine T. H. Davies, Iain D. Kendall, Jonna Koponen, Kit Wong, Eduardo Follana, Elvira Gmiz, G. Peter Lepage, Eike H. Mller, Heechang Na, and Junko Shigemitsu (HPQCD Collaboration), *Phys. Rev. D* 83, 014506 (2011).
- [3] Nikolai Zerf, *PoS RADCOR2015*, 089 (2015).
- [4] T.C. Hammant, A.G. Hart, G.M. von Hippel, R.R. Horgan, and C.J. Monahan, *Phys. Rev. Lett.* 107, 112002 (2011).
- [5] R.J. Dowdall, C.T.H. Davies, T.C. Hammant, and R.R. Horgan, *Phys. Rev. D* 86, 094510 (2012).
- [6] A. Gray, I. Allison, C. T. H. Davies, E. Gulez, G. P. Lepage, J. Shigemitsu, and M. Wingate (HPQCD and UKQCD Collaborations), *Phys. Rev. D* 72, 094507 (2005).
- [7] J.M. Flynn, F. Mescia, and A.S.B. Tariq, *JHEP* 0307, 066 (2003).

- [8] Claude Bernard, Tom Burch, Kostas Orginos, Doug Toussaint, Thomas A. DeGrand, Carleton DeTar, Saumen Datta, Steven Gottlieb, Urs M. Heller, and Robert Sugar, Phys. Rev. D64, 054506 (2001).
- [9] C.T.H. Davies, E. Follana, I.D. Kendall, G.P. Lepage, and C. McNeile, Phys. Rev. D81, 034506 (2010).
- [10] A. Bazavov *et al.*, Rev. Mod. Phys. 82, 1349 (2010), hep-lat/0903.3598.
- [11] K. Orginos and D. Toussaint, Phys. Rev. D59, 014501 (1998).
- [12] K. Orginos, D. Toussaint, and R. L. Sugar, Phys. Rev. D60, 054503 (1999).
- [13] UKQCD collaboration, Ken C. Bowler, Balint Joo, Richard D. Kenway, Chris M. Maynard and Robert J. Tweedie, JHEP 0508:003, 2005 (arXiv:hep-lat/0411005v2)
- [14] Silas R. Beane, Kostas Orginos, and Martin J. Savage, Phys. Lett. B654 (2007) 20-26
- [15] M. Tanabashi *et al.* (Particle Data Group), Phys. Rev. D98, 030001 (2018) and 2019 update.
- [16] Zachary S. Brown, William Detmold, Stefan Meinel, and Kostas Orginos, Phys. Rev. D90, 094507 (2014).
- [17] Nora Brambilla, Antonio Vairo, and Thomas Rösch, Phys. Rev. D72, 034021 (2005).
- [18] Xin-Zhen Weng, Xiao-Lin Chen, and Wei-Zhen Deng, Phys. Rev. D97, 054008 (2018).

Chapter 5

Tetraquark

Very recently, the possible existence of tetraquarks particularly heavy tetraquarks $Z_b(10610)$ and $Z'_b(10650)$, having minimal quark content of four quarks ($b\bar{b}u\bar{d}$) been reported by the Belle Collaboration [1, 2]. These states are thought to be a few MeV above the thresholds of $B^*\bar{B}(10604)$ and $B^*\bar{B}^*(10649.4)$. Along with the heavy tetraquarks possible existence of lighter tetraquarks have been reported in experiments [3, 4, 5, 6]. The Z_b and Z'_b states can couple to at least eight decay channels. Therefore instead of ($b\bar{b}u\bar{d}$) theoretically simpler ($bb\bar{u}\bar{d}$) or ($\bar{b}\bar{b}ud$) states have been extensively studied in the literature. In this thesis we investigate the ($bb\bar{u}\bar{d}$) system. The stability of $QQ\bar{l}\bar{l}$ state in the infinite quark mass limit had been studied in [7, 8, 9] which raised the possibility of existence of heavy four quark bound states below the $Q\bar{l} - Q\bar{l}$ threshold.

Around the same time, lattice QCD has been employed to investigate the bound and/or molecular nature of the heavy tetraquark states, not only to understand the above experimentally observed states but also to identify other possible bound tetraquark states in both 0^+ and 1^+ channels. In the charm sector, some early lattice studies involve T_{cc} and T_{cs} tetraquark states [10], $cc\bar{c}\bar{c}$ [11], $X(3872)$ and $Y(4140)$

[12] and more recently $D_{s_0}^*(2317)$ [13]. The bottom sector received intense attention where, instead of $B^*\bar{B}$ or $B^*\bar{B}^*$, as mentioned before relatively simpler BB , BB^* systems are studied. The lattice investigations this far involve four bottom $bb\bar{b}\bar{b}$ [14] and two bottom tetraquark states $\bar{b}b\bar{l}_1l_2$, where $l_1, l_2 \in c, s, u, d$, [15, 16, 17, 18]. An important observation of these lattice studies is that the possibility of the existence of $bb\bar{l}_1\bar{l}_2$ tetraquark bound states increases with decreasing light quark masses, while they become less bound with decreasing heavy (anti)quark mass.

Besides the usual lattice simulations, the heavy tetraquark systems have also been studied using QCD potential and Born-Oppenheimer approximation [19, 20, 21, 22]. The main idea in this method is to investigate tetraquark states with two heavy (anti)quarks, which was $\bar{b}b$ in the study, and two lighter quarks using quantum mechanical Hamiltonian containing screened Coulomb potential. This approach has been used to explain our two different choices of light u/d quark masses for different classes of tetraquark states.

In the next section we discussed the construction of tetraquark states, having quark content $bb\bar{l}_1\bar{l}_2$ in 1^+ both below and above $B - B^*$ threshold, by a combination of lattice operators and tuning quark masses based on quantum mechanical potential calculation. Here we also explore through variational/GEVP analysis how the trial states created by our operators contribute to the energy eigenstates.

5.1 Doubly bottom tetraquark

For doubly bottom tetraquark we have considered two different kind of operators – the mesonic local diquark-antidiquark tetraquark and molecular 4-quark states. Let us recall that the b quark is expressed in terms of two component ψ_h fields. In Eq.

(3.14), we defined the four component spinor as,

$$Q \equiv \begin{pmatrix} \psi_h \\ 0 \end{pmatrix}. \quad (5.1)$$

The local tetraquark operators for $bb\bar{u}\bar{d}$ having quantum number $I(J^P) = 0(1^+)$ can be constructed as [23]

$$\mathcal{O}_{M_1} \equiv \mathcal{O}_{B^*B} = [\bar{l}_1^a(x)\gamma_k Q^a(x)] [\bar{l}_2^b(x)\gamma_5 Q^b(x)] \quad (5.2)$$

$$\mathcal{O}_{M_2} \equiv \mathcal{O}_{B^*B^*} = \epsilon_{ijk} [\bar{l}_1^a(x)\gamma_j Q^a(x)] [\bar{l}_2^b(x)\gamma_k Q^b(x)] \quad (5.3)$$

$$\mathcal{O}_D \equiv \mathcal{O}_{\mathcal{Q}^*\tilde{\pi}} = [Q^{aT}(x)C\gamma_k Q^b(x)] [\bar{l}_1^a(x)C\gamma_5 (\bar{l}_2^b(x))^T] \quad (5.4)$$

where a, b are color indices. In literature the operators in (5.2) and (5.3) are often referred as ‘‘molecular’’. The diquark-antidiquark 1^+ four quark state $bb\bar{l}_1\bar{l}_2$ with $l_1 \neq l_2$ in (5.4) can actually be defined in two ways [24],

$$\begin{aligned} \mathcal{O}_{\mathcal{Q}^*\tilde{\pi}} &= [Q^{aT}C\gamma_k Q^b] [\bar{l}_1^a C\gamma_5 \bar{l}_2^{bT} - \bar{l}_1^b C\gamma_5 \bar{l}_2^{aT}] \\ \mathcal{O}_{\mathcal{Q}\tilde{\pi}^*} &= [Q^{aT}C\gamma_5 Q^b] [\bar{l}_1^a C\gamma_k \bar{l}_2^{bT} + \bar{l}_1^b C\gamma_k \bar{l}_2^{aT}] \end{aligned} \quad (5.5)$$

with $l_1, l_2 \in u, d$. The subscripts \mathcal{Q}^* and $\tilde{\pi}$ in the operator $\mathcal{O}_{\mathcal{Q}^*\tilde{\pi}}$ are in $\bar{3}_c$ and 3_c respectively, while \mathcal{Q} and $\tilde{\pi}^*$ in the operator $\mathcal{O}_{\mathcal{Q}\tilde{\pi}^*}$ are in 6_c and $\bar{6}_c$. But both $\mathcal{O}_{\mathcal{Q}^*\tilde{\pi}}$ and $\mathcal{O}_{\mathcal{Q}\tilde{\pi}^*}$ correspond to the 1^+ state. Of these the $\mathcal{O}_{\mathcal{Q}^*\tilde{\pi}}$ is our desired ‘‘bound’’ tetraquark operator because one-gluon-exchange interaction is attractive for a heavy quark pair in $\bar{3}_c$ diquark configuration [8] and spin dependent attraction exists for light quark pairs in ‘‘good diquark’’ configuration characterized by color $\bar{3}_c$, spin $J = 0$ and isospin $I = 0$ or $1/2$ [25]. The two terms in $\mathcal{O}_{\mathcal{Q}^*\tilde{\pi}}$ contribute identically in the final correlator, hence we consider only the first term in the calculation. With these considerations

in mind, the operator for the bound tetraquark state is $\mathcal{O}_{\Omega^*\bar{\pi}}$ and the corresponding correlator is

$$C_{DD}(t) = \sum_{\vec{x}} \text{Tr} \left[(G^{ad}(x, 0))^T \gamma_k \gamma_4 \gamma_2 G^{bc}(x, 0) \gamma_4 \gamma_2 \gamma_k \right] \times \text{Tr} \left[\gamma_4 \gamma_2 M_1^{\dagger da}(x, 0) \gamma_4 \gamma_2 \left(\gamma_5 M_2^{\dagger cb}(x, 0) \gamma_5 \right)^T \right] \quad (5.6)$$

The molecular state tetraquark correlators constructed from the operators \mathcal{O}_{B^*B} and $\mathcal{O}_{B^*B^*}$ are

$$C_{M_1 M_1}(t) = \sum_{\vec{x}} \text{Tr} \left[\gamma_5 M_1^{\dagger}(x, 0) \gamma_5 \gamma_k G(x, 0) \gamma_k \right] \times \text{Tr} \left[M_2^{\dagger}(x, 0) G(x, 0) \right] - \sum_{\vec{x}} \text{Tr} \left[G(x, 0) M_2^{\dagger}(x, 0) G(x, 0) \gamma_k \gamma_5 M_1^{\dagger}(x, 0) \gamma_5 \gamma_k \right] \quad (5.7)$$

$$C_{M_2 M_2}(t) = \sum_{\vec{x}} \epsilon_{kij} \epsilon_{klm} \text{Tr} \left[\gamma_5 M_1^{\dagger}(x, 0) \gamma_5 \gamma_i G(x, 0) \gamma_l \right] \times \text{Tr} \left[\gamma_5 M_2^{\dagger}(x, 0) \gamma_5 \gamma_j G(x, 0) \gamma_m \right] - \sum_{\vec{x}} \epsilon_{kij} \epsilon_{klm} \text{Tr} \left[G(x, 0) \gamma_m \gamma_5 M_2^{\dagger}(x, 0) \gamma_5 \gamma_j G(x, 0) \gamma_l \gamma_5 M_1^{\dagger}(x, 0) \gamma_5 \gamma_i \right] \quad (5.8)$$

As we are doing GEVP analysis we need off-diagonal terms also. One such cross correlator is

$$C_{DM_1}(t) = \sum_{\vec{x}} \left[G^{ad}(x, 0) \gamma_k \gamma_5 M_1^{\dagger da}(x, 0) \gamma_5 \gamma_2 \gamma_4 \gamma_5 \right]_{\mu\nu} \times \left[\gamma_2 \gamma_k \gamma_4 G^{bc}(x, 0) \gamma_5 \gamma_5 M_2^{\dagger cb}(x, 0) \gamma_5 \right]_{\mu\nu} \quad (5.9)$$

Traces in Eqs. (5.7) and (5.8) are taken over both the spin and color indices but only over spin indices in Eq. (5.6). The term $\text{Tr} \left[G M_2^{\dagger} G M_1^{\dagger} \right]$ appears only in $C_{M_1 M_1}$, $C_{M_2 M_2}$, $C_{M_1 M_2}$ and $C_{M_2 M_1}$ correlators. The diquark and the anti-diquark part of

\mathcal{O}_D in (5.4) do not have free spinor index and, therefore, we do not have similar $\text{Tr} \left[GM_2^\dagger GM_1^\dagger \right]$ term in C_{DD} . The remaining correlators C_{DM_1} , C_{DM_2} , C_{M_1D} and C_{M_2D} can not be expressed in compact $\text{Tr} \left[GM_1^\dagger \right] \times \text{Tr} \left[G, M_2^\dagger \right]$ form. Like before the heavy quark propagator $G(x, 0)$ has to be rotated to the MILC basis before implementing the equations (5.6), (5.7), (5.8) and (5.9) using the unitary matrix defined in Eq. (3.17).

5.1.1 Quark mass tuning

For molecular tetraquark mass calculation, the m_b tuned in the Chapter 4 is made use of while for $m_{u/d}$ the situation is little tricky. In our previous study [26] we found that the B -meson tuned $m_{u/d}$ reproduces the mass of Σ_b baryon but not that of Λ_b . Therefore, we tuned $m_{u/d}$ to two different values depending on the construction of the pairs $[ud]$ and $[bu]$ or $[bd]$. The motivation to do so followed from the observation that substantial mass difference exist among singly heavy baryons having same quark content and same J^P . For instance, the mass differences between the $J^P = \frac{1}{2}^+$ pairs $(\Lambda_b, \Sigma_b [bdu])$, $(\Lambda_c, \Sigma_c [cdu])$, $(\Xi_b, \Xi'_b [bsu])$ and $(\Xi_c, \Xi'_c [csu])$ are in the range 110–190 MeV. The Λ_b , Λ_c , Ξ_b and Ξ_c baryons are characterized by the spin of the $[l_1 l_2]$ (where $l_{1,2} \in u, d, s$) light-light diquark $s_l = 0$ while Σ_b , Σ_c , Ξ'_b and Ξ'_c by $s_l = 1$. This differences in their wave functions alone cannot generate such mass differences [27] but can at most account for a difference of about 30 MeV. The heavy hadron chiral perturbation theory calculations [28, 29] for Λ_Q and Σ_Q , where $Q \in b, c$, demonstrated that the mass differences get large correction of the order ≈ 150 MeV. A correction of similar magnitude is anticipated in our NRQCD-HISQ heavy baryon / tetraquark systems, but the relevant χ PT for which is yet to be available. To include such a correction in our calculations, we propose this unique method of tuning the $[\bar{u}\bar{d}]$ diquark system to Λ_b -baryon and $[b\bar{u}]$ to B -meson.

We tried to understand this tuning scheme in more details with the help of relativised quark model [30, 31] and Hartree-Fock calculation. The basic idea is that $m_{u/d}$ has to be tuned to two different values corresponding to two different constructions of the pairs $[\bar{u}\bar{d}]$ and $[b\bar{u}]$. In the operator $\mathcal{O}_D \equiv [bb][\bar{u}\bar{d}]$, the antiquark part formed with two light u/d quarks is the same that appear in the baryonic operator $\Lambda_b \equiv (u^T C \gamma_5 d) b$, and hence, we use experimental Λ_b mass 5620 MeV to tune the bare $am_{u/d}$. For the operators \mathcal{O}_{M_1/M_2} , the diquark part is formed between heavy quark and light antiquark $[b\bar{u}]$ which is the same as in the B -meson $(\bar{b}\gamma_{(5,k)}u)$ or $\Sigma_b \equiv (Q^T C \gamma_5 u) u$. In such case we tend to use B -meson mass 5279 MeV to tune the $am_{u/d}$.

For molecular tetraquark state, we assumed that the light antiquark wave functions do not overlap with each other significantly and they are effectively in the potential of their respective heavy b quarks [20] *i.e.* a two B -meson like system shown in Figure 5.1.

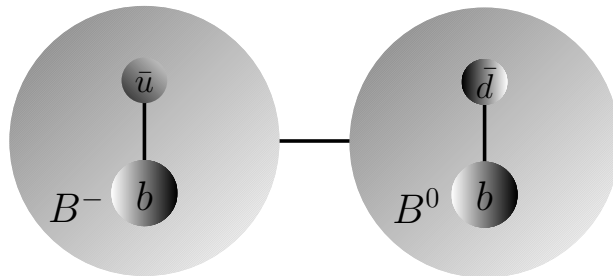


Figure 5.1: Molecular tetraquark state viewed as bound state of two B mesons, which is similar to two hydrogen atoms forming a hydrogen molecule.

Then for each B meson, the light \bar{u}/\bar{d} antiquark is taken to be in the field of “static” b quark and we solve the problem by considering the radial part of the Schrödinger equation numerically using suitably modified Herman-Skillman code [32]. Employing the relativised quark model we numerically calculate the mass of B meson

using the light antiquark mass as parameter.

$$-\frac{1}{2m_{u/d}} \frac{d^2 U(r)}{dr^2} + V(r)U(r) = EU(r) \quad (5.10)$$

Here $U(r) = r\psi(r)$ and the potential $V(r)$ is given by

$$V(r) = -\frac{4\alpha}{3r} + \beta r \quad (5.11)$$

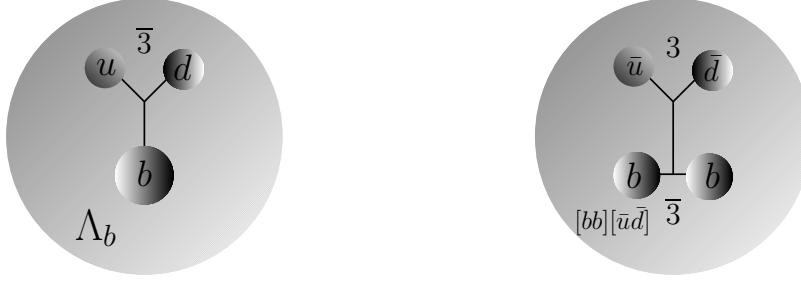
The B meson mass M_B is, therefore, determined from the energy eigenvalue E ,

$$M_B = m_b + m_{u/d} + E \quad (5.12)$$

where $m_b = 4.18$ GeV ($\overline{\text{MS}}$) is the mass of the bottom quark, the $\alpha = \pi/16$ [21] and $\beta = 0.18$ GeV² [30]. For $M_B = 5.279$ GeV, the light quark mass obtained is $m_{u/d} \approx 0.227$ GeV.

For bound tetraquark state, we assumed that the heavy b quarks stay close to each other and they form nearly static heavy “nucleus” which gets surrounded by light \bar{u}, \bar{d} antiquark cloud. The light \bar{u}, \bar{d} antiquarks are assumed to form spin antisymmetric “good antiquark” in bound tetraquark state. This picture of bound tetraquark has striking similarity with Λ_b baryon where the heavy b quark gets surrounded by light u, d quark cloud. The u, d quarks also form spin antisymmetric “good diquark” in Λ_b . In Figure 5.2 we schematically depicted the similarity between Λ_b and bound tetraquark.

With this motivation we solve for Λ_b baryon using Hartree-Fock method. Like before, we numerically calculated Λ_b baryon mass using the light antiquark mass as



(a) u/d quarks in Λ_b baryons form a $\bar{3}_c$ diquark in presence of a b quark. (b) Like Λ_b , two b quarks form a (nearly) static nucleus surrounded by \bar{u}, \bar{d} cloud.

Figure 5.2: Schematic diagram of helium-like Λ_b and $[bb][\bar{u}\bar{d}]$ tetraquark state used for Hartree-Fock treatment.

parameter. The Hamiltonian for Λ_b baryon is

$$\begin{aligned}
 H = & -\frac{1}{2m_{u/d}}\nabla_1^2 - \frac{2\alpha}{3r_1} + \frac{\beta r_1}{2} - \frac{1}{2m_{u/d}}\nabla_2^2 - \frac{2\alpha}{3r_2} + \frac{\beta r_2}{2} \\
 & -\frac{2\alpha'}{3r_{12}} + \frac{\beta' r_{12}}{2}
 \end{aligned} \tag{5.13}$$

where r_{12} is the relative distance between two light quarks “orbiting” the heavy b quark and their interaction potential is the last two terms in the equation (5.13) with coefficient α' and β' . For the Hartree-Fock calculation of the energy E , we take $\beta' = \beta$ and $\alpha' = 0.6$ [30].

To solve the Hamiltonian (5.13), we consider the trial wave function, which is space-symmetric and spin-antisymmetric, in terms of Slater determinant

$$\Psi^{\text{HF}} = \frac{1}{\sqrt{2}} \begin{vmatrix} \chi_1(x_1) & \chi_1(x_2) \\ \chi_2(x_1) & \chi_2(x_2) \end{vmatrix}, \tag{5.14}$$

where $x_i \equiv (\vec{r}, s)$ collectively denotes the space and spin indices, $\chi_i(\vec{r}, s) = \phi_{is}(\vec{r}) \mathfrak{S}(s)$ with $\phi(\vec{r})$ being the 1S state. Therefore, the expectation value of the the Hamiltonian

can be written as

$$\begin{aligned}
\langle \Psi^{\text{HF}} | H | \Psi^{\text{HF}} \rangle &= \langle T \rangle + \int \rho(\vec{r}) V_{\text{ext}}(\vec{r}) d\vec{r} - \frac{Z'}{2} \iint \frac{\rho(\vec{r})\rho(\vec{r}_1)}{|\vec{r} - \vec{r}_1|} d\vec{r} d\vec{r}_1 \\
&+ \frac{B'}{2} \iint \rho(\vec{r}) \rho(\vec{r}_1) |\vec{r} - \vec{r}_1| d\vec{r} d\vec{r}_1 \\
&+ \frac{Z'}{2} \sum_{i,j,s} \iint \frac{\phi_{i,s}^*(\vec{r}) \phi_{j,s}^*(\vec{r}_1) \phi_{i,s}(\vec{r}_1) \phi_{j,s}(\vec{r})}{|\vec{r} - \vec{r}_1|} d\vec{r} d\vec{r}_1 \\
&- \frac{B'}{2} \sum_{i,j,s} \iint \phi_{i,s}^*(\vec{r}) \phi_{j,s}^*(\vec{r}_1) \phi_{i,s}(\vec{r}_1) \phi_{j,s}(\vec{r}) |\vec{r} - \vec{r}_1| d\vec{r} d\vec{r}_1
\end{aligned} \tag{5.15}$$

where, we have used

$$\begin{aligned}
\langle T \rangle &= \sum_{i,s} \left\langle \phi_{i,s}(\vec{r}) \left| -\frac{1}{2m_{u/d}} \nabla^2 \right| \phi_{i,s}(\vec{r}) \right\rangle \\
&= -\frac{1}{2m_{u/d}} \sum_{i,s} \int \phi_{i,s}^*(\vec{r}) \nabla^2 \phi_{i,s}(\vec{r}) d\vec{r} \\
\rho(\vec{r}) &= \sum_{i,s} |\phi_{i,s}(\vec{r})|^2 = \sum_{i,s} \phi_{i,s}^*(\vec{r}) \phi_{i,s}(\vec{r}) \\
V_{\text{ext}}(\vec{r}) &= -\frac{2\alpha}{3r} + \frac{\beta r}{2} \\
Z' &= \frac{2\alpha'}{3} \quad \text{and} \quad B' = \frac{\beta'}{2}.
\end{aligned}$$

Here the integrations over $d\vec{r}$ or $d\vec{r}_1$ in equation (5.15) and in the subsequent ones denote the volume integration. In contrast to the helium atom, the presence of linear r -terms *i.e.* the terms containing β or β' in the Hamiltonian given in equation (5.13) leads to additional exchange-energy terms in the calculation. Variation with respect to $\phi_{i,s}^*(\vec{r})$

$$\frac{\delta}{\delta \phi_{i,s}^*(\vec{r})} [\langle \Psi^{\text{HF}} | H | \Psi^{\text{HF}} \rangle - E \langle \Psi^{\text{HF}} | \Psi^{\text{HF}} \rangle] = 0 \tag{5.16}$$

and using $\frac{\delta\phi_{j_s}^*(\vec{r}_1)}{\delta\phi_{i_s}^*(\vec{r})} = \delta(\vec{r}_1 - \vec{r}) \delta_{ij}$ leads to the Hartree-Fock equation

$$\begin{aligned}
E \phi_{i_s}(\vec{r}) = & \left[-\frac{1}{2m_{u/d}} \nabla^2 + V_{\text{ext}}(\vec{r}) - Z' \int \frac{\rho(\vec{r}_1)}{|\vec{r} - \vec{r}_1|} d\vec{r}_1 + B' \int \rho(\vec{r}_1) |\vec{r} - \vec{r}_1| d\vec{r}_1 \right] \phi_{i_s}(\vec{r}) \\
& - B' \sum_{j,s} \int \phi_{j_s}^*(\vec{r}_1) \phi_{i_s}(\vec{r}_1) \phi_{j_s}(\vec{r}) |\vec{r} - \vec{r}_1| d\vec{r}_1 \\
& + Z' \sum_{j,s} \int \frac{\phi_{j_s}^*(\vec{r}_1) \phi_{i_s}(\vec{r}_1) \phi_{j_s}(\vec{r})}{|\vec{r} - \vec{r}_1|} d\vec{r}_1
\end{aligned} \tag{5.17}$$

We solve for E in equation (5.17) iteratively and, eventually, the Λ_b mass is calculated from

$$M_{\Lambda_b} = m_b + 2m_{u/d} + E \tag{5.18}$$

The PDG value of $\Lambda_b(5620)$ is obtained by setting the $m_{u/d}$ to 0.157 GeV.

In Table 5.1, we compare the nonperturbatively tuned $m_{u/d}$ on our lattices with those obtained by solving the equations (5.10) and (5.17). The bare lattice light quark masses cannot be directly compared to the parameter $m_{u/d}$ in these equations mainly because of the use of renormalized b quark mass (in $\overline{\text{MS}}$ scheme) in the Hartree-Fock calculation. Therefore, the $m_{u/d}$'s in the above calculation return a sort of “renormalized constituent” quark mass. Nonetheless it is obvious that we need two different $m_{u/d}$ for two different systems, namely B and Λ_b . So by comparing the two sets, we simply wish to point out that the lattice tuned $m_{u/d}$'s are in same order of magnitude as Schrödinger equation based quark model but have a difference of 10 – 15%. This helps us to understand the possible physics behind two different tuning of light quark mass in determining the masses of single bottom hadron(s) and double bottom tetraquark states.

Lattice	B meson: $m_{u/d} = 227$ MeV		Λ_b baryon: $m_{u/d} = 157$ MeV	
	$am_{u/d}$	$m_{u/d}$ (MeV)	$am_{u/d}$	$m_{u/d}$ (MeV)
$16^3 \times 48$	0.155	204	0.105	138
$20^3 \times 64$	0.118	194	0.083	137
$28^3 \times 96$	0.087	191	0.064	143

Table 5.1: Comparison of $m_{u/d}$ obtained from various lattices with quark mass parameters in the equations (5.10) and (5.17).

5.1.2 $bb\bar{u}\bar{d}$ spectrum

In the Figure 5.3 we presented the variation of tetraquark mass with the entire range of bare u/d quark masses given in the Table 4.4. For clarity in comparing with existing results, we choose to plot our results for $16^3 \times 48$ lattice. The vertical lines denote the u/d and s bare quark masses at which the shown hadronic states are achieved.

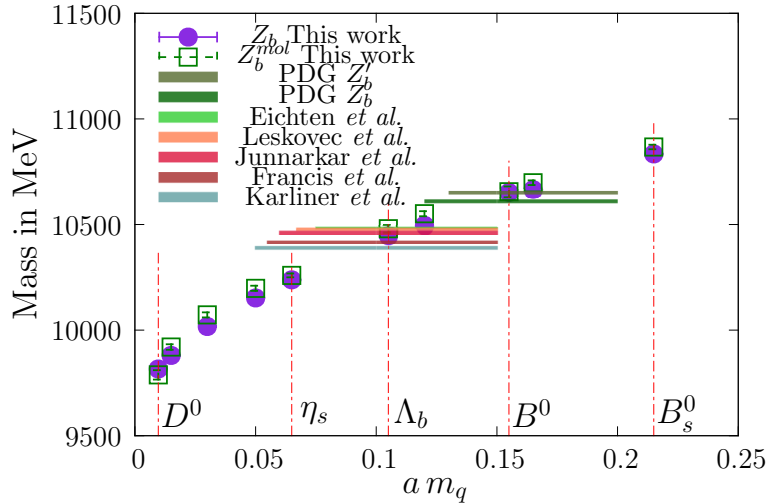


Figure 5.3: Variation of tetraquark mass in MeV versus am_q . The $am_q = 0.105$ and 0.155 are the Λ_b and B^0 tuned u/d quark masses.

It is interesting to note that the lattice results Eichten *et al.* [8], Karliner *et al.* [9], Francis *et al.* [15], Junnarkar *et al.* [17], Luka *et al.* [18] and the PDG value [37] are clustered around two significantly different masses. All the lattice data sort of

overlap at Λ_b data point supporting the possibility of capturing a bound tetraquark state $[bb][\bar{l}\bar{l}]$ much like $b[l_1l_2]$ state like Λ_b . But the PDG results agree rather well with our data at B^0 point implying a likely molecular state of the form $[b\bar{l}][\bar{b}l]$ which aligned with the idea that $Z_b(10610)$ and $Z'_b(10650)$ decay mostly into $\bar{B}B^*$ and \bar{B}^*B^* respectively. The masses of these states also lie a few MeV above the corresponding thresholds. This picture seems to favour the molecular configuration for Z_b and Z'_b .

To understand the “goodness” of our various tetraquark operators and to have an idea of possible fit range we plot the effective masses of $|D\rangle$ and $|M_1\rangle$ states obtained at different lattice spacings together with the lattice thresholds for easy comparison. The colored bands represent fitted am_{eff} values. The superscripts Λ_b and B denote the light quark tuning.

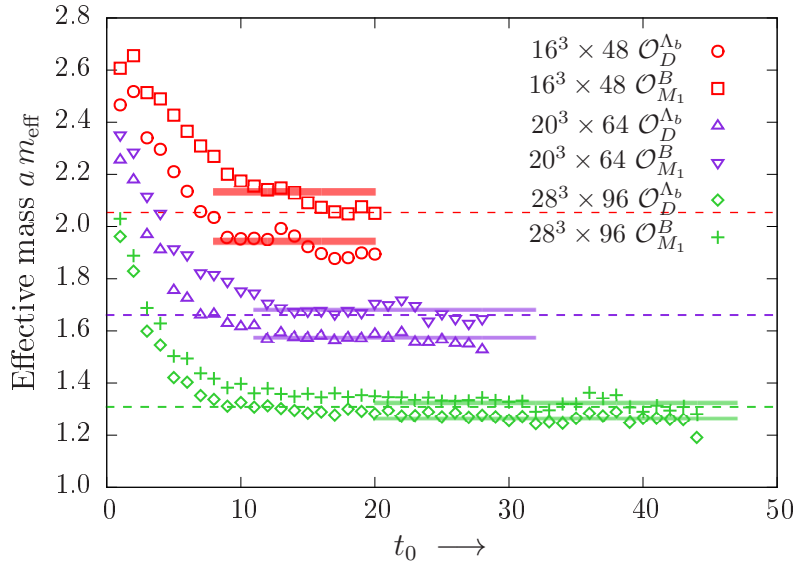


Figure 5.4: Effective mass plot of the states of the operators \mathcal{O}_D and \mathcal{O}_{M_1} calculated on $16^3 \times 48$, $20^3 \times 64$ and $28^3 \times 96$ lattices. Dashed lines are $B - B^*$ thresholds for different lattices. For easy viewing, the effective masses and thresholds on $20^3 \times 64$ (purple colored) are multiplied by a common factor of 0.85, while that of $28^3 \times 96$ (green colored) by 0.70.

In the Tables 5.2 and 5.3, we present our results of the tetraquark states corre-

sponding to the operators given in the expressions (5.2, 5.3, 5.4). We call these states $\mathcal{O}_X^\dagger|\Omega\rangle \equiv |X\rangle$ as trial states. We use two-exponential uncorrelated fit to the correlation functions, the fitting range being chosen by looking at the positions of what we consider plateau in the effective mass plots. We present the masses in lattice unit $a E_{\text{latt}}$ in Table 5.2 and in physical unit M_{latt} (MeV) in Table 5.3, the notations being introduced in equation (4.3). The errors quoted are statistical, calculated assuming the lattice configurations of different lattice spacings are statistically uncorrelated. The second column of both the Tables shows the tuning used for the corresponding states. In the last column of Table 5.3 we provide the masses averaged over all the lattice ensembles.

Operators	Tuning	$16^3 \times 48$	$20^3 \times 64$	$28^3 \times 96$
		aE_{latt}	aE_{latt}	aE_{latt}
$\mathcal{O}_D = [bb][\bar{u}\bar{d}]$	Λ_b	1.944(5)	1.852(3)	1.803(5)
$\mathcal{O}_{M_1} = [b\bar{u}][b\bar{d}]$	B	2.133(7)	1.977(4)	1.892(6)
$\mathcal{O}_{M_2} = \epsilon_{ijk}[b\bar{u}]_j[b\bar{d}]_k$	B	2.124(7)	1.974(4)	1.890(5)
$B = b\gamma_5\bar{u}$	B	1.022(3)	0.974(3)	0.931(3)
$B^* = b\gamma_k\bar{u}$	B^*	1.032(3)	0.980(3)	0.938(2)

Table 5.2: Masses of tetraquark states for different $am_{u/d}$ tuning in lattice unit aE_{latt} . We also include the B and B^* states that are used for threshold calculation.

Operators	Tuning	$16^3 \times 48$	$20^3 \times 64$	$28^3 \times 96$	Average (MeV)
		M_{latt}	M_{latt}	M_{latt}	
$\mathcal{O}_D = [bb][\bar{u}\bar{d}]$	Λ_b	10418(7)	10422(5)	10407(11)	10417(9)
$\mathcal{O}_{M_1} = [b\bar{u}][b\bar{d}]$	B	10667(10)	10628(5)	10602(13)	10638(27)
$\mathcal{O}_{M_2} = \epsilon_{ijk}[b\bar{u}]_j[b\bar{d}]_k$	B	10655(8)	10623(5)	10560(10)	10623(35)
$B = b\gamma_5\bar{u}$	B	5274(4)	5290(3)	5268(3)	5279(10)
$B^* = b\gamma_k\bar{u}$	B^*	5288(4)	5300(4)	5284(3)	5292(8)

Table 5.3: Masses of tetraquark states for different $am_{u/d}$ tuning (M_{latt}) in MeV.

From the Fig. 5.4 and Table 5.3 it is clear that the trial state generated by our \mathcal{O}_D operator is below $B - B^*$ threshold which possibly indicates a bound state. On

the other hand, the states generated by \mathcal{O}_{M_1} and \mathcal{O}_{M_2} are just above it. We tabulate the difference of the masses from their respective thresholds $\Delta M_{D/M_1/M_2} = M_{D/M_1/M_2} - M_B - M_{B^*}$ in the Table 5.4. In this table, we calculated the following correlator ratio to determine the mass differences which gives us an estimate of the binding energy,

$$C_{X-B-B^*}(t) = \frac{C_X(t)}{C_B(t) \times C_{B^*}(t)} \sim e^{-(M_X - M_B - M_{B^*})t} \quad (5.19)$$

Here we want to inform the reader that though Eq.(5.19) is commonly used to determine the mass splittings but it can lead to false plateaus [35]. This can happen due to the fact that the $B - B^*$ scattering states can contribute differently in $|D\rangle$, $|M_1\rangle$, $|M_2\rangle$ excited states which might persist at large t . In the present analysis, we have assumed these contributions are of same order of magnitude and cancel each other at moderately large t .

Operators	Lattices	$a \Delta M_X$	ΔM_X in MeV	$\overline{\Delta M_X}$ (MeV)
\mathcal{O}_D	$16^3 \times 48$	-0.125(12)	-164(16)	-167(19) this work
	$20^3 \times 64$	-0.108(10)	-177(16)	-215(12) [9]
	$28^3 \times 96$	-0.070(10)	-155(22)	-189(10) [15]
				-143(34) [17]
				-128(34) [18]
\mathcal{O}_{M_1}	$16^3 \times 48$	0.070(12)	92(16)	65(29) this work
	$20^3 \times 64$	0.026(11)	43(18)	see Table VI [18]
	$28^3 \times 96$	0.024(9)	53(20)	
\mathcal{O}_{M_2}	$16^3 \times 48$	0.070(16)	92(21)	63(30) this work
	$20^3 \times 64$	0.022(9)	36(20)	
	$28^3 \times 96$	0.020(10)	44(21)	

Table 5.4: Mass differences of “bound” $|D\rangle$ and “molecular” $|M_1\rangle$, $|M_2\rangle$ states from $B - B^*$ threshold. The X subscript denotes any of the D , M_1 , M_2 .

In the last column, we calculate our lattice average of ΔM_X in MeV and compare with some of the previous lattice results. To our knowledge, the binding energies of

the $|M_1\rangle, |M_2\rangle$ states have been calculated in the framework of chiral quark model [36] for $B - \bar{B}^*$ and $B^* - \bar{B}^*$ states but there are no lattice results. But the binding energies for the first excited states, along with the ground states, obtained on different lattice ensembles are given in [18]. Though their tuning of light quark mass is very different compared to ours, still we can use their result as a reference.

As we know, on lattice the operators for states having the same quantum numbers can mix and, therefore, a GEVP analysis can help resolve the issue of mutual overlap of various states on the energy eigenstates. In this work, rather than the energies of the eigenstates, we are more interested to learn the overlap of our trial states, namely $|D\rangle, |M_1\rangle$ and $|M_2\rangle$ on the first few energy eigenstates, where $|0\rangle$ is the ground state and $|1\rangle, |2\rangle$ etc. are the excited states.

5.1.3 Variational analysis

For the 2-bottom tetraquark system with quantum number 1^+ , we consider the three local operators – “good” diquark \mathcal{O}_D , molecular \mathcal{O}_{M_1} and vector meson kind \mathcal{O}_{M_2} as defined above in the expressions (5.2 – 5.4) – to capture the ground state ($|0\rangle, \mathcal{E}_0$) and possibly the first excited state ($|1\rangle, \mathcal{E}_1$).

As is generally understood, these operators are expected to have overlap with the desired ground and excited states of the tetraquark system of our interest. The variational analysis can be performed to determine the eigenvalues and the eigenvectors from the mixed states formed by lattice operators. This is typically achieved by constructing a correlation matrix involving the lattice operators \mathcal{O}_X and \mathcal{O}_Y ,

$$\begin{aligned}
C_{XY}(t) &= \langle \mathcal{O}_X(t) \mathcal{O}_Y^\dagger(0) \rangle \\
&= \sum_{m=0}^{\infty} \langle \Omega | \mathcal{O}_X | m \rangle \langle m | \mathcal{O}_Y^\dagger | \Omega \rangle e^{-E_m t}
\end{aligned} \tag{5.20}$$

where X, Y can either be all or any two combinations of D, M_1, M_2 in the expressions (5.2 – 5.4). The terms $\langle n | \mathcal{O}_X^\dagger | \Omega \rangle$ are the coefficients of expansion of the trial states $\mathcal{O}_X^\dagger | \Omega \rangle$, where $|\Omega\rangle$ is the vacuum state, and expanded in the energy eigenbasis $|m\rangle$ as,

$$\mathcal{O}_X^\dagger | \Omega \rangle = \sum_m |m\rangle \langle m | \mathcal{O}_X^\dagger | \Omega \rangle \equiv \sum_m Z_X^m |m\rangle \quad (5.21)$$

Presently, we are interested in expressing the energy eigenstates in terms of the trial states to understand the contribution of each to the former. If we confine ourselves to the first few energy eigenstates, we can write

$$|m\rangle = \sum_X v_m^X \mathcal{O}_X^\dagger | \Omega \rangle \Rightarrow \langle l | m \rangle = \delta_{lm} \approx \sum_X v_m^X Z_X^l \quad (5.22)$$

The v_m^X are equivalent to the eigenvector components obtained by solving a GEVP w.r.t a suitably chosen reference time t_0 [13],

$$C(t) v_m(t, t_0) = \lambda_m(t) C(t_0) v_m(t, t_0). \quad (5.23)$$

The eigenvalues $\lambda_m(t)$ are directly related to energy of m -th state, *i.e.* ground and the first few excited states of our system through the relation

$$\lambda_m(t) = A_m e^{-\mathcal{E}_m(t-t_0)} \quad (5.24)$$

The component of eigenvectors $v_m(t, t_0)$ gives information about the relative overlap of the three local operators to the m -th eigenstate. The eigenvectors v_m 's are normalized to 1.

To determine the parameter t_0 , we solve the GEVP and found that the ground and excited state energies are almost independent for $t_0 = 3, 5, 7, 9$ as demonstrated

in the Fig. 5.5. In this plot, we showed our results for Λ_b -tuned $am_{u/d}$ for all the operators \mathcal{O}_X but the results are similar with B tuning and, hence, not shown. We want to mention here in passing that we have used the Λ_b tuning whenever all three \mathcal{O}_D , \mathcal{O}_{M_1} , \mathcal{O}_{M_2} operators are made use of. We chose $t_0 = 5$ for our calculations.

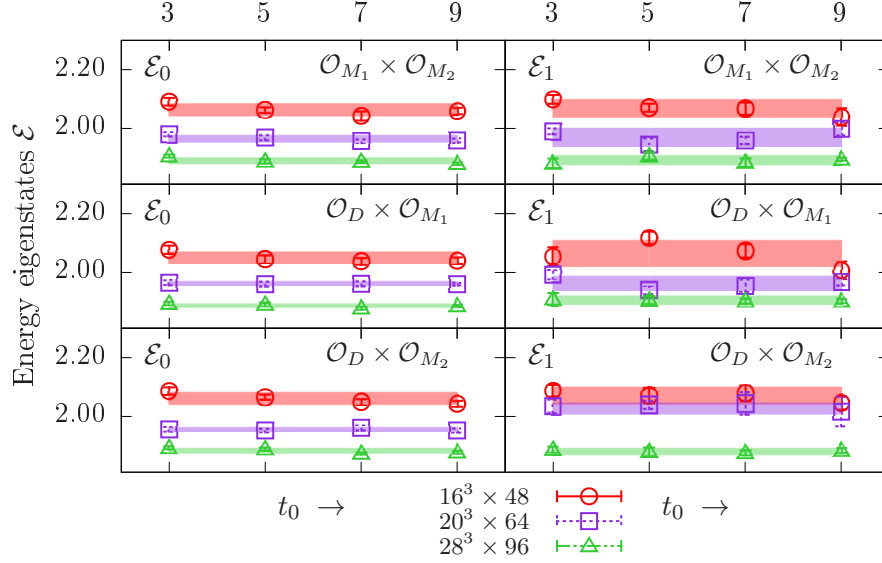


Figure 5.5: Variation of ground and excited state energies \mathcal{E}_m of the equation (5.24) with t_0 , obtained by solving 2×2 GEVP of the correlation matrices $\mathcal{O}_{M_1} \times \mathcal{O}_{M_2}$, $\mathcal{O}_D \times \mathcal{O}_{M_1}$ and $\mathcal{O}_D \times \mathcal{O}_{M_2}$. In this plot we used Λ_b -tuned $am_{u/d}$ for all the operators.

The GEVP analysis has been carried out in two steps because of differences in the tuning of $am_{u/d}$ for the “molecular” states $|M_1\rangle$, $|M_2\rangle$ and “good” diquark state $|D\rangle$. In the first step, we will do a GEVP with the B -tuned molecular operators and determine the difference of its lowest energy state from the threshold, as these states are found to coincide with experimentally observed states. In the next step, we have done the GEVP analysis with all three operators using Λ_b tuning to understand the state(s) below the threshold.

In the Table 5.5 we have shown our GEVP results of B -tuned $\mathcal{O}_{M_1} \times \mathcal{O}_{M_2}$ and the Λ_b -tuned $\mathcal{O}_D \times \mathcal{O}_{M_1} \times \mathcal{O}_{M_2}$ correlation matrices. The energy eigenstates $\mathcal{E}_{0,1,2}$ correspond to the \mathcal{E}_m of the expression (5.24). In the Table 5.6, we calculated the energy difference of the eigenstates $|0\rangle, |1\rangle$ etc. from their corresponding thresholds. Values given in the first row for each lattices are in lattice units while in the second row they are presented in MeV. We often find the energies of the highest states are very noisy and consequently the separation from the thresholds $\Delta\mathcal{E}$ have large errors, hence their entries are kept vacant. We can only reliably quote the lowest for 2×2 , and first two lowest energies for 3×3 correlator matrices.

Correlation matrix	Tuning	Energy	$16^3 \times 48$	$20^3 \times 64$	$28^3 \times 96$
$\mathcal{O}_{M_1} \times \mathcal{O}_{M_2}$	B meson	\mathcal{E}_0	2.063(10)	1.959(12)	1.888(7)
		\mathcal{E}_1	2.071(10)	1.969(20)	1.906(18)
$\mathcal{O}_D \times \mathcal{O}_{M_1} \times \mathcal{O}_{M_2}$	Λ_b baryon	\mathcal{E}_0	1.898(7)	1.846(5)	1.784(12)
		\mathcal{E}_1	1.905(10)	1.851(7)	1.816(8)
		\mathcal{E}_2	1.917(18)	1.856(15)	1.820(22)

Table 5.5: Energy eigenvalues in lattice unit from GEVP analysis of the B -tuned $\mathcal{O}_{M_1} \times \mathcal{O}_{M_2}$ and Λ_b -tuned $\mathcal{O}_D \times \mathcal{O}_{M_1} \times \mathcal{O}_{M_2}$.

Lattice	Threshold	$\mathcal{O}_{M_1} \times \mathcal{O}_{M_2}$		$\mathcal{O}_D \times \mathcal{O}_{M_1} \times \mathcal{O}_{M_2}$		
		$\Delta\mathcal{E}_0$	$\Delta\mathcal{E}_1$	$\Delta\mathcal{E}_0$	$\Delta\mathcal{E}_1$	$\Delta\mathcal{E}_2$
$16^3 \times 48$ (0.15 fm)	2.054(3) 10562	0.010(7) 13(9)	0.016(6) 21(8)	-0.154(10) -202(13)	-0.149(15) -196(20)	-0.137(23) -
$20^3 \times 64$ (0.12 fm)	1.954(3) 10590	0.010(9) 16(15)	- -	-0.110(9) -181(15)	-0.104(10) -173(17)	-0.099(19) -
$28^3 \times 96$ (0.09 fm)	1.869(3) 10552	0.012(10) 26(22)	- -	-0.085(10) -186(22)	-0.053(10) -117(22)	- -

Table 5.6: Energy differences from the $B - B^*$ threshold of the GEVP values of Table 5.5 for the $\mathcal{O}_{M_1} \times \mathcal{O}_{M_2}$ and Λ_b -tuned $\mathcal{O}_D \times \mathcal{O}_{M_1} \times \mathcal{O}_{M_2}$ correlation matrices. Threshold values are taken from Table 5.2.

Next we look at the contribution of \mathcal{O}_{M_1} and \mathcal{O}_{M_2} in constructing the lowest molecular energy eigenstate $|0\rangle$.

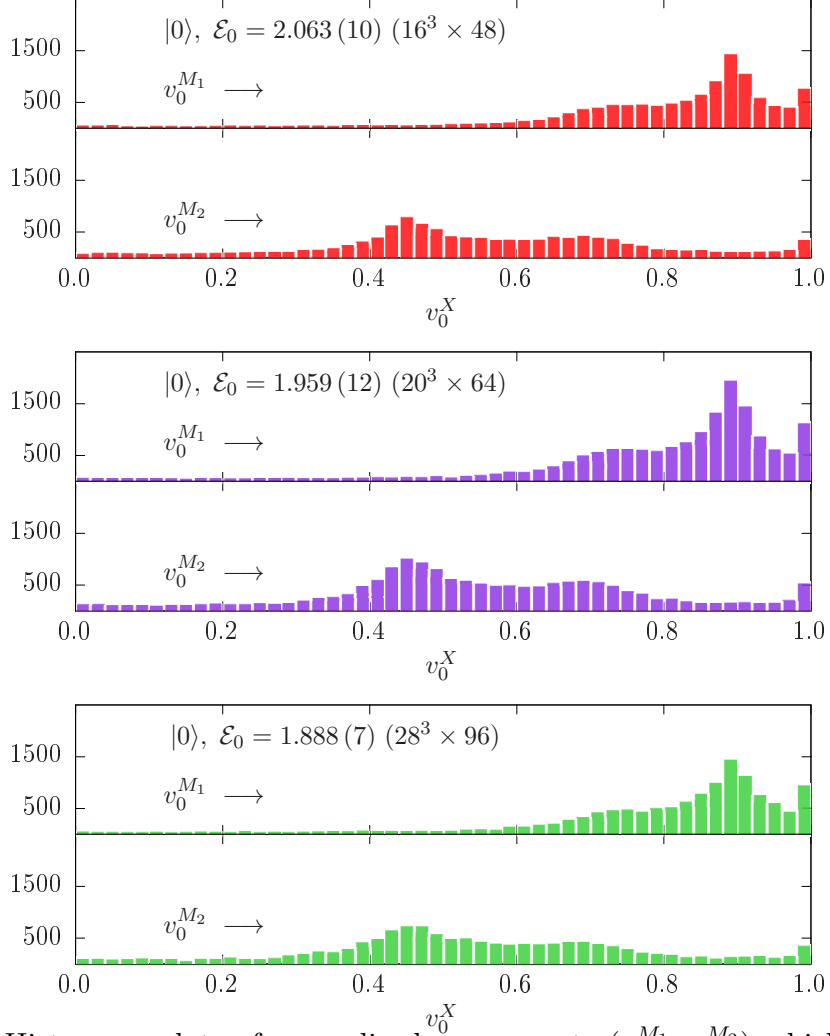


Figure 5.6: Histogram plots of normalized components $(v_0^{M_1}, v_0^{M_2})$ which define the energy eigenstate $|0\rangle = v_0^{M_1}|M_1\rangle + v_0^{M_2}|M_2\rangle$.

In the Fig. 5.6, we plot the histogram of the components of the normalized eigenvectors

$$v_0 = (v_0^{M_1}, v_0^{M_2})$$

corresponding to the lowest energy \mathcal{E}_0 for all three lattices. Assuming that the coefficients $v_0^{M_1, M_2}$ approximately remain the same on all time slices and for all the individual gauge configurations of an ensemble, the histogram figures are obtained

by plotting the M_1 , M_2 components of normalized eigenvector v_0 for all time points and individual gauge configurations. As is expected, all three lattices return identical histogram of the coefficients and hence, in the subsequent histogram plots we will show only the results from $28^3 \times 96$. The eigenvector component $v_0^{M_1}$ shows a peak around 0.9 indicating the lowest energy state $|0\rangle$ receives dominant contribution from $|M_1\rangle$ trial state. We recall here that \mathcal{O}_{M_1} corresponds to the $B - B^*$ molecular state as defined in the equation (5.2).

However, the first excitation $|1\rangle$, for which our data is rather noisy to reliably estimate ΔM , the $|M_1\rangle$ and $|M_2\rangle$ states appear to have comparable contribution and are broadly distributed over different time slices and vary significantly over configurations. This is evident from the histogram plot in the Fig. 5.7. This may have a bearing with the fact that above the threshold, the molecular tetraquark can couple to multiple decay channels resulting in a broad spectrum.

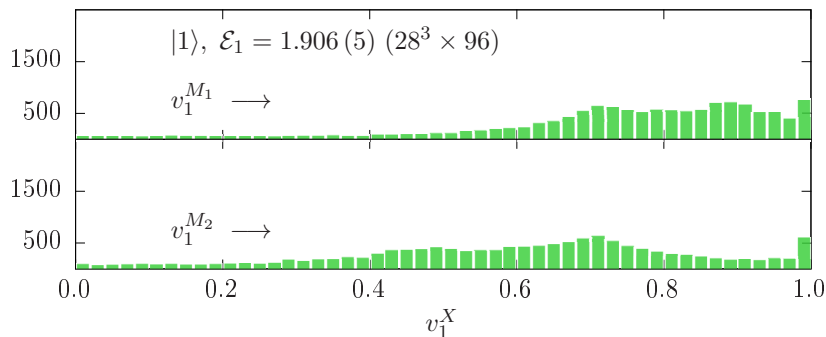


Figure 5.7: The histogram plot of $v_1^{M_1}$ and $v_1^{M_2}$ that define the energy eigenstate $|1\rangle = v_1^{M_1}|M_1\rangle + v_1^{M_2}|M_2\rangle$.

Including \mathcal{O}_D along with the \mathcal{O}_{M_1} and \mathcal{O}_{M_2} to form a 3×3 correlation matrix requires using either Λ_b tuned $am_{u/d}$ in all three trial states. An important issue here is to interpret what Λ_b tuning meant for $B - B^*$ meson system (or, conversely, what

B tuning is meant for Λ_b like system). Certainly, a B -tuned bound $|D\rangle$ state above threshold is not well-defined and we find it has statistically small and varying overlap with the energy eigenstates much like in Fig. 5.7. On the other hand, Λ_b tuned molecular states can possibly have finite overlap to the eigenstates below threshold. However, we always expect dominance of $|D\rangle$ in $|0\rangle$ because of the difference in construction of wave functions of the $|M_1\rangle$ and $|M_2\rangle$.

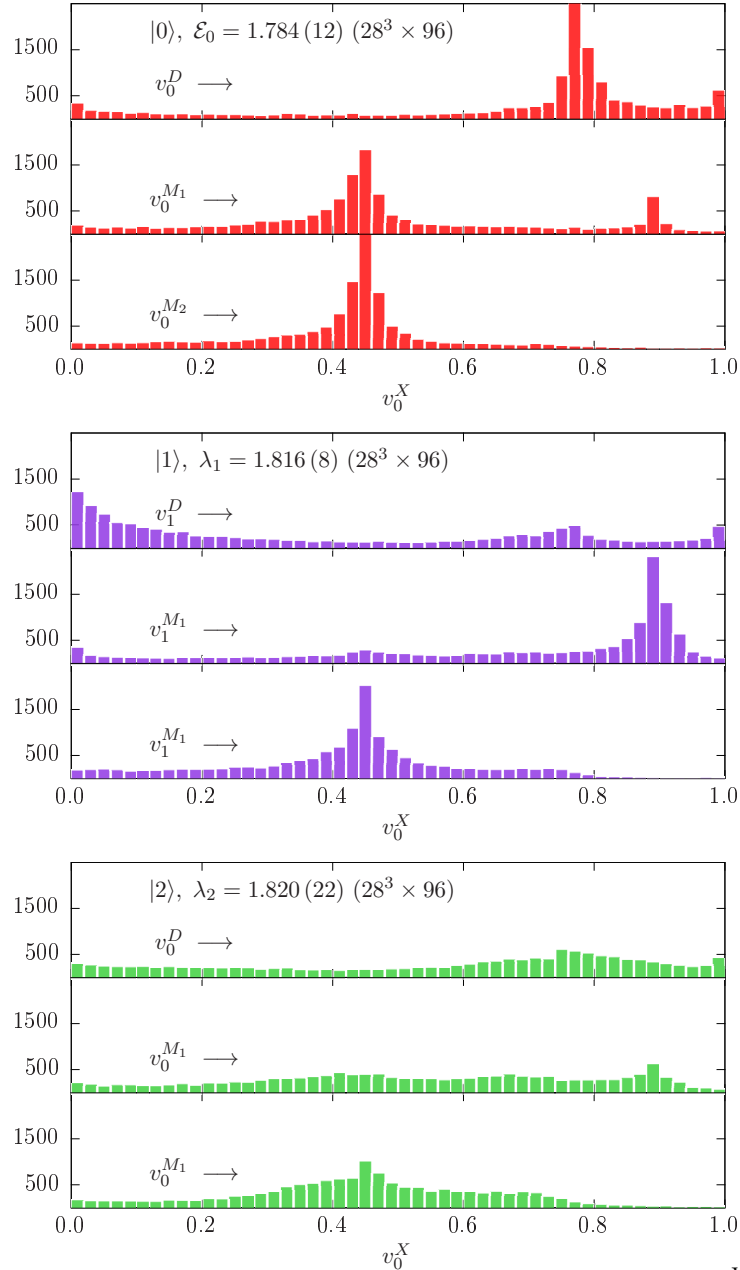


Figure 5.8: Histogram plots of normalized eigenvector components v_0^X , v_1^X and v_2^X of 3×3 correlation matrix, where $X = D, M_1, M_2$, on $28^3 \times 96$ lattice.

The histogram of the eigenvector components of 3×3 correlation matrix are shown in the Fig. 5.8 for the $28^3 \times 96$ lattices. The lowest energy eigenstate $|0\rangle$ is clearly dominated by $|D\rangle$ showing peak around 0.8, although it receives sizeable

overlap from both $|M_1\rangle$ and $|M_2\rangle$ peaking around 0.45. But overlap of $|D\rangle$ on $|1\rangle$ is rather small and it is mostly molecular $|M_1\rangle$ despite the excited state energy \mathcal{E}_1 is below the threshold. Our data for $|2\rangle$ is too noisy to extract much information. Based on this Λ_b tuned 3×3 GEVP analysis, we get our final binding energy number for $bb\bar{u}\bar{d}$ tetraquark system to be $-189(18)$ MeV, where the error is statistical.

5.2 Bottom-charm tetraquark

The use of HISQ action for $c, s, u/d$ plays out well for the bottom baryons and two-bottom tetraquark states explored so far. We have problem in forming $(l_1 C \gamma_k l_2)$ diquark with HISQ l_1 and l_2 , which we addressed by replacing one of the light quarks with a b quark denoted by Q . In $bc\bar{u}\bar{d}$ tetraquark simulation, use of NRQCD b and HISQ c, u, d quarks gives rise to a different problem. The operators that are necessary to calculate the binding energy of bottom-charm tetraquarks are

$$\mathcal{O}_{B^*D} = [\bar{l}_1^a(x) \gamma_k Q^a(x)] [\bar{l}_2^b(x) \gamma_5 c^b(x)] \quad (5.25)$$

$$\mathcal{O}_{B_c \bar{\pi}} = [Q^{aT}(x) C \gamma_i c^b(x)] [\bar{l}_1^a(x) C \gamma_5 (\bar{l}_2^b(x))^T] \quad (5.26)$$

The correlator for \mathcal{O}_{B^*D} is

$$C_{B^*D}(t) = \sum_{\vec{x}} \text{Tr} \left[\gamma_5 M_1^\dagger(x, 0) \gamma_5 \gamma_k G(x, 0) \gamma_k \right] \times \text{Tr} \left[\gamma_5 M_2^\dagger(x, 0) \gamma_5 \gamma_5 M_c(x, 0) \gamma_5 \right] \quad (5.27)$$

while the corresponding correlator for the operator $\mathcal{O}_{B_c \bar{\pi}}$ is

$$C_{B_c \bar{\pi}}(t) = \sum_{\vec{x}} \text{Tr} \left[(G^{ad}(x, 0))^T \gamma_k \gamma_4 \gamma_2 M_c^{bc}(x, 0) \gamma_4 \gamma_2 \gamma_k \right] \times \text{Tr} \left[\gamma_4 \gamma_2 M_1^{\dagger da}(x, 0) \gamma_4 \gamma_2 \left(\gamma_5 M_2^{\dagger cb}(x, 0) \gamma_5 \right)^T \right] \quad (5.28)$$

The $M_c(x, 0)$ is the HISQ propagator for the c quark. The operators defined in the Eqs. (5.25) and (5.26) are qualitatively different. The first one \mathcal{O}_{B^*D} is molecular tetraquark states where the two mesons are bound by the residual strong interaction. The corresponding baryonic analogue is the deuteron, where the neutron and proton are bound by the residual strong nuclear force. The second operator $\mathcal{O}_{B_c\bar{\pi}}$ corresponds to a deeply bound tetraquark state. The mass difference between the two states for the corresponding doubly bottom tetraquark is about 100 MeV. Therefore, we can expect some mass difference for the bottom-charm tetraquarks too. Since the NRQCD propagator $G(x, 0)$ has vanishing lower components and HISQ propagators have same Kawamoto-Smit multiplicative factor $\Omega(x)$ as defined in Eq(2.29), the above correlators in Eqs. (5.27) and (5.28) yield identical results which prevented us to simulate $bc\bar{u}\bar{d}$ tetraquark states.

Bibliography

- [1] A.E. Bondar, A. Garmash, A.I. Milstein, R. Mizuk and M.B. Voloshin, Phys. Rev. D **84**, 054010 (2011).
- [2] A. Bondar *et al.* (Belle Collaboration), Phys. Rev. Lett. **108**, 122001 (2012).
- [3] R. Aaij *et al.* (LHCb Collaboration), Phys. Rev. Lett **112**, 222002 (2014).
- [4] R.F. Lebed, R.E. Mitchell and E.S. Swanson, Prog. Part. Nucl. Phys. **93**, 143 (2017).
- [5] A. Esposito, A. Pilloni and A.D. Polosa, Phys. Rep. **668**, 1 (2017).
- [6] S.L. Olsen, T. Skwarnicki and D. Zieminska, Rev. Mod. Phys. **90**, 015003 (2018).
- [7] A.V. Manohar and M.B. Wise, Nucl. Phys. **B399**, 17 (1993).
- [8] E.J. Eichten and C. Quigg, Phys. Rev Lett. **119**, 202002 (2017).
- [9] Marek Karliner and Jonathan L. Rosner, Phys. Rev Lett. **119**, 202001 (2017).
- [10] Y. Ikeda, B. Charron, S. Aoki, T. Doi, T. Hatsuda, T. Inoue, N. Ishii, K. Murano, H. Nemura and K. Sasaki, Phys. Lett. **B729**, 85 (2014).
- [11] Marc Wagner *et al.* 2014 J. Phys.: Conf. Ser. **503**, 012031.
- [12] M. Padmanath, C.B. Lang and S. Prelovsek, Phys. Rev. D **92**, 034501 (2015).

- [13] C. Alexandrou, J. Berlin, J. Finkenrath, T. Leontiou and M. Wagner, Phys. Rev. D **101**, 034502 (2020).
- [14] C. Hughes, E. Eichten and C.T.H. Davies, Phys. Rev. D **97**, 054505 (2018).
- [15] A. Francis, R.J. Hudspith, R. Lewis and K. Maltman, Phys. Rev. Lett. **118**, 142001 (2017)
- [16] A. Francis, R.J. Hudspith, R. Lewis and K. Maltman, Phys. Rev. D **99**, 054505 (2019).
- [17] P. Junnarkar, N. Mathur and M. Padmanath, Phys. Rev. D **99**, 034507 (2019).
- [18] L. Leskovec, S. Meinel, M. Pflaumer and M. Wagner, Phys. Rev. D **100**, 014503 (2019).
- [19] P. Bicudo, and M. Wagner, Phys. Rev. D **87**, 114511 (2013).
- [20] P. Bicudo, K. Cichy, A. Peters, B. Wagenbach and M. Wagner, Phys. Rev. D **92**, 014507 (2015).
- [21] P. Bicudo, J. Scheunert and M. Wagner, Phys. Rev. D **95**, 034502, (2017).
- [22] P. Bicudo, M. Cardoso, A. Peters, M. Pflaumer and M. Wagner, Phys. Rev. D **96**, 054510 (2017).
- [23] P. Mohanta and S. Basak, Phys. Rev. D **102**, 094516 (2020).
- [24] J. Jiang, W. Chen and S. Zhu, Phys. Rev. D **96**, 094022 (2017).
- [25] R.L. Jaffe, Phys. Rep. **409**, 1 (2005).
- [26] P. Mohanta and S. Basak, Phys. Rev. D **101**, 094503 (2020).
- [27] K. C. Bowler *et al.*, (UKQCD Collaboration), Phys. Rev. D **54**, 3619 (1996).

- [28] B.C. Tiburzi, Phys. Rev. D **71**, 034501 (2005).
- [29] Z.S. Brown, W. Detmold, S. Meinel, and K. Orginos, Phys. Rev. D **90**, 094507 (2014).
- [30] S. Godfrey and N. Isgur, Phys. Rev. D **32**, 189 (1985).
- [31] S. Capstick and N. Isgur, Phys. Rev. D **34**, 2809 (1986).
- [32] folk.uib.no/nfylk/Hartree/lindex.html
- [33] D. R. Hartree and W. Hartree, Proc. R. Soc. Lond. A150: 933, (1935).
- [34] V. Fock, Z. Physik 61, 126148 (1930).
- [35] T. Iritani *et al.* (HAL QCD Collaboration), JHEP 1610 (2016) 101.
- [36] G. Yang, J. Ping, and J. Segovia, Phys. Rev. D **101**, 014001 (2020)
- [37] M. Tanabashi *et al.* (Particle Data Group), Phys. Rev. D **98**, 030001 (2018) and 2019 update.

Chapter 6

Summary and Outlook

In this final chapter, we highlight our main results on bottom baryon spectra and the important inferences drawn from them in relation to the broad picture of heavy baryon spectroscopy in lattice. The B meson physics obtained from lattice QCD calculations have significantly influenced heavy flavor theories and experiments. Similarly, the masses and other properties of heavy baryons containing one or more b quark(s) from first principle calculation can serve as important input in both theoretical studies and experimental investigations. This becomes particularly true for those baryon states that are yet to be observed in experiments and, for which, lattice calculations can be used as guide. However, bottom baryon spectroscopy from lattice can be derived from a handful varieties of u/d , s and c quark actions (b quark action is almost always NRQCD) and consequently complete understanding of all the sources of systematic uncertainties, including finite lattice spacings, volumes and discretization errors, have to worked out before world averaging of the data can be attempted. This serves as our motivation for the present work where we address lattice QCD determination of single and multiple bottom baryon masses and mass splittings using NRQCD action for the b -quark and HISQ action for the c , s and u/d quarks. This combination of

NRQCD and HISQ has previously been employed in [1] for bottom mesons, although the exact implementation was rather different. In this work, we converted the one component HISQ propagators to 4×4 matrices by the Kawamoto-Smit transformation and the two component NRQCD propagators to 4×4 matrices using the prescription suggested in the reference [2].

The first step of a spectroscopy study is to construct creation / annihilation operators with correct quantum numbers for the hadronic states of interest. The use of HISQ action for lighter quarks gives rise to difficulties for constructing operators motivated by HQET for single bottom baryons. The problem is essentially in constructing diquarks of the form $q^T C \gamma_k q$ as demanded by HQET but which becomes identically equal to zero with two HISQ quarks. To get around, we propose to use $Q^T C \gamma_k q$ instead. Here Q represents the b quark field. We discussed in details this construction along with two and three b baryon operators.

For some of the baryons, we have multiple operators for the same state *i.e.* a baryon having the same quantum numbers. It would be natural in such cases to construct correlation matrices and obtain lowest lying *i.e.* ground states by solving the generalized eigenvalue problem (GEVP). But we cannot always use all such operators because often one of the operators turns out to be lot noisier than the other(s). Hence we refrained for performing GEVP analysis in this work.

Single bottom baryons can have isodoublets with the same overall quantum numbers J^P . For instance, there exist three isodoublets of Ξ_b which are not radially or orbitally excited states [3]. These states have been categorized by the spin of the us or ds diquark denoted by j and the spin-parity of the baryon. These baryons are referred to as $\Xi_b(j = 0, J^P = \frac{1}{2}^+)$, $\Xi'_b(j = 1, J^P = \frac{1}{2}^+)$ and $\Xi_b^*(j = 1, J^P = \frac{3}{2}^+)$. The same pattern is observed in Ξ_c states [4]. The mass difference between Ξ'_b and Ξ_b is about 143 MeV. So depending upon the choice of the wave function having the

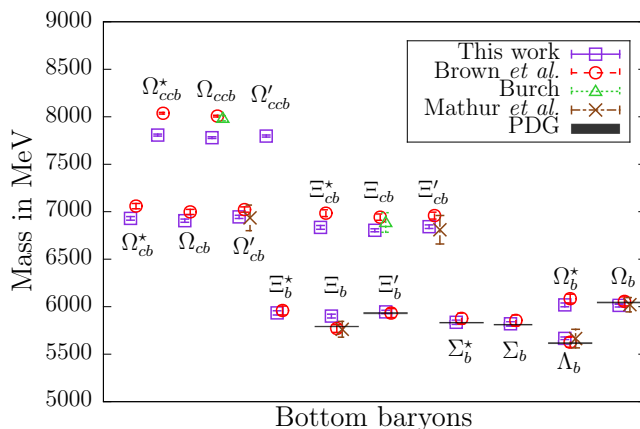


Figure 6.1: Comparison of our single bottom baryon spectra with Brown *et al.* [2], Burch [5], Mathur *et al.* [6] and PDG [4] where available.

same overall quantum numbers, we can have different baryon states. If we choose $(s^T C \gamma_5 d) Q$ as our $j = 0$ baryon operator then we will be simulating Ξ_b state and if we project out the spin-1/2 state of $j = 1$ operator $(s^T C \gamma_k d) Q$ then we will get the Ξ'_b state.

For reason discussed before, we cannot define $j = 1$ light-light diquark state. In our case, the wave function that corresponds to Ξ'_b is $(Q^T C \gamma_5 s) d$. Constructing operator in this way allows the s and d quarks to have parallel spin configurations. By simple physical reasoning, we can argue that explicit construction of $j = 0$ diquark for Ξ_b is more likely to have significant overlap with physical Ξ_b compared to Ξ'_b ($j = 1$) upon gauge averaging. However the operator $(Q^T C \gamma_5 s) d$ is expected to have a good overlap with Ξ'_b state and this is also supported by our result. For anti-parallel s and d spin configuration, Ξ'_b can also have an overlap with the Ξ_b state. On lattice, operators for states having same quantum numbers can mix and, therefore, a detailed GEVP analysis can only resolve the issue of mutual overlap of Ξ_b and Ξ'_b states, which we have not included in this work. This is perhaps the reason we see discrepancies in their values with PDG and others in the Figure 6.1.

The b quark mass has been tuned to modified $\Upsilon - \eta_b$ spin average mass while c quark simply to $J/\psi - \eta_c$ spin average mass. The s quark required to be tuned to both the fictitious η_s and B_s mass since we expect the bottom-strange bound state to be more appropriate than $s - \bar{s}$ bound state in bottom baryons. For the light u/d quarks, we have considered a wide range of bare masses and tune it using B meson. Here in passing, we want to mention that the B and B_s meson tuned u/d and s quark masses correspond to pion and kaon masses that are significantly larger than the physical pion and kaon masses. However, this scheme of tuning u/d quarks has not worked for Λ_b . There u/d are tuned to capture the 190 MeV mass difference $\Sigma_b - \Lambda_b$. This specially tuned $m'_{u/d}$, which is used only for Λ_b , gives it a mass of 5667 MeV. The PDG value for Λ_b mass is 5620 MeV. We demonstrated the variation of bottom baryons as well as hyperfine splittings against varying m_s and $m_{u/d}$. We showed that the hyperfine splittings are almost independent of s and u/d quark masses.

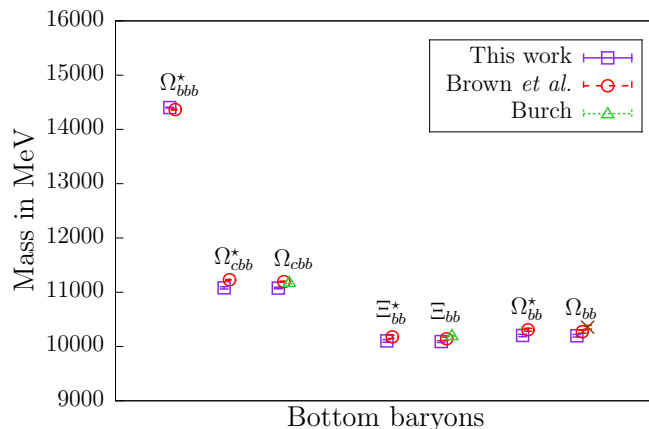


Figure 6.2: Comparison of our triple and double bottom baryon spectra with Brown *et al.* [2] and Burch [5].

We compare our bottom baryon results with other works, mostly with the references [2, 5, 6], in the Figures 6.1 and 6.2. NRQCD has been standard action of choice for the b quark in these three cited studies, but the actions used for c quark are all

different – NRQCD, Clover-Wilson and relativistic heavy quark action [7]. Whatever differences we see in the results for single b baryons with c quark, particularly in the cases with two c , possibly have stemmed from the differences in actions. However, in this work we do not address the systematics involved, which could be significant, because of these differences. The uncertainties for the heavy-hadron masses and mass splittings shown in this thesis represent only the statistical uncertainties. (The study of such systematics needed to arrive at phenomenologically relevant numbers will be reported elsewhere.) But otherwise, the results of bottom baryon spectra in the present study with NRQCD b quark and HISQ $c, s, u/d$ quarks appear to agree with each other.

The previous lattice studies of bottom baryon have all emphasised on calculating the hyperfine splittings *i.e.* mass differences between spin-3/2 and 1/2 bottom baryon states with same quark content. These splittings are also phenomenologically important numbers. We have determined the hyperfine splittings for a host of states. Among these, only the $\Sigma_b^* - \Sigma_b$ splitting have entry in PDG. The comparison of the hyperfine splittings we obtained with other works are shown in the Figure 6.3.

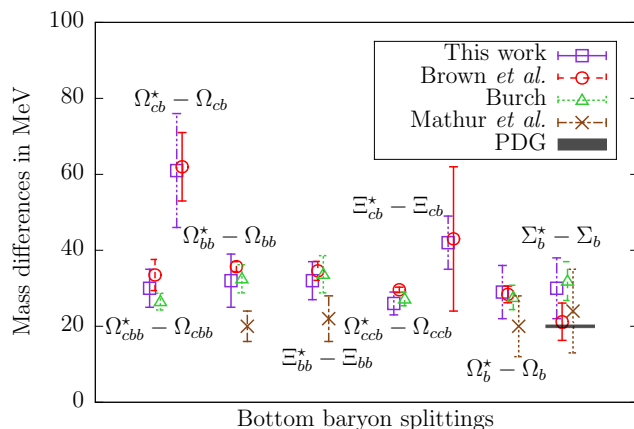


Figure 6.3: Comparison of our hyperfine splittings with Brown *et al.* [2], Burch [5], Mathur *et al.* [6] and PDG [4] where available.

Apart from the hyperfine splittings, a few other mass splittings calculated in this work are assembled in the Table 6.1. The bottom baryon spectra and various mass splittings reported in this thesis and those appearing in [2, 4] are well comparable given the wide choice of actions and tuning employed in achieving them.

Mass splittings	This work	Brown <i>et al.</i> [2]	PDG [4]
$\Omega'_b - \Lambda_b$	398(9)	–	426.4(2.2)
$\Xi_b^* - \Xi_b$	133(36)	189(29)	155.5
$\Xi_b - \Lambda_b$	166(9)	–	172.5(0.4)
$\Lambda_b - B$	406(21)	–	339.2(1.4)
$\Sigma_b^* - \Lambda_b$	201(13)	251(46)	213.5

Table 6.1: Bottom baryon mass differences in MeV. PDG values without error is simply the differences of the two states.

In the study of doubly heavy tetraquark states, we constructed NRQCD- Staggered deeply bound and molecular tetraquark state operators in “good” diquark configuration characterized by color 3_c and spin $J = 0$. In generating the molecular tetraquark state $|M_1\rangle$ and $|M_2\rangle$, we used the same set of tuning for b and u/d quarks as in bottom baryon spectroscopy. The tetraquark spectrum obtained yields an interesting picture validating our $m_{u/d}$, one at Λ_b point and the other at B^0 point. The mass of deeply bound tetraquark state $|D\rangle$ obtained from $m_{u/d}$ at Λ_b agrees closely with the previously available lattice results for bound states. Whereas, the $m_{u/d}$ at B^0 , tuned specifically for (bu) type diquark, gives molecular diquark ($|M_1\rangle$) mass that agrees with the experimental mass of Z_b . This favours the idea of Z_b being molecular tetraquark state. But our scheme of using NRQCD b quark with HISQ c quark prevented us from constructing bottom-charm (bc) tetraquark operators. We found that by construction $[bc][\bar{l}_1\bar{l}_2]$ and $[b\bar{l}_1][c\bar{l}_2]$ operators correspond to the same state with identical correlator.

Bibliography

- [1] Eric B. Gregory, Christine T. H. Davies, Iain D. Kendall, Jonna Koponen, Kit Wong, Eduardo Follana, Elvira Gmiz, G. Peter Lepage, Eike H. Mller, Heechang Na, and Junko Shigemitsu (HPQCD Collaboration), Phys. Rev. D83, 014506 (2011).
- [2] Zachary S. Brown, William Detmold, Stefan Meinel, and Kostas Orginos, Phys. Rev. D90, 094507 (2014).
- [3] R. Aaij *et al.* (LHCb Collaboration), Phys. Rev. Lett. 114, 062004 (2015).
- [4] M. Tanabashi *et al.* (Particle Data Group), Phys. Rev. D98, 030001 (2018) and 2019 update.
- [5] Tommy Burch, arxiv:1502.00675
- [6] N. Mathur, R. Lewis, and R.M. Woloshyn, Phys. Rev. D66, 014502 (2002).
- [7] S. Aoki, Y. Kuramashi, and S. Tominaga, Prog. Theor. Phys. 109, 383 (2003).

Summary

We studied the spectra of singly, doubly and triply bottom baryons and doubly bottom tetraquark using Nonrelativistic QCD (NRQCD) bottom and Highly Improved Staggered Quark (HISQ) charm, strange, up and down quarks on $N_f = 2 + 1$ MILC Asqtad lattices. While studying bottom baryon, we considered all possible combinations of bottom quark(s) with u/d , s and c quarks of the form (bbl) , (bll) and (bl_1l_2) , where l_1 , l_2 and l are the lighter quarks. As the upper and lower components decouple in NRQCD, bottom quarks are described by two-component spinors instead of the usual four component spinor. We discussed operator construction for the above baryons in details along with the operator construction of heavy-heavy, heavy-light and light-light mesons. These mesons are used for tuning of various quark masses.

We noticed that the problem of constructing baryonic operator for spin-3/2 baryons using HISQ propagators persists for singly bottom baryons. The natural choice of interpolating operator for singly heavy baryon as motivated by HQET, is $(\mathcal{O}_k^{l_1l_2h})_\alpha = \epsilon_{abc} (l_1^a C \gamma_k l_2^b) Q_\alpha^c$ where Q represents the heavy bottom quark field, α is the spinor index and a, b, c are the color indices. Though the above operator couples to both spin-1/2 and spin-3/2 states but as the HISQ propagators have same Kawamoto-Smit multiplicative factor $\Omega(x) = \prod_{\mu=1}^4 (\gamma_\mu)^{x_\mu} = \gamma_1^{x_1} \gamma_2^{x_2} \gamma_3^{x_3} \gamma_4^{x_4}$ the contribution of the two spin states can not be separated from the corresponding two-

point function. To get around this problem we have defined our (hl_2l_1) operator as $(\mathcal{O}_k^{hl_2l_1})_\alpha = \epsilon_{abc} (Q^{aT} C \gamma_k l_2^b) l_{1\alpha}^c$. Here we can separate the contribution of different spin states using appropriate projection operator. In the same spirit we defined the doubly bottom baryon operator. Having defined the operators we obtained spectra for singly, doubly and triply bottom baryon. We matched our results with other groups and PDG values where available and found that the results agree well with each other.

Next we considered the spectrum of doubly bottom tetraquark $(bb\bar{u}\bar{d})$. We constructed operators for both molecular and deeply bound states. Here we came across the issue of different tuning of u/d quark mass. The B -meson tuned u/d quark mass reproduces the spectra of both singly and doubly bottom baryons as well as the masses of molecular tetraquark states but fails for Λ_b baryon. On the other hand Λ_b tuned u/d quark mass reproduces the mass of deeply bound tetraquark state. This discrepancy originates due to the fact that various single heavy baryon like Σ_b and Λ_b gets large corrections from χ PT and our deeply bound tetraquark operator has similar structure as of Λ_b baryon and thus is expected to have similar correction. We tried to understand this discrepancy using relativized quark model. We solved for quantum mechanical Hamiltonians of B -meson and Λ_b baryon using Schrödinger equation and Hartree-Fock method. We found that these two systems are solved for two different values of light (u/d) quark mass. With this motivation we carried out GEVP analysis. From 3×3 Λ_b tuned correlation matrix, we get our final binding energy number for $bb\bar{u}\bar{d}$ tetraquark system to be $-189(18)$ MeV.

Appendix A

Zeroth Order NRQCD

Let's consider the Foldy-Wouthuysen transformation of free Dirac field. Our objective is to decouple the Dirac field into top and bottom components. This is obtained through the following transformation.

Let's take the free Dirac equation

$$H\psi = i\frac{\partial\psi}{\partial t}$$

where

$$H = \vec{\alpha} \cdot \vec{P} + m\beta \tag{A.1}$$

and change the field as $\psi' = e^{iS}\psi$, with $S = -i\beta\vec{\alpha} \cdot \hat{P}\delta$, where $\tan 2\delta = \frac{P}{m}$.

The Hamiltonian changes as

$$\begin{aligned}
H' &= e^{iS} H e^{-iS} \\
&= e^{\beta \vec{\alpha} \cdot \hat{P} \delta} (\vec{\alpha} \cdot \vec{P} + m\beta) e^{-\beta \vec{\alpha} \cdot \hat{P} \delta} \\
&= (\vec{\alpha} \cdot \vec{P} + m\beta) e^{-2\beta \vec{\alpha} \cdot \hat{P} \delta} \quad (\text{Using } \alpha^k \beta = -\beta \alpha^k) \\
&= (\vec{\alpha} \cdot \vec{P} + m\beta) \left(1 - \beta \vec{\alpha} \cdot \hat{P} 2\delta - \frac{(2\delta)^2}{2!} + \beta \vec{\alpha} \cdot \hat{P} \frac{(2\delta)^3}{3!} + \dots \right) \\
&= (\vec{\alpha} \cdot \vec{P} + m\beta) (\cos 2\delta - \beta \vec{\alpha} \cdot \hat{P} \sin 2\delta) \\
&= (\vec{\alpha} \cdot \vec{P} + m\beta) \left(\frac{m - \beta \vec{\alpha} \cdot \hat{P} P}{\sqrt{P^2 + m^2}} \right) \\
&= \frac{\beta P^2 + \beta m^2}{\sqrt{P^2 + m^2}} \\
&= \beta \sqrt{P^2 + m^2} \tag{A.2}
\end{aligned}$$

In the Dirac representation of gamma matrices β is give as

$$\beta = \gamma^0 = \begin{pmatrix} I_2 & 0 \\ 0 & -I_2 \end{pmatrix} \tag{A.3}$$

Here I_2 is 2×2 identity matrix. Hence form Eq(A.2) we can see that the Foldy-Wouthuysen transformation results into an Hamiltonian where the upper and lower component of the Dirac field can be decoupled and which gives the energy of the free particle in its rest frame.

Appendix B

Triply light baryon

If we want to realize the spin of a baryon as a vector sum of the spin of the quarks then the simplest operator which can be used to simulate spin-3/2 baryons is given by

$$(\mathcal{O}_k^{l_1 l_2 l_3})_\alpha = \epsilon_{abc} (l_1^{aT} C \gamma_k l_2^b) l_{3\alpha}^c \quad (\text{B.1})$$

Here the diquark part is Lorentz vector, therefore the spin of the diquark is one (in units of \hbar). When we add another quark then according to angular momentum addition rule the above operator will contain both spin-1/2 and 3/2 states.

$$1 \otimes \frac{1}{2} = \frac{3}{2} \oplus \frac{1}{2} \quad (\text{B.2})$$

Here we are assuming that the spin of the baryon is coming solely from the spin of the quarks *i.e.* the quarks don't have any angular momentum. Therefore we can hope to capture the lowest lying states of a baryon with the aforementioned operator.

Hermitian conjugate of such a operator is given by

$$\begin{aligned}
(\mathcal{O}_k^{l_1 l_2 l_3})^\dagger_\delta &= \epsilon_{fgh} (l_3^\dagger)_\delta^h \left[l_2^{g\dagger} \gamma_k \gamma_2 \gamma_4 (l_1^{f\dagger})^T \right] \\
&= \epsilon_{fgh} (\bar{l}_3 \gamma_4)_\delta^h \left[\bar{l}_2^g \gamma_k \gamma_2 \gamma_4 (l_1^{f\dagger} \gamma_4)^T \right] \\
&= \epsilon_{fgh} (\bar{l}_3 \gamma_4)_\delta^h \left[\bar{l}_2^g \gamma_k \gamma_2 \gamma_4 (\bar{l}_1^f)^T \right]
\end{aligned} \tag{B.3}$$

Here we used $\gamma_4^2 = I$ and $\gamma_4^T = \gamma_4$ (in Dirac and MILC-Weyl representation of γ matrices). The corresponding two-point function becomes

$$\begin{aligned}
C_{jk,\alpha\delta}^{l_1 l_2 l_3}(t) &= \sum_{\vec{x}} \langle 0 | [\mathcal{O}_j^{l_1 l_2 l_3}(x)]_\alpha [\mathcal{O}_k^{l_1 l_2 l_3}(0)]_\delta^\dagger | 0 \rangle \\
&= \sum_{\vec{x}} \epsilon_{abc} \epsilon_{fgh} \langle 0 | l_{1\mu}^a(x) (C\gamma_j)_{\mu\nu} l_{2\nu}^b(x) \\
&\quad l_{3\alpha}^c(x) \bar{l}_{3\beta}^h(0) \gamma_{4\beta\delta} \bar{l}_{2\rho}^g(0) (\gamma_k \gamma_2 \gamma_4)_{\rho\sigma} \bar{l}_{1\sigma}^f(0) | 0 \rangle \\
&= \sum_{\vec{x}} \epsilon_{abc} \epsilon_{fgh} M_{3\alpha\beta}^{ch}(x, 0) \gamma_{4\beta\delta} \\
&\quad (\gamma_4 \gamma_2 \gamma_j)_{\mu\nu} M_{2\nu\rho}^{bg}(x, 0) (\gamma_k \gamma_2 \gamma_4)_{\rho\sigma} M_{1\mu\sigma}^{af}(x, 0) \\
&= \sum_{\vec{x}} \epsilon_{abc} \epsilon_{fgh} [M_3^{ch}(x, 0) \gamma_4]_{\alpha\delta} \times \\
&\quad \text{Tr} \left[\gamma_4 \gamma_2 \gamma_j M_2^{bg}(x, 0) \gamma_k \gamma_2 \gamma_4 M_1^{afT}(x, 0) \right]
\end{aligned} \tag{B.4}$$

As we haven't taken any parity projection while defining the interpolating operator in Eq.(B.1), the correlation function given in Eq.(B.4) gets contribution from both positive and negative parity states [1, 2]. At large t the two-point function approaches the following form

$$\begin{aligned}
C_{ij}^{l_1 l_2 l_3}(t) &= Z_{3/2} \Pi_+ P_{ij}^{3/2} e^{-E_{3/2} t} + Z_{1/2} \Pi_+ P_{ij}^{1/2} e^{-E_{1/2} t} \\
&\quad + Z_{3/2}^P \Pi_- P_{ij}^{3/2} e^{-E_{3/2}^P t} + Z_{1/2}^P \Pi_- P_{ij}^{1/2} e^{-E_{1/2}^P t}
\end{aligned} \tag{B.5}$$

where $\Pi_+ = (1 + \gamma_4)/2$, $\Pi_- = (1 - \gamma_4)/2$, are the parity projection operators and $P_{ij}^{1/2} = \gamma_i \gamma_j / 3$, $P_{ij}^{3/2} = \delta_{ij} - \gamma_i \gamma_j / 3$ are the spin projection operators. Therefore in order to extract the contribution of a particular state one needs to multiply the correlation function (Eq.(B.4)) not only by spin projection operators $P_{ij}^{1/2,3/2}$ but also with parity projection operators $\Pi_{+,-}$.

As we are using HISQ propagators for light quarks we can not use the operator defined in Eq.(B.1) in our simulation for reasons discussed in chapter 3. However we can simulate spin-1/2 baryons with the following operator

$$(\mathcal{O}_5^{l_1 l_2 l_3})_\alpha = \epsilon_{abc} (l_1^{aT} C \gamma_5 l_2^b) l_{3\alpha}^c \quad (\text{B.6})$$

Two-point function for this operator has the same form as in Eq.(B.4) with γ_j and γ_k replaced by γ_5 . Like before correlation function of this operator gets contribution from both positive and negative parity states [2]

$$C_5^{l_1 l_2 l_3}(t) = Z_{1/2} \Pi_+ e^{-E_{1/2} t} + Z_{1/2}^P \Pi_- e^{-E_{1/2}^P t} \quad (\text{B.7})$$

Here the contribution of a particular state can be extracted by multiplying the correlation function only by $\Pi_{+,-}$.

Bibliography

- [1] K. C. Bowler, R. D. Kenway, O. Oliveira, D. G. Richards, P. Ueberholz, L. Lellouch, J. Nieves, C. T. Sachrajda, N. Stella, and H. Wittig (UKQCD Collaboration) , Phys. Rev. D54, 3619 (1996).

- [2] J.M. Flynn, F. Mescia, and A.S.B. Tariq, JHEP 0307, 066 (2003).

Heavy hadron spectrum on lattice with NRQCD bottom and HISQ lighter quarks

Protick Mohanta
PHYS11201204013

Thesis Highlight

- Construction of singly, doubly and triply bottom baryon and doubly bottom tetraquark operator.
- Modifications are made in construction of singly bottom baryon operators to get around the problem of HQET inspired light-light diquark involving staggered quarks.
- For doubly bottom baryons spectrum obtained from the modified operator and the conventional HQET motivated operator are matched and they agree with each other quite well.
- Two different tuning of up/down quark mass namely the B -meson tuning and Λ_b tuning were used to compensate the corrections coming from heavy hadron chiral perturbation theory.
- Two tuning are explained using quantum mechanical Hamiltonian with Cornell potential.
- Single bottom baryon spectra obtained are found to have good overlap with the experimentally observed PDG values.
- Based on this agreement several other singly and doubly bottom baryon spectra are calculated and found to have good overlap with the values obtained by other groups.
- The nature of doubly heavy tetraquark are shown to depend on the tuning of up/down quark mass.
- The doubly bottom tetraquark spectrum obtained using B -meson tuning overlaps with PDG values of $Z_b(10610)$ and $Z'_b(10650)$ indicating possible molecular structure.
- The spectrum of the deeply bound tetraquark state obtained using Λ_b tuned up/down quark mass exhibits a binding energy of $-189(18)$ Mev.